The role of auxin during pattern formation in *Arabidopsis thaliana*

Dissertation

der Mathematisch-Naturwissenschaftlichen Fakultät

der Eberhard Karls Universität Tübingen

zur Erlangung des Grades eines

Doktors der Naturwissenschaften

(Dr. rer. nat.)

vorgelegt von

Ole Herud

aus Hamburg

Tübingen

2016

The role of auxin during pattern formation in Arabidopsis thaliana

Gedruckt mit Genehmigung der Mathematisch-Naturwissenschaftlichen Fakultät der Eberhard Karls Universität Tübingen.

Tag der mündlichen Qualifikation: 22.04.2016

Dekan: Prof. Dr. Wolfgang Rosenstiel

1. Berichterstatter: Prof. Dr. Gerd Jürgens

2. Berichterstatter: Prof. Dr. Marja Timmermans

3. Berichterstatter: Prof. Dr. Christian S. Hardtke

Acknowledgements

I would like to express my gratitude to all the people making this doctoral thesis possible. Especially I want to thank my parents and my girlfriend for their constant support, for their encouragement and for believing in me. My various friends I want to thank for all the distractions and discussions.

My friends from Hamburg for their encouragement, even 10 years after I left the city; my rowing teams, which always accepted my early leave for the lab, and of course all my colleagues who did the same. For general discussions about science and their friendship I am especially grateful to Andrey Fadeev, Julia Kamenz, Stephanie Heinrich, Andreas Boland, and Jörg Braun.

My rowing teams and dance partners for all the training sessions and the small victories, especially Nikolas Pietrzik, Rainer Huhn, Andreas Wild, Gitta Bertram, Eva Neumann, Gesa Wilken, and Caro Fischer.

I would also like to mention all the PhD representatives, PhDnet members and rowing club managing committee members, who worked with me to improve the conditions for all of us.

I would also like to thank Gerd Jürgens for allowing me to follow up on my ideas, past and present members of his Lab for fruitful discussions in the beginning of my PhD work, Andrey Fadeev and Daniel Slane for critical reading of this thesis and Gerd Jürgens and Marja Timmermans for evaluating it.

Contents

Acknowledgements 2
Contents 3
Abbreviations 5
Summary 7
Zusammenfassung 8
Personal contribution: accepted publications 10
Lau, S., D. Slane, O. Herud, J. Kong and G. Jürgens (2012). "Early embryogenesis in flowering plants: setting up the basic body pattern." Annu Rev Plant Biol 63: 483-506. 10
Herud, O., D. Weijers, S. Lau and G. Jürgens (2016). "Auxin responsiveness of the MONOPTEROS-BODENLOS module in primary root initiation critically depends on the nuclear import kinetics of the Aux/IAA inhibitor BODENLOS." Plant J. 85, 269-277. 10
Personal contribution: Manuscripts in preparation 10
Herud, O., A. Stiel, B. Höcker and G. Jürgens (In preparation). "Direct visualization of the phytohormone auxin via semi-rational design of a biosensor." 10
Introduction 11
The establishment of polarity 11
The role of auxin response in embryogenesis and directional root growth 12
Mechanism of auxin perception 13
Nuclear transport in plants 16
Attempts to determine intracellular auxin concentration 18
Biosensors and the principles of FRET 20
Design of novel protein function 25
Auxin metabolism 26
Aims of this thesis 30
Results and Discussion 31
Review of the embryogenesis of flowering plants (Lau *et al.* 2012) 31
Developing programs to analyze the splicing pattern in a splice-factor mutant 31
On the kinetics of BDL nuclear uptake (Herud *et al.* 2016) 31
The development of a sensor for the phytohormone auxin 34
Future perspectives 46
References 48

Accepted Publications 62

Lau, S., D. Slane, O. Herud, J. Kong and G. Jürgens (2012). "Early embryogenesis in flowering plants: setting up the basic body pattern." Annu Rev Plant Biol 63: 483-506. 62

Herud, O., D. Weijers, S. Lau and G. Jürgens (2016). "Auxin responsiveness of the MONOPTEROS-BODENLOS module in primary root initiation critically depends on the nuclear import kinetics of the Aux/IAA inhibitor BODENLOS." Plant J. 85, 269-277. 89

Manuscripts in Preparation 123

Herud, O., A. Stiel, B. Höcker and G. Jürgens (In preparation). "Direct visualization of the phytohormone auxin via semi-rational design of a biosensor." 123

Abbreviations

2,4-D	2,4-dichlorophenoxyacetic acid
AFB	AUXIN SIGNALING F BOX PROTEIN
ARE	AUXIN RESPONSIVE ELEMENT
ARFs	AUXIN RESPONSE FACTORs
ATP	Adenosine triphosphate
Aux/IAA	INDOLE-3-ACETIC ACID INDUCIBLE
BDL	BODENLOS
Ca^{2+}	Calcium
CWC15	CELL CYCLE CONTROL PROTEIN 15
DII	Degradation domain of IAA28
ϵ_A	Excitation coefficient of the acceptor
E_{FRET}	Energy transferred
EMB	Embryo lethal
FG	Phenylalanin and glycine rich
FLIM	Fluorescence lifetime imaging
FRET	Förster resonance energy transfer
GFP	GREEN FLUORESCENT PROTEIN
IAA	Indole-3-acetic acid
IAA-Cl	Carboxyl conjugated auxin
IAA-Glc	Glucose conjugated IAA
IAAGlu	Indole-3-acetyl glutamate
IAA-N	Nitrogen conjugated auxin
IAAsp	Indole-3-acetyl aspartic acid
IAN	Indole-3-acetonitrile
IAOx	Indole-3-acetaldoxime
IBA	Indole-butyric acid
ILR	IAA-LEUCINE RESISTANT
IMPα	Importin α
IMPα6	IMPORTIN ALPHA 6
IMPβ	Importin beta

IPA	Indole-3-pyruvic acid
ITC	Isothermal titration calorimetry
J(λ)	Spectral overlap
κ	Dipole orientation factor
MP	MONOPTEROS
n	Refraction index
N_A	Avogadro number
NAA	1-naphthalene acetic acid
NLS	Nuclear localization sequence
NTC	Nineteen-complex
oxIAA	Oxindole-3-acetic acid
oxIAA-Glc	Hexose conjugated oxIAA
PIN	PIN-FORMED
QD	Quantum yield of the donor
R0	Förster distance
RanGEF	Ran nucleotide exchange factors
RNAseq	RNA sequencing
SCF	Skp, Cullin, F-box containing complex
TAA	TRYPTOPHAN AMINOTRANSFERASE
TIR1	TRANSPORT INHIBITOR RESPONSE 1
TrpR	Tryptophan repressor
TrpR	Tryptophan
YUC	YUCCA

Summary

Even the most complex organism has its origin in a single cell. During development the descendants of this cell adopt diverse fates in response to a variety of endogenous and exogenous factors, giving rise to the overwhelming diversity of life. Plants use the phytohormone auxin as a major patterning factor. Auxin controls asymmetric growth in response to photo- and gravitropic stimuli, suppresses shoot branching and promotes lateral root initiation.

Because of the stereotypic cell division pattern in early *Arabidopsis thaliana* embryogenesis, the role of auxin in embryonic root formation is particularly well understood (Lau *et al.* 2012). Auxin degrades the Aux/IAA protein BODENLOS (BDL), thereby releasing the AUXIN RESPONSE FACTOR (ARF) MONOPTEROS (MP), and MP in turn initiates primary root formation.

To study the regulation of the auxin response mediated by the MP-BDL module, we employed a suppressor screen on the root initiation defect of the *bdl* mutant which expresses a stabilized version of the BDL inhibitor. This screen resulted in the identification of the nuclear import receptor *IMPORTIN ALPHA 6* (*IMPα6*) as a critical determinant of auxin response. In *impα6-1 bdl* double mutants the primary root initiation defect of *bdl* is partially rescued, presumably because of a reduced nuclear uptake of bdl into the nucleus. Incorporation of delayed nuclear import into a previously established computational model auxin-modulated MP-BDL interaction revealed that such a delay can be sufficient to trigger an auxin response in *bdl* after a short auxin pulse (Herud *et al.* 2016).

Traditionally auxin localization is inferred from the expression of reporter genes under the control of the auxin-inducible promoter *DR5*. The presence of reporter signal is usually referred to as an auxin-response maximum, and it is assumed that each reporter-signal maximum represents a local auxin maximum. Quantitative measurements indicate that this is not necessarily the case. We employed the similarities between auxin and tryptophan to develop an auxin sensor based on Förster resonance energy transfer (FRET) by semi-rational redesign of an established

tryptophan sensor. This sensor enables us to visualize auxin directly and with high temporal and spatial resolution.

Zusammenfassung

Die Entwicklung auch des komplexesten Organismus beginnt mit einer einzelnen Zelle. Eine große Anzahl von endogenen und exogenen Faktoren beeinflusst die Spezifizierung aller Organe aus den Nachkommen dieser Zelle. In Pflanzen ist das Phytohormon Auxin ein sehr wichtiger Musterbildungsfaktor. Auxin kontrolliert z.B. asymmetrisches Wachstum während des Photo- und Gravitropismus, unterdrückt die Ausbildung sekundärer Sprossachsen und fördert die Bildung von lateralen Wurzeln.

Aufgrund des stereotypischen Zellteilungsmusters in der Embryogenese von *Arabidopsis thaliana* ist die Wirkung von Auxin in der embryonalen Wurzelinitiierung besonders gut verstanden (Lau *et al.* 2012). Auxin degradiert Aux/IAA Proteine wie BODENLOS (BDL) und befreit dadurch AUXIN RESPONSE FACTORS (ARFs) wie MONOPTEROS (MP) von ihrer Inhibierung. Während der Primärwurzelinitiation wird BDL in den inneren Zellen des apikalen Proembryos degradiert, dadurch kann MP die Wurzel initiieren.

Um die Regulation der Auxinantwort besser zu verstehen, haben wir nach Mutanten gesucht, die den Wurzelinitiierungsdefekt von *bdl* retten; die *bdl* Mutante exprimiert ein stabilisiertes BDL Protein. Dabei haben wir den Kerntransportrezeptor *IMPORTIN ALPHA 6* (*IMPα6*) als wichtigen Teil der Auxinantwort identifiziert. In *impα6-1 bdl* Doppelmutanten tritt der Wurzelinitiierungsdefekt seltener auf, vermutlich weil bdl langsamer in den Zellkern aufgenommen wird. Indem wir einen verlangsamten Import in ein etabliertes Model der Auxinantwort eingefügt haben, konnten wir zeigen, dass dies ausreichend sein kann, um in der *bdl* Mutante eine Auxinantwort nach einer kurzen Erhöhung der Auxinkonzentration auszulösen.

Traditionell wird die Auxinkonzentration aus der Expression von Reportergenen unter der Kontrolle des artifiziellen, auxin-induzierbaren Promotors *DR5* geschlossen. Der Bereich, in dem das Reportergen exprimiert ist, wird als Auxinantwort-Maximum bezeichnet, und es wird angenommen, dass jedes Auxinantwort-Maximum auch ein

Maximum der Auxinkonzentration ist. Quantitative Messung zeigen jedoch, dass Auxinkonzentration und *DR5* Aktivität nicht immer korrelieren. Wir haben die Ähnlichkeit von Tryptophan (Trp) und Auxin ausgenutzt, um einen auf Förster-Resonanz-Energie-Transfer basierten Trp-Sensor zu einem Auxin-Sensor zu machen. Mit diesem Sensor können wir Auxin in einer hohen zeitlichen und räumlichen Auflösung visualisieren.

Personal contribution: accepted publications

Lau, S., D. Slane, O. Herud, J. Kong and G. Jürgens (2012). "Early embryogenesis in flowering plants: setting up the basic body pattern." Annu Rev Plant Biol 63: 483-506.

The chapter “RADIAL PATTERNING AND PROTODERM SPECIFICATION“ was mainly written by me. In addition I assisted the other authors with figures and critical reading of the manuscript.

Herud, O., D. Weijers, S. Lau and G. Jürgens (2016). "Auxin responsiveness of the MONOPTEROS-BODENLOS module in primary root initiation critically depends on the nuclear import kinetics of the Aux/IAA inhibitor BODENLOS." Plant J. 85, 269-277.

This study was designed by me, Steffen Lau, Dolf Weijers and Gerd Jürgens. Except the initial screen for a suppression of the *bdl* phenotype, all experiments were performed by me, similar the manuscript was mainly written by me.

Personal contribution: Manuscripts in preparation

Herud, O., A. Stiel, B. Höcker and G. Jürgens (In preparation). "Direct visualization of the phytohormone auxin via semi-rational design of a biosensor."

This project was planned and performed mainly by me. In some experiments I was assisted by Helen Schäfer and Ana-Cristina Barragan Lopez. Crystal structures and dissociation constants were determined by André Stiel and Sooruban Shanmugaratnam. André Stiel and Birte Höcker analyzed crystal structures to facilitate the design process. The manuscript was mainly written by me and André Stiel.

Introduction

The establishment of polarity

The development of an organism begins with the fusion of a sperm with an egg cell, resulting in the formation of a zygote. How this cell and its progenitors establish polarity and initiate all the organs of the organism is one of the fundamental questions in biology. Remarkably, different species use widely different arrays of signaling and gene networks to organize these processes.

While fertilization and sperm entry define the final axis in *amphibians* and *ascidians* (Lane and Sheets 2002), in most animal species the anterior-posterior axis is only recognizable at the end of the gastrulation stage (Kimelman and Martin 2012). In contrast, many species of the spermatophytes exhibit a clear polarity already at the zygote stage (Ueda and Laux 2012). But in the very same spermatophytes, in which the apical-basal axis of the progeny is already predefined by the position of the egg cell in the embryo sac, microspore embryogenesis and callus cultures prove that the polarity can also be established *de novo* (Luo and Koop 1997, Tang *et al.* 2013).

Experiments in *Oryza sativa* showed that the sperm entry site does not correlate with the apical-basal axis of the proembryo (Nakajima *et al.* 2010) but several other groups reported a role of the zygote cell wall. In microspore embryogenesis of *Brassica napus* the axis correlates with the exine opening, suggesting that mechanical stress might influence the polarity (Tang *et al.* 2013). Similarly in *Nicotiana tabacum*, polarity seems to be correlated with zygote elongation, eventually influenced by cell wall proteins. He *et al.* (2007) could show that even a loosely attached fragment of the cell wall appears sufficient.

Extensive research is aimed at understanding the molecules that pattern the subsequent specification events in the early embryo. One of the popular models explaining how a complex pattern can arise from a single pole is the French flag model. Originally proposed by Wolpert (1969), the model predicts a complex pattern arising from a single morphogen gradient. Different downstream modules are purportedly induced by different concentrations of the morphogen (Figure 1a). A good example for this mode of patterning is the pattern formation in the syncytial *Drosophila melanogaster* embryo

(Kimelman and Martin 2012). The dorso-ventral axis is defined by the ventral activation of *dorsal (Reeves and Stathopoulos 2009)*. *Dorsal* induces the expression of *twist*, and together they control several target genes. The different affinities of the transcription factors for promoters of their target genes enable the establishment of distinct expression zones. Simultaneously, *dorsal* represses other promoters, preventing the expression of the corresponding genes in the ventral expression domain of *dorsal* and *twist* (Figure 1b) (Reeves and Stathopoulos 2009).

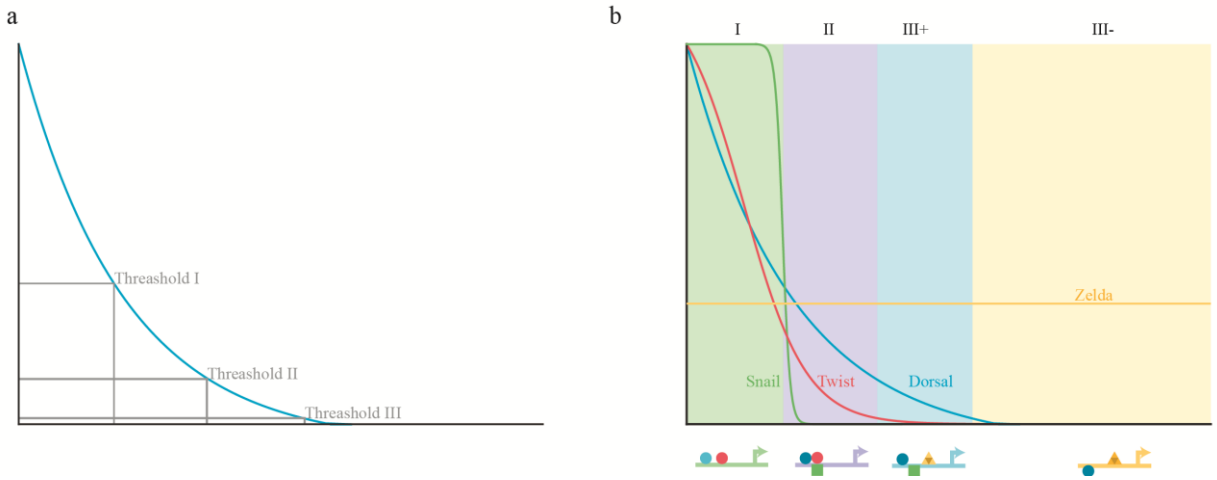

Figure 1: French Flag model and the expression domains along the dorsoventral axis of *D. melanogaster*.

a) French Flag model with 3 different thresholds.

b) Simplified illustration of the dorso-ventral patterning in *D. melanogaster*, modified from Reeves and Stathopoulos (2009). *Snail* (green) is only expressed at high *dorsal* (blue) levels and represses the expression of the Domain II and III+ genes, which only require low *dorsal* levels. In domain III *zelda* acts as transcriptional activator, while domain-III genes are repressed by *dorsal*.

The role of auxin response in embryogenesis and directional root growth

A major patterning factor in plants is the phytohormone auxin. Some researchers propose a role for auxin already in the patterning of the female gametophyte (Pagnussat *et al.* 2009) but this notion has been challenged (Lituiev *et al.* 2013). Nonetheless, auxin participates in the establishment of the apical-basal axis after the first cell division of the zygote at the latest. In the mutants that are defective in auxin perception or transport, for example *bodenlos* (*bdl*), *monopteros* (*mp*), and *pin-formed 7* (*pin7*), the apical daughter

cell division is not reliably vertical, and therefore does not follow the stereotypical division pattern of *Arabidopsis thaliana* (Hamann *et al.* 1999, Friml *et al.* 2003).

Later in embryo development, *bdl* and *mp* exhibit additional defects in root specification and cotyledon initiation (Hamann *et al.* 1999). Furthermore, mutations affecting auxin transport or perception can lead to the absence of leaves (Okada *et al.* 1991), abnormally patterned or absent inflorescences (Yamaguchi *et al.* 2013), and the absence of photo- and gravitropism (Zadnikova *et al.* 2015).

The effect of auxin on organ patterning is largely controlled by localized transport. Grieneisen *et al.* (2007) developed a model of auxin transport and response. They showed that in the root, patterning can be recapitulated by directed transport, independently of the biosynthetic source of auxin. This model predicts an auxin maximum in the organizing center of the root meristem, where auxin concentration is higher than in the rest of the root by two orders of magnitude. The main transport route of auxin in the root is summarized in Figure 2a. Auxin is transported downwards through the vasculature by PIN1. Below the organizing center of the root, in the gravity-sensing columella cells, PIN3 transports auxin laterally and then PIN2 transports it upwards the root again.

Under gravity-stimulation, amyloplasts in the columella cells follow the gravity vector and trigger calcium (Ca^{2+}) release from the endoplasmic reticulum (Vandenbrink *et al.* 2014). This triggers the relocation of PIN3 towards the lower side of the root within a few minutes (Friml *et al.* 2002) and thereby establishes a 2-fold increase of auxin levels on the lower side of the root (Band *et al.* 2012). This results in root bending until an angle of 40° toward the gravity vector is reached after about 100 min (Band *et al.* 2012).

Mechanism of auxin perception

Auxin controls organ and cell shape by transcriptional and non-transcriptional responses (Chen *et al.* 2015). Whereas the mechanism of non-transcriptional response is still debated (Gao *et al.* 2015), the transcriptional response is well understood, with the main factors illustrated in Figure 2b. At low auxin concentrations, proteins of the INDOLE-3-ACETIC ACID INDUCIBLE (Aux/IAA) family inhibit the ARF transcription factors by heterodimer formation and potentially multimerization (Korasick *et al.* 2014). In addition,

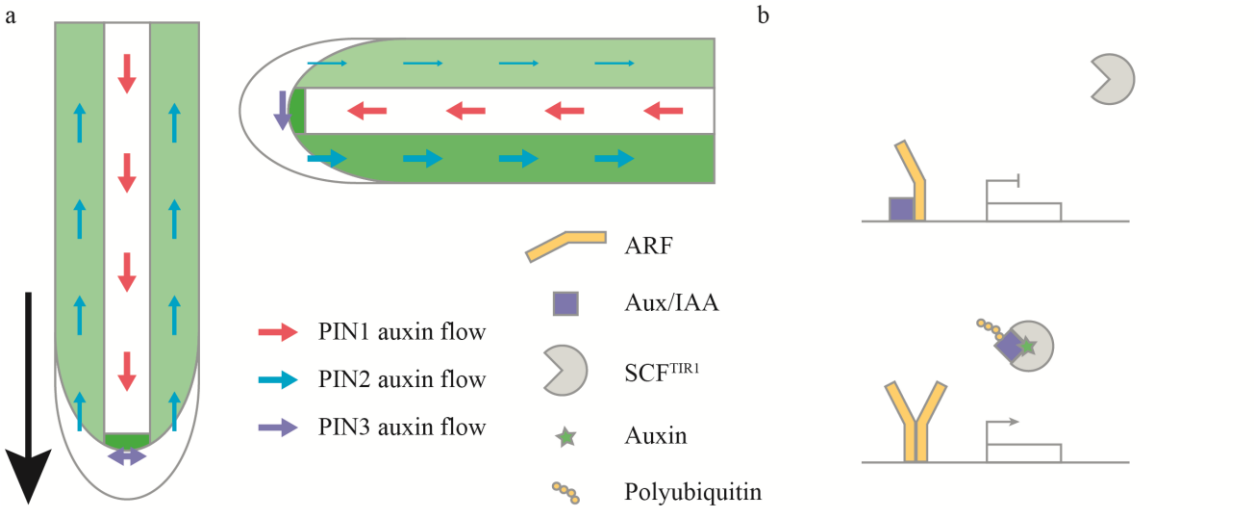

Figure 2: Auxin transport and mechanism of auxin response.

a) Auxin is transported through the root by PIN proteins; (right) relocalization of PIN3 protein in response to gravity stimulation increases auxin concentration on the lower side of the root. The black arrow indicates the gravity vector. Increasing auxin concentrations are highlighted by green coloration. Modified from (Petrasek and Friml 2009).

b) Scheme of the auxin response. Aux/IAA proteins (purple) inhibit ARF transcription factors (yellow). In the presence of auxin, the Aux/IAA proteins are polyubiquitinated and the ARFs induce the expression of their target genes.

Aux/IAA proteins contain ETHYLENE RESPONSE FACTOR-associated amphiphilic repression motifs and mediate repression employing the histone deacetylase TOPLESS (Szemenyei *et al.* 2008). Auxin functions as a molecular glue between Aux/IAA proteins and TRANSPORT INHIBITOR RESPONSE 1 (TIR1) / AUXIN-SIGNALING F-BOX PROTEINs (AFBs) 1 – 5. These F-Box proteins are a part of a specialized SKP, Cullin, F-box (SCF) complex resulting in $SCF^{TIR1/AFB}$. $SCR^{TIR1/AFB}$ auxin-dependently polyubiquitinates Aux/IAA proteins which are in turn degraded by the 26S proteasome. The ARFs are released from inhibition and activate or repress genes with AUXIN-RESPONSIVE ELEMENTS (AREs) in their promoters (Pierre-Jerome *et al.* 2013).

This auxin response is regulated on several levels: transcriptionally, post-transcriptionally, and post-translationally (Table 1). *ARF* genes are transcribed in a tissue-specific manner (Rademacher *et al.* 2011), the mRNAs of some *ARF* genes are further restricted by miRNAs (Mallory *et al.* 2005, Wang *et al.* 2005, Liang *et al.* 2015),

and some ARF proteins are regulated by phosphorylation (Vert *et al.* 2008, Cho *et al.* 2014). Furthermore, the F-Box proteins are miRNA targets as well and regulated by S-nitrosylation (Navarro *et al.* 2006, Terrile *et al.* 2012). Such regulation might enable the plant to regulate different sets of target genes at similar auxin concentrations and incorporate exogenous factors into patterning decisions, e.g. nutrient supply into the root architecture (Liang *et al.* 2015).

Target	Modification	Effect	Reference
ARF10, ARF16, ARF17	Degradation by miR160	Mediating root cap formation, lateral root number, and primary root length. miR160 is induced by nitrogen, sulphur and carbon deprivation.	(Mallory *et al.* 2005, Wang *et al.* 2005, Liang *et al.* 2015)
ARF8	Degradation by miR167	Nitrogen represses miR167 and thereby regulates lateral root initiation and emergence.	(Gifford *et al.* 2008)
TIR1, AFB2, AFB3	Degradation by miR393	Repression of the auxin response as part of the immune response towards *Pseudomonas syringae*.	(Navarro *et al.* 2006)
ARF2	Phosphorylation by BIN2	Brassinosteroid promotes auxin response by inactivation of inhibiting ARFs.	(Vert *et al.* 2008)
ARF7, ARF19	Phosphorylation by BIN2	Inhibition of ARF – Aux/IAA interaction during lateral root development.	(Cho *et al.* 2014)
TIR1, AFB2	S-nitrosylation	Enhances F-Box – Aux/IAA interaction in response to changes in the redox potential.	(Terrile *et al.* 2012)

Table 1: Examples of the regulation of transcriptional auxin response by different signals.

A further leverage point of auxin response modulation is the size of the involved gene families. Auxin concentration is translated into a specific response by a large family of 29 Aux/IAAs, 22 ARFs, and 6 TIR1/AFB proteins. Most, but not all Aux/IAA proteins are degraded in response to auxin; others are auxin-insensitive or also degraded in the absence of auxin, while the Aux/IAA-TIR1/AFB co-receptor complexes exhibit different affinities for particular Aux/IAAs and natural auxins (Shimizu-Mitao and Kakimoto 2014). In addition, ARFs and Aux/IAAs exhibit various affinities to each other and thereby allow the co-existence of different response modules (Calderon Villalobos *et al.* 2012, Piya *et al.* 2014). Modelling is further complicated by functionally different classes of ARF proteins, which are commonly referred to as activating or repressing. This classification is based on protoplast experiments and homology of the DNA-binding domains. But rescue experiments with the “repressive” ARF *ETTIN/ARF3* revealed that only a transcriptional activation domain fused ARF3 rescues the *arf3* phenotype, while a repressor-domain fusion does not (Pekker *et al.* 2005).

Weijers *et al.* (2005) demonstrated that the stabilization of the Aux/IAA proteins BDL and IAA3 triggers specific responses and interferes mainly with different target genes. Furthermore, the suspensor-expressed *IAA10* (Rademacher *et al.* 2012) and *BDL*, genes which are expressed in largely complementary domains in early embryogenesis, exhibit different auxin sensitivities in the presence of TIR1 or AFB2. While the auxin sensitivities of most Aux/IAAs in the presence of TIR1 and AFB2 are similar, IAA10 shows a 2-fold higher sensitivity in the presence of AFB2, and BDL exhibits a 2-fold higher sensitivity in the presence of TIR1 (Shimizu-Mitao and Kakimoto 2014). Thus auxin controls the expression of a wide number of target genes, for example in the root where the auxin responsiveness correlates loosely with the position (Bargmann *et al.* 2013), but the specific readout in a single cell is influenced by many more factors.

One of the best studied auxin responses is the initiation of the primary root meristem in early embryogenesis (Lau *et al.* 2012). Auxin degrades the Aux/IAA protein BODENLOS (BDL), thereby releasing the AUXIN RESPONSE FACTOR (ARF) MONOPTEROS (MP), MP in turn initiate the primary root formation. Auxin response takes place in the nucleus since ARFs, Aux/IAAs and TIR1/AFB family members are localized in the nucleus (Abel *et al.* 1994, Dharmasiri *et al.* 2005, Weijers *et al.* 2006). If bdl is excluded from the nucleus by fusing it with the ligand-binding domain of the glucocorticoid receptor, it does not inhibit MP unless it is translocated into the nucleus upon dexamethasone treatment (Weijers *et al.* 2006).

Nuclear transport in plants

Small proteins up to the size of GREEN FLUORESCENT PROTEIN (GFP) can passively diffuse into the nucleus, but the enrichment in the nucleus is achieved by active transport (Figure 3). Proteins with nuclear localization sequences (NLS) are either bound by the import receptor of the importin beta (IMPβ) family, or indirectly through interaction with proteins of the importin α (IMPα) family (Merkle 2011). The complex is then transported through the nuclear pore complex. Here the transport receptors interact with the intrinsically disordered phenylalanin and glycine rich (FG)-repeats of the nuclear pore proteins. The transport receptors can pass this barrier within milliseconds (Yang *et al.* 2004) because they possess a high number of FG binding sites which the FG repeats can transiently interact with (Hough *et al.* 2015). Additional to this canonical pathway at

least in yeast atypical interactions are common: predicted NLS, nuclear localization, and interaction with IMPα correlate only weakly (Lange *et al.* 2007).

Within the nucleus the complex dissociates after binding guanine triphosphate (GTP)-bound Ras-related nuclear protein (Ran). RanGTP-bound IMPβ is transported directly back, IMPα proteins are transported with the help of the specific exportin Exportin2. Similarly, proteins with nuclear export sequences shuttle to the cytoplasm with other exportin proteins (Figure 3).

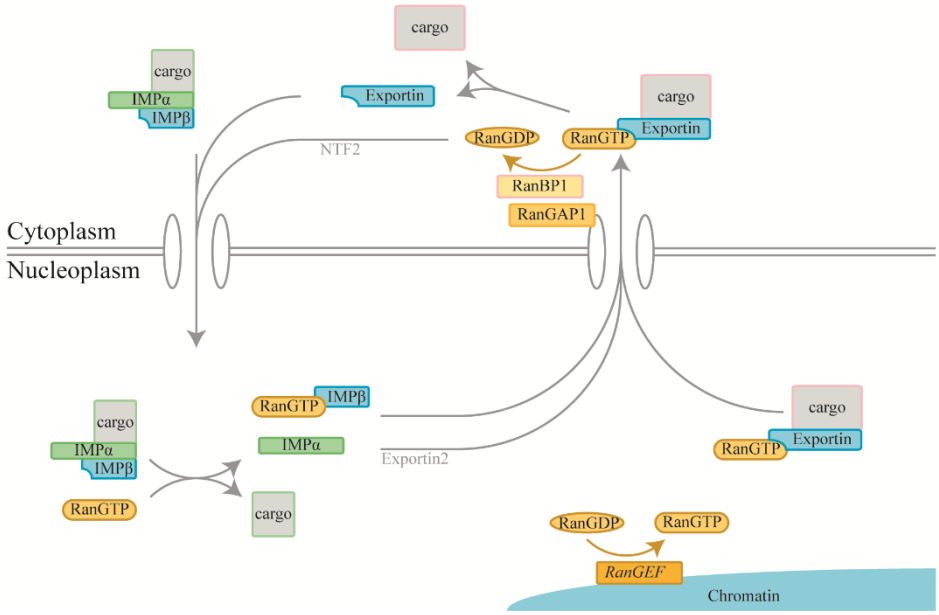

Figure 3: Nuclear import and export cycle.

The energy for this process is provided by RanGTP. In the nuclei of yeast and vertebrates, Ran nucleotide exchange factors (RanGEF) promote the exchange of guanine diphosphate (GDP) against GTP. No homolog has been found in plants yet, but a similar mechanism is likely to exist. The hydrolysis of RanGTP in the cytoplasm is mediated by Ran-specific binding protein 1 (RanBP1) and GTPase-activating protein (RanGAP). Then RanGDP is transported by NUCLEAR TRANSPORT FACTOR 2 (NTF2) back into the nucleus (Figure 3) (Merkle 2011).

Aux/IAAs are constantly synthesized and degraded, therefore the auxin response depends on the complete functionality of protein biosynthesis and nuclear transport. Inhibition of the protein biosynthesis, e.g. with the ribosome inhibitor cycloheximide, and protein import defects both stimulate the expression of auxin-inducible genes because

their pool can be rapidly depleted (Abel *et al.* 1995, Parry *et al.* 2006). In contrast to this, inhibition of protein degradation by the 26S proteasome inhibitor MG132 stabilizes Aux/IAAs and prevents auxin responses (Dharmasiri *et al.* 2005).

Attempts to determine intracellular auxin concentration

Although difficult to obtain, to understand the function of auxin in any given process, knowledge about its exact localization is essential. Commonly, auxin concentration is inferred from the expression of reporter genes like *β-glucuronidase* or *GFP* under the control of a tandem multimer of the ARE with the sequence TGTCTC, termed *DR5* (Ulmasov *et al.* 1997, Sabatini *et al.* 1999). Another ARE, which was designed using the crystal structure of ARF1 and ARF5, exhibits a higher affinity and shows further auxin response maxima (Liao *et al.* 2015). Unfortunately, both reporter constructs unfortunately show a switch-like response, while direct quantification of auxin in the root indicates a smooth gradient in the root (Petersson *et al.* 2009). This suggests that auxin-responsive promoters are active when certain auxin concentration thresholds are reached. Possible response curves resulting from the incorporation of changes in the ARF-ARE affinities into an established model (Lau *et al.* 2011) are illustrated in Figure 4.

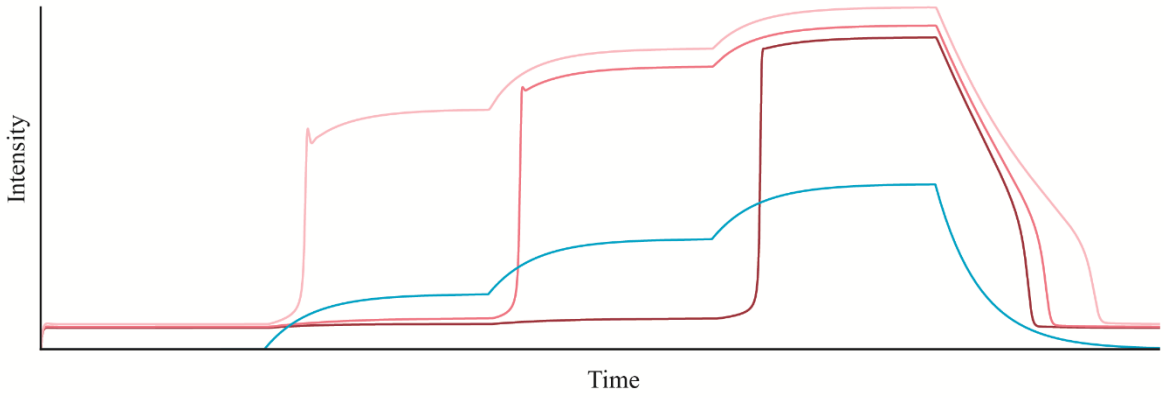

Figure 4: Auxin switches modelled with different dissociation constants.

Various ARF promoter affinities result in different auxin response thresholds. Blue: auxin, red: expression strength of ARF genes with different affinities of ARFs to the promoter of the corresponding Aux/IAA and its own promoter. Only auxin and the expression levels of the ARFs are shown.

The model predicts different sets of ARFs being activated at different auxin concentrations and thereby demonstrates how various auxin reporters can give rise to different results. This is further corroborated by early studies on the expression of Aux/IAAs. Abel *et al.* (1995) showed the wide range of expression responses upon treatment with auxin: the concentration of auxin necessary to induce expression of Aux/IAAs differs by several orders of magnitude. In addition, the temporal response curves studied by Abel *et al.* (1995) are in agreement with the idea that each ARF has an activating influence on the subsequent ARF-Aux/IAA pair, similar to the time-dependent gene activation model proposed by Meinhardt (2015). Therefore expression-based sensors can only have a very limited dynamic range, mainly exhibiting “on” or “off” response, and do not correlate well with auxin concentrations. This critique has also been raised when *DR5* expression in young and old leaves was compared to direct auxin quantifications (Ljung *et al.* 2010).

Some of the problems associated with the usage of expression-based reporters have been circumvented by a novel sensor, directly employing auxin-dependent degradation of Aux/IAA proteins. Brunoud *et al.* (2012) fused the degradation domain of IAA28 (DII) with the fast maturing yellow fluorophore Venus, resulting in *DII-Venus*. With this tool they generated a negative auxin response map, where cells exposed to high auxin concentrations exhibit no fluorescence. This sensor is independent of *ARFs* and *Aux/IAAs* and is degraded in response to auxin within a similar timeframe as auxin induces the expression of *DR5* mRNA, but without the time lag originating from protein maturation. By addition of a non-degradable DII version fused to a red fluorophore, the expression can be monitored and the absence of the sensor can be attributed reliably to an increased auxin concentration (Liao *et al.* 2015). *DR5* is known to oscillate in the timeframe of hours at the lateral root initiation sites (Xuan *et al.* 2015); if no faster oscillation takes place in plants, the irreversible DII-Venus degradation should offer a high enough temporal resolution.

Besides the abovementioned approaches which employ the plant auxin response machinery, antibodies and mass spectrometry can be used to quantify auxin. The highest spatial resolution can be achieved by immunolocalization, but auxin is a hapten, a molecule too small to trigger an immune response (Caruso *et al.* 1995). Therefore

antibodies have been raised not against free auxin but against carboxyl (IAA-C1) or nitrogen (IAA-N) conjugated auxin. In contrast to IAA-N binding antibodies which also bind free auxin, IAA-C1 antibodies are only specific for conjugated auxin, but exhibit a higher sensitivity (Caruso *et al.* 1995). Benkova *et al.* (2003) used antibody staining to demonstrate auxin maxima in root tips and lateral root primordia, confirming the results obtained with *DR5* (Sabatini *et al.* 1999).

Quantitative readouts can be obtained by mass spectrometry. The combination of this technique with tissue-specific fluorescent cell sorting was used to generate an auxin concentration map in the root, auxin concentrations reaching up to 50 µM in the root meristem (Petersson *et al.* 2009). The need for relatively high numbers of cells allows only statements on auxin distribution in cell populations, but also this method suggests an auxin maximum in the root tip, an observation that was confirmed by phenotypical analysis (Sabatini *et al.* 1999). Small differences are found in the developing vasculature of the embryo, the metaxylem of the root, trichoblasts, and the root cap (Petersson *et al.* 2009, Liao *et al.* 2015).

Biosensors and the principles of FRET

In contrast to these methods, which only give qualitative readouts of the concentration of their target molecule or only exhibit a limited special and temporal resolution, genetically encoded sensors can typically be employed to monitor concentrations in the range of two orders of magnitude; they can even resolve Ca^{2+} spikes that result from a single action potential (Okumoto *et al.* 2012).

The development of genetically encoded sensors was pioneered by R. Tsien´s group. Miyawaki et al. (1997) designed FRET-based sensors to quantify Ca^{2+} concentrations in living cells. The sensor consists of a blue and a green or yellow fluorescent protein fused to calmodulin and the M13 peptide. Upon Ca^{2+}-binding the M13 peptide and the calmodulin domain interact with each other and change the orientation of the fluorophores (Figure 5a,b). Fluorescent probes transfer energy to each other when the chromophore dipoles are arranged in parallel and the distance between them is in the order of few Å. The change of the conformation of the fluorophores is thereby translated into a change in the blue and yellow emission intensities (Figure 5a-c). Other biosensors

are based on changes in the properties of fluorescence proteins, like the reduction of the florescence intensity or a shift of the emission maxima (Okumoto et al. 2012).

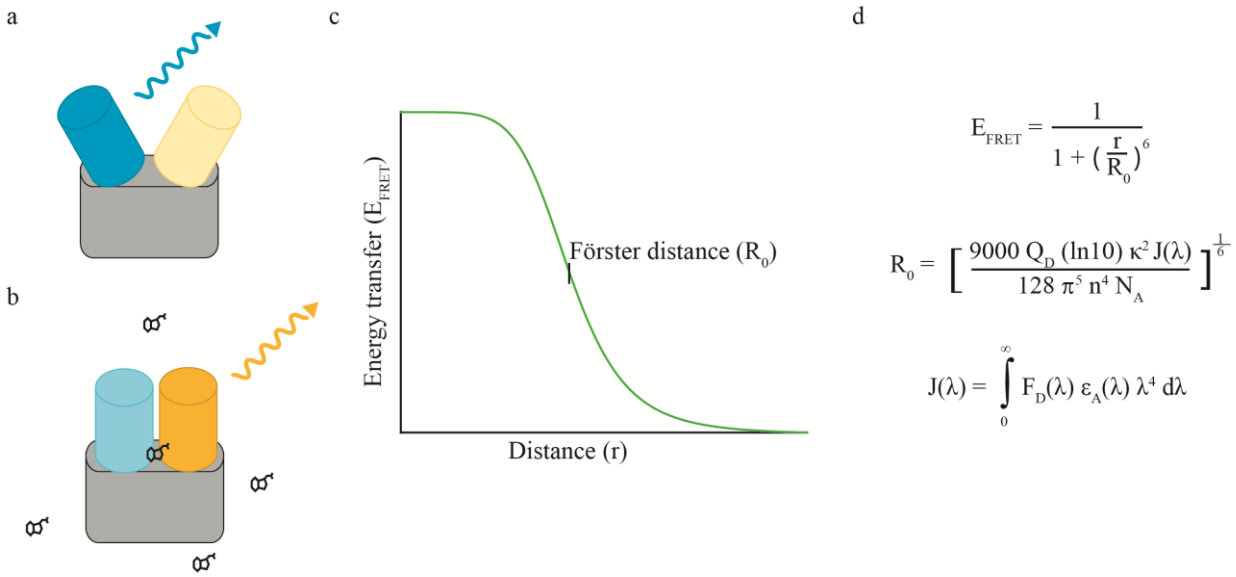

Figure 5: The principle of FRET.

a, b) Scheme of a FRET sensor.

a) In the absence of the ligand, the two fluorophores are too distant, or their chromophore dipoles are perpendicular to each other: the donor (blue) is excited and directly emits photons.

b) When the ligand (black) is bound, the orientation or distance changes and energy is directly transferred from the donor to the acceptor, which then emits more photons, while the photon emission of the donor is quenched.

c) The energy transferred (E_{FRET}) from the donor to the acceptor depends on the sixth power of the distance. See also (d).

d) Formulas to calculate E_{FRET}, Förster distance (R_0), and the spectral overlap $J(\lambda)$. R_0 depends on the quantum yield of the donor Q_D, the dipole orientation factor κ, the spectral overlap $J(\lambda)$, the refraction index n, and the Avogadro number N_A. The spectral overlap also depends on the excitation coefficient of the acceptor (ϵ_A).

The percentage of energy transferred (E_{FRET}) depends on the distance between the fluorophores and the Förster distance (R_0) (Figure 5c,d). The typical distance is between 50 Å for the traditional eCFP-Venus and 63 Å for the optimized Clover-mRuby2 pair (Lam *et al.* 2012). The constants which can be optimized by the use of improved fluorophores are: 1) the quantum yield of the donor (Q_D) which gives the probability of a

photon being absorbed; 2) the spectral overlap between the emission spectra of the donor and the excitation spectra of the acceptor (Figure 6a); 3) the excitation coefficient, which defines the brightness of the acceptor (Figure 5d).

All these factors only affect R_0 in the one-sixth power; if the Q_D is increased by a factor of 2 the R_0 is only increased by 12% and even a 120-fold change in the overlap integral results in only a 2.2-fold increased R_0 (Lakowicz 2006). This exemplifies that small alterations in the properties do not cause large changes in R_0 (Figure 6b-g).

In contrast to the parameters Q_D, ε_A, and $J(\lambda)$, which are given by the fluorophores used, κ and r are much more complicated to optimize. Okumoto *et al.* (2012) first used *periplasmic binding proteins* as a biosensor scaffold, because they undergo large conformational changes upon ligand binding, hence a large change in r. They found that similar ratio changes can be obtained when the donor and acceptor fluorophores were fused to the same linker, indicating that changes in the dipole orientation, κ, dominate the observed FRET ratio change. No clear rules can be defined for the optimal connection of the fluorophores. Long linkers (around one hundred amino acids) are believed to be more likely to create a distance-dependent FRET sensor whereas short and rigid linkers fix fluorophores in specific orientations and result in orientation-dependent sensors (Hamers *et al.* 2014). Similarly, weakly dimerizing fluorophores give the highest FRET contrast. Grunberg *et al.* (2013) used a weak interaction domain to increase the FRET contrast. This was additionally demonstrated by the development of the CyPet-YPet pair. This optimized FRET pair was designed by directed evolution but the remarkable FRET properties were not due to enhanced fluorescence properties and might be caused by increased dimerization of the fluorophores (Vinkenborg *et al.* 2007).

Further complications in the observation of FRET stem from the method used. The most commonly used calculation of the ratio between donor and acceptor fluorescence (ratiometric) is very easy to perform, but suffers from cross-excitation, the direct excitation of the acceptor upon excitation of the donor, and cross-bleeding from the donor emission into the acceptor channel (Figure 6a,f-g). Therefore acceptor photobleaching is frequently used to quantify FRET, but it strongly depends on the bleaching efficiency. If only 70% of the acceptor is bleached the error is 50%, furthermore the error rate increases between 70 - 100% bleaching efficiency and even

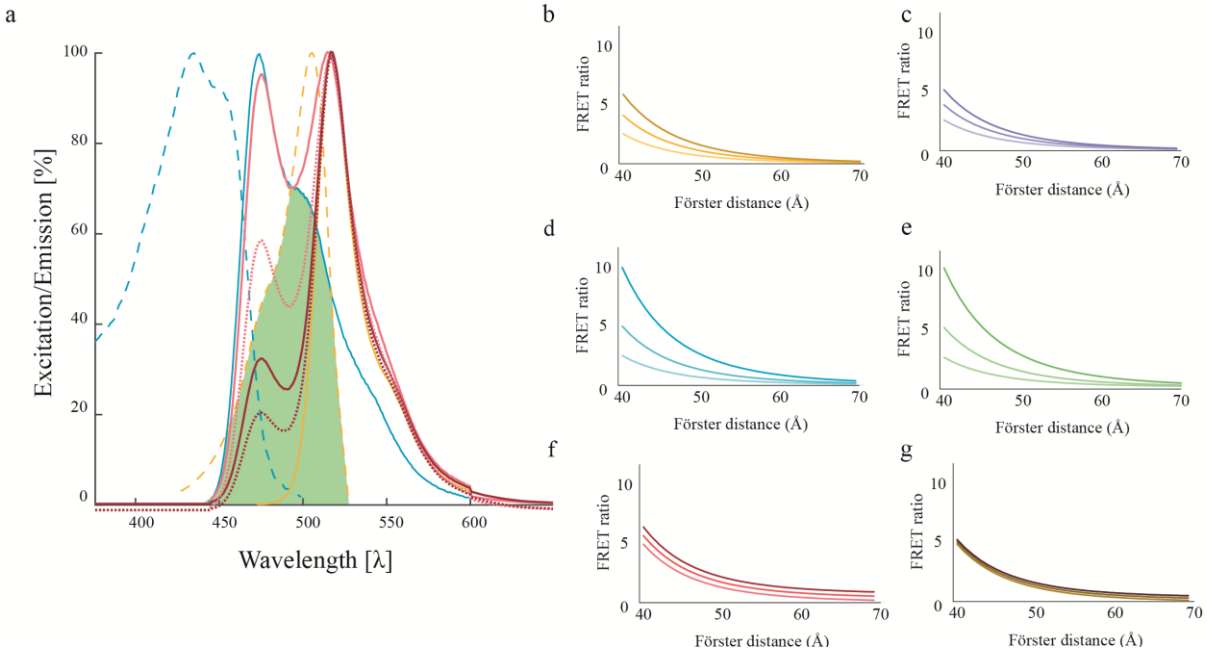

Figure 6: Optimization of the FRET effect and the effect of cross-talk, based on the Aquamarine – mNeonGreen pair.

a) Excitation (dashed) and Emission (solid) spectra of donor (blue) and acceptor (yellow), as well as the resulting emission spectra of the FRET-pair at r =65 Å (pink) and r = 50 Å (red). The solid line is the theoretical result without cross-talk, the dotted line considers cross-talk.

b – g) The theoretical FRET ratio under consideration of the different optimized variants.

b) Q_D varies between 0.4 and 0.9 for the commonly used enhanced CYAN FLUORESCENT PROTEIN (eCFP, pale) and most advanced variants like Aquamarine (dark).

c) ϵ_A varies between 60 000 and 120 000 for eGFP (pale) and more advanced variants like mNeonGreen (dark). Most variants used are close to the optimum.

d) The spectral overlap has a bigger effect on the FRET ratio change because the available fluorescent proteins can exhibit very different excitation and emission spectra.

e) κ^2 has the biggest effect. Here only variants between $^1/_3$ and $^4/_3$ are shown, but in theory values between 0 (dipoles are perpendicular to each other) and 4 (dipoles are parallel) are possible; for free-floating fluorophores κ^2 is assumed to be $^2/_3$. In addition, κ^2 is not a constant defined by the properties of the fluorophores and might change upon substrate binding. In this case the κ^2-induced changes would occur on top of distance-caused changes.

f) Observed ratio changes, when cross-excitation of up to 20 % (dark) is considered.

g) Observed ratio changes, when cross-bleeding of the acceptor into the donor channel of up to 40 % (dark) is considered.

100% photobleaching can provide 10% error (Berney and Danuser 2003). Fluorescence lifetime imaging (FLIM) can reduce these artifacts, as FLIM only depends on the reduced lifetime of the donor. But because most natural fluorophores do not follow a mono-exponential decay, relatively bright signals are necessary for careful quantification (Lakowicz 2006) and the equipment necessary is not widely available.

As most researchers focus on quantitative differences between genotypes and tissues, the precise quantification is not the biggest concern and the quality of the data obtained depends on the dynamic response of the sensor and the signal-to-noise ratio of the sensor in the tissue. Since the original publication of the Ca^{2+} sensor by Miyawaki *et al.* (1997) the sensor readout change was increased to 11 000 % (Zhao *et al.* 2011), and sensors for metabolites, morphogens and hormones have been developed (Kaper *et al.* 2007, Shimozono *et al.* 2013, Jones *et al.* 2014).

All examples shown are based on endogenous proteins which were fused to fluorescent proteins. For example Jones *et al.* (2014) and Waadt *et al.* (2014) fused the two abscisic acid receptor complex proteins PYR1/PYL1 and ABI1(PP2C) with each other and with the fluorescent proteins into a single polypeptide chain and expressed it under the strong *35S* promoter of the *Cauliflower mosaic virus*. This resulted in ABA-hypersensitivity of the transgenic plants, exemplifying the risks of this approach (Jones *et al.* 2014).

Kaper *et al.* (2007) used the tryptophan repressor (TrpR) to quantify tryptophan (Trp) *in planta*. The TrpR protein from *Escherichia coli* represses the expression of several genes involved in the biosynthesis of Trp. Upon binding of Trp, TrpR forms a complete helix-turn-helix motif and subsequently binds DNA, preventing RNA polymerase from interacting with DNA (Somerville 1992). TrpR forms a dimer that non-cooperatively binds Trp with a dissociation constant (K_d) of 14.6 µM and indole-3-acetic acid (IAA) with 72.9 µM (Marmorstein *et al.* 1987). Therefore the TrpR repressor is active as long as the cellular Trp concentration is in the normal range of 70 – 150 µM, an order of magnitude higher than the K_d of the main Trp-consuming enzyme Trp-tRNA synthetase with a K_d of 5 µM (Somerville 1992).

Design of novel protein function

If the use of a protein from another kingdom is not suitable or no protein is available, interactions between the sensor and the organism and hence possible interferences with the natural processes can be minimized by *de novo* protein design or by modification of unrelated proteins (Marvin and Hellinga 2001, Looger *et al.* 2003, Hamers *et al.* 2014). Different approaches have been taken in the past to develop enzymes with novel properties. In general a scaffold with a limited affinity is chosen, by mRNA display of a random-sequence library (Keefe and Szostak 2001), by computational design (Siegel *et al.* 2010), by natural diversity-guided design (Jochens and Bornscheuer 2010) or by literature-based search for a protein with minimal affinity (Bornscheuer and Kazlauskas 2004) (Figure 7). These engineered proteins are commonly screened for binding or catalytic activity, but computational design was also successfully used to design sensors for diverse ligands, such as L-lactate, serotonin and zinc (Marvin and Hellinga 2001, Looger *et al.* 2003).

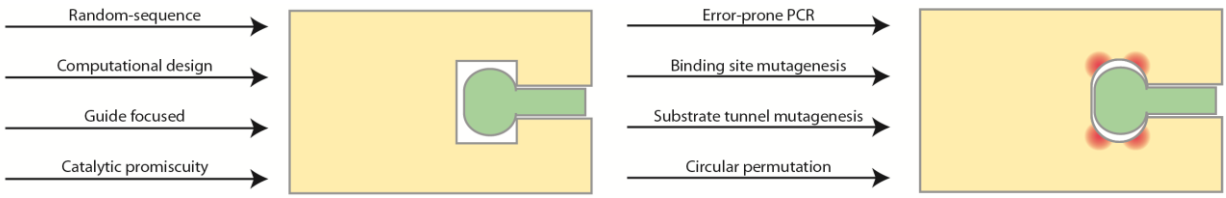

Figure 7: Design of a novel protein function.
Different methods can be employed to find a scaffold with minimal affinity (left). They provide suboptimal binding, which can be further improved to give rise to highly efficient catalysts or sensors (right).

Keefe and Szostak (2001) could show that random-sequence libraries yield proteins with a minimal affinity towards their target molecule adenosine triphosphate (ATP) with a frequency of 1 in 10^{11}. Several rounds of mutagenesis with error-prone PCR and *in vitro* selection resulted in a protein with ATP affinity of 100 nM. Computational design allows the screening of even bigger libraries. Siegel *et al.* (2010) used *de novo* protein design screening a library of 10^{19} possible active sites by modelling a defined active site of substrates and catalytic residues into 207 stable protein scaffolds. After computational optimization 84 designs were tested and 2 showed the desired Diels-Alderase activity, which was further improved by mutating the residues within the active site in direct

contact with the transition state. Smaller libraries can be screened if biological knowledge is incorporated into the design. Jochens and Bornscheuer (2010) incorporated multiple sequence alignments and information about the important residues to identify promising candidates; within just 520 variants screened, 36 members exhibited higher enantio-selectivity.

Those methods did not only differ in regard to finding the scaffold, but also the way in which the activity of the enzyme was further enhanced. While Siegel *et al.* (2010) specifically mutated the residues facing the transition state, and Keefe and Szostak (2001) increased binding by error-prone PCR, circular permutation (Böttcher and Bornscheuer 2010) and mutation in the substrate tunnel (Banas *et al.* 2006) can also be used to increase catalytic efficiency (Figure 7).

Auxin metabolism

Like the natural receptors optimized by millions of years of evolution, these newly designed sensors might also bind other components present in the organism. The F-Box proteins of the TIR1 family for example bind not only the main auxin IAA but also several natural auxins such as 4-chloroindole-3-acetic acid and phenylacetic acid (Shimizu-Mitao and Kakimoto 2014), as well as the synthetic auxins 2,4-dichlorophenoxyacetic acid (2,4-D) and 1-naphthalene acetic acid (NAA) (Tan *et al.* 2007). But because an artificial sensor would not be shaped by evolution to prevent IAA metabolites or storage forms to trigger signaling, these structurally similar compounds have to be taken into account if an artificial sensor is desired.

In Figure 8 the current knowledge about auxin metabolism is summarized in a simplified form. The main auxin pathway of *A. thaliana* is shown in black. Auxin is synthesized from Trp via indole-3-pyruvic acid (IPA) by the sequential action of the TRYPTOPHAN AMINOTRANSFERASE 1 (TAA1) and YUCCA (YUC) gene family proteins (Zhao *et al.* 2001, Stepanova *et al.* 2008). Degradation occurs mainly through oxidization to oxindole-3-acetic acid (oxIAA) and hexose conjugated to oxIAA (oxIAA-Glc) (Ostin *et al.* 1998). Feeding experiments additionally showed conversion to indole-3-acetyl aspartic acid (IAAsp) and indole-3-acetyl glutamate (IAAGlu). Especially the conjugation to IAAsp does not show any sign of saturation, even at the very high rates of 143 µM/h (Kramer and Ackelsberg 2015); however, its role under normal conditions is less clear.

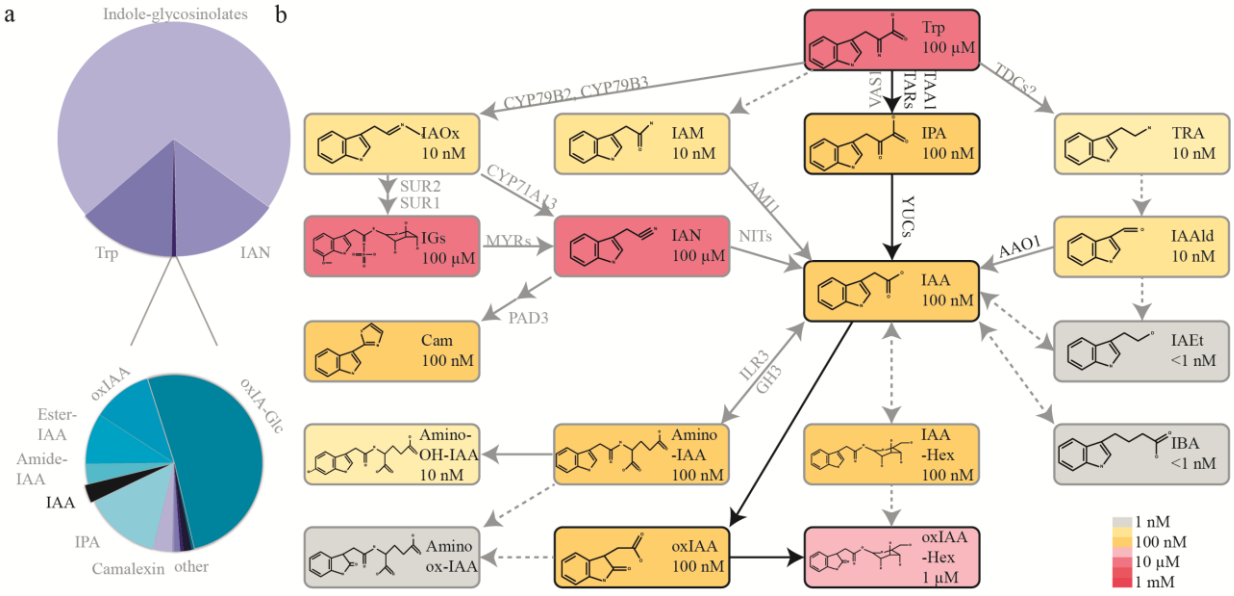

Figure 8: Auxin metabolism and quantification of the specific compounds.

a) Composition of the indole derivatives in plants. Only a minority of the indole derivatives are part of the IAA metabolism, the highest concentrations are reached by the defense components Indole-Glucosinolates (about 300 µM) and IAN (about 70 µM).

b) Overview of the auxin and indole glucosinolate metabolism (Ostin *et al.* 1998, Kai *et al.* 2007, Bednarek *et al.* 2009, Sugawara *et al.* 2009, Normanly 2010, Ludwig-Müller 2011, Zandalinas *et al.* 2012, Ljung 2013). The order of magnitude of the concentrations *in planta* is indicated by the color code. (Kowalczyk and Sandberg 2001, Brown *et al.* 2003, Kai *et al.* 2007, Bednarek *et al.* 2009, Sun *et al.* 2010, Novak *et al.* 2012, Peer *et al.* 2013, Böttcher *et al.* 2014). Solid lines refer to established steps. The main route is highlighted in black.

Beside biosynthesis and degradation, reversible conjugation is also important for auxin homeostasis. GH3 proteins conjugate IAA to amides, and while IAAsp and IAAGlu are irreversibly inactivated, the leucine and alanine conjugates are hydrolyzed back to IAA by IAA-LEUCINE RESISTANT 1 (ILR1) and other hydrolases (Ludwig-Müller 2011). A similar role has been proposed for indole-butyric acid (IBA) (Ludwig-Müller 2007), but it could not be detected by Novak *et al.* (2012) in *A. thaliana* seedlings. Interestingly, IBA does not produce the same response as IAA, but induces lateral root initiation at concentrations which IAA is ineffective at, arguing against a direct conversion of IBA to

IAA. Additionally, a mutant that is resistant to IBA is also resistant to the synthetic auxin 2,4-D but not to IAA or NAA (Ludwig-Müller 2007).

But beside this main pathway, other pathways are also important in *A. thaliana*, for example the *Brassicaceae*-specific indole-3-acetaldoxime (IAOx) pathway (Zhao *et al.* 2002), or the poorly understood Trp-independent pathway affecting early embryo development (Wang *et al.* 2015). Ljung *et al.* (2001) showed that sources and degradation routes of IAA in *Pinus sylvestris* change during seedling development. Similarly the contributions of the individual auxin biosynthesis and catabolism pathways as well as the concentrations of the individual components might change during the development of *A. thaliana*. Furthermore, metabolic rates differ tremendously between species. *Zea mays* exhibits biosynthesis and hydrolysis rates an order of magnitude higher than those observed in eudicots (Kramer and Ackelsberg 2015).

The majority of Trp metabolized in *A. thaliana* is not shuffled into the auxin biosynthesis, but into the defense pathway (Figure 8). Brassicaceae use glucosinolates for antifungal defense (Bednarek *et al.* 2009). They are mainly stored in the vacuole, especially in reproductive organs and the flower stalk, where cells with exceptionally high glucosinolate concentrations are accompanied by idioblasts, which break during insect feeding and release a wide array of bioactive compounds, including thiocyanates and nitriles (Grubb and Abel 2006). At fungal entry sites high concentrations are achieved by active transport of the β-thioglucoside glucohydrolase PENETRATION 2 (Bednarek *et al.* 2009).

Because of the very high levels of glucosinolates in comparison to auxin metabolites and their degradation to IAN and IAA, as well as underestimated Trp conversion, early papers overestimated the amount of amide-bound IAA and free IAA. More than $^2/_3$ of the putative IAA and IAA-amide conjugates can be attributed to glucosinolates or IAN (Llic *et al.* 1996, Yu *et al.* 2015).

Beside the absolute concentration, also the location is of great importance for the interfering potential of the different compounds. The data available in this regard are highly encouraging. All enzymes of the Trp biosynthesis pathway are putatively localized in the chloroplast (Maeda and Dudareva 2012), and the glucosinolates are believed to

be sequestered in the vacuole or specialized cells where they reach concentrations of up to 130 mM (Grubb and Abel 2006, Jorgensen *et al.* 2015). In addition there may be multiple pools of indole-3-acetonitrile (IAN), not all of which are available for IAA synthesis (Normanly 2010), indicating compartmentalization. Furthermore, glucose-conjugated IAA (IAA-Glc) reaches high concentration in the vacuole (Ranocha *et al.* 2013). These substances would therefore not interfere with the quantification of IAA in the cytoplasm or nucleus. IBA would be expected, at least partially, to be present in the peroxisome where it is to be oxidized to IAA (Spiess and Zolman 2013), while IAA-conjugating enzymes are located in the ER (Rampey *et al.* 2004), a notion that is supported by the ER-localized PIN-LIKE (PIL) proteins (Barbez *et al.* 2012). The PIN-LIKEs are evolutionarily older than PINs mediating cell-cell transport, supporting the idea that intracellular compartmentalization is a conserved mechanism, present already in unicellular algae (Barbez *et al.* 2012).

Aims of this thesis

This thesis is aimed to better understand pattern formation of *A. thaliana* and in particular its major patterning factor, the phytohormone auxin. To address this topic we employed semi-rational protein design to engineer a dynamic and direct fluorescence resonance energy transfer sensor. This approach additionally resulted in a better understanding of the sensor binding pocket. Several approaches undertaken to optimize the readout, can furthermore be employed for general improvements of FRET sensor design. Thereby we aim to provide a tool for the plant science community to gain further insights into auxin-controlled processes.

The characterization of *IMPORTIN ALPHA 6* and the modeling of the auxin response should further facilitate the understanding of hormone response pathways and auxin-dependent organ initiation.

Results and Discussion

Review of the embryogenesis of flowering plants (Lau *et al.* 2012)

This review describes the successive establishment of the polarity axes during plant embryogenesis as well as the regulatory networks controlling it. Examples focus on experiments from *A. thaliana* and are supplemented by studies on other dicots and monocots. The expression patterns of genes involved in radial pattern as well as their gene regulatory network are summarized and highlight the signaling within the protoderm cell.

Developing programs to analyze the splicing pattern in a splice-factor mutant

By chance we generated a line mutated in the splice factor *CELL CYCLE CONTROL PROTEIN 15* (*CWC15*). This line showed cell division defects in embryogenesis. To analyze the defects observed in *cwc15* embryogenesis in molecular detail, we developed tools to process comparative RNA sequencing data from wild-type and mutant.

The primary data generated by an RNAseq experiment are a high number of sequences, but most commercially available tools only allow the mapping to whole genes. They usually provide a readout consisting of the number of reads per gene or kilobase of a gene. To understand the NTC component CWC15 we developed tools to map RNAseq data to all exons and introns of *A. thaliana* and search for genes differently spliced between mutant and wildtype. These data were used to compare the splicing pattern of every gene between mutant and wildtype.

On the kinetics of BDL nuclear uptake (Herud *et al.* 2016)

Screens for suppression of auxin resistance phenotypes identified members of the nuclear pore complex (NPC) (Parry *et al.* 2006). Furthermore, several studies on different members of the plant import machinery showed a high sensitivity of the auxin response towards perturbation of the nuclear transport (Kim and Roux 2003, Ferrandez-Ayela *et al.* 2013, Boeglin *et al.* 2016).

In our screen for suppressors of the *bdl* phenotype we identified the nuclear import receptor *IMPORTIN ALPHA 6* (*IMPα6*) as an important component of the bdl import. In *bdl impα6-1* the penetrance of the root initiation defect of *bdl* is reduced, but no other phenotypic difference was found. The *A. thaliana* primary root initiation is a particularly sensitive readout of the auxin response. The specification requires an auxin response before the hypophysis divides, thus within a relatively short timeframe (Weijers *et al.* 2006). In the *bdl impα6-1* double mutant the hypophysis divides frequently horizontally and not vertically as in the *bdl* mutant, thus the *impα6-1* mutation rescues the causative defect in root initiation (Figure 9a).

Furthermore, this phenotype is strongly dose-dependent. Results by Weijers *et al.* (2005) and our own results show that the penetrance differs strongly between individual lines transformed with *pBDL::bdl* or *pBDL::bdl:GUS*. In some lines, hemizygous plants frequently fail to develop a root, whereas in others even homozygous plants frequently show no defect. Interestingly, several plants hemizygous for *pBDL::bdl:3xGFP* exhibit a root initiation defect with an even higher penetrance. This suggests that the GFP fusion stabilizes the bdl protein. Taken together our results show a high sensitivity of the root initiation to the bdl protein level.

By fluorescence recovery after photobleaching we confirmed that the rescue of the *bdl* phenotype by *impα6-1* is correlated with a reduced nuclear translocation of bdl:3xGFP into the nucleus, and does lead to a reduced transcription of MP targets in protoplast transient-expression assays. This indicates that *impα6-1* mutants fail to facilitate the translocation of bdl into the nucleus to the extent necessary to inhibit MP-dependent root initiation (Herud *et al.* 2016). The presumable mechanism is summarized in Figure 9b.

To understand if the suppression of the *bdl* phenotype is specific for *impα6-1*, we generated *impα3-1 impα6-1 bdl:GUS/-* triple mutants and found a further reduction of the *bdl* phenotype. In their screen for suppressors of *auxin-resistant 1*, Parry *et al.* (2006) also found two NPC components. Thus, the suppression of an auxin-resistant phenotype is not very specific to single components, but appears to be a general effect of nuclear transport defects.

To understand why the auxin response is particularly sensitive to nuclear transport defects, we used an established model of the auxin-dependent *MP-BDL* module (Figure 9, solid) (Lau *et al.* 2011). We integrated a reduced degradation into the existing model to account for the *bdl* mutant phenotype. This *MP-bdl* module fails to exhibit an auxin response after a short auxin pulse, recapitulating the root initiation defect in *bdl* (Figure 9, dashed). To account for the *impα6-1* mutation, we additionally introduced a delay of the import of bdl (Figure 9, dotted). Simulations showed that upon a small delay of the bdl import the switch becomes responsive again, even in the presence of stabilized bdl.

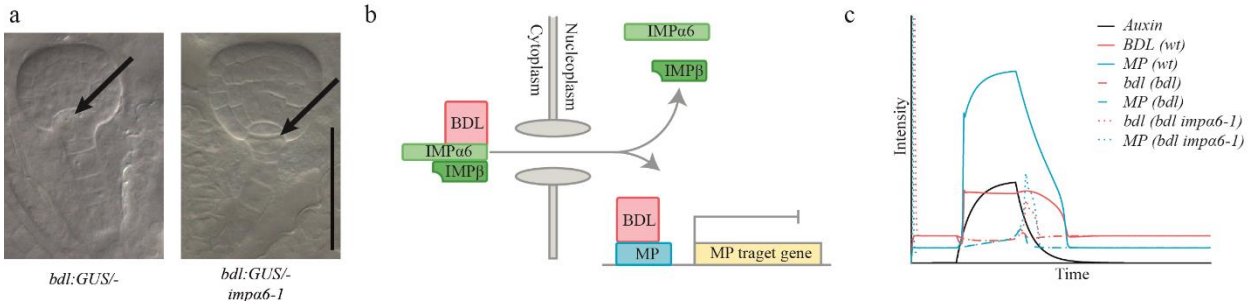

Figure 9: Summary of the work on the function of *IMPα6*

a) The vertical cell division of the hypophysis in the *bdl* mutant embryo is frequently rescued by *impα6-1* (arrows). Modified from (Herud *et al.* 2016).

b) Model of the nuclear transport of BDL. BDL is translocated with the help of IMPα6 into the nucleus where it inhibits the activity of MP.

c) Computational simulations of the *MP-BDL* module in wild type (solid line) and in the *bdl* mutant (dashed). The dotted line shows the induction of MP in the presence of bdl if its import is delayed by 0.5 ‰ of the time axis. Modified from (Herud *et al.* 2016).

In comparison to the *bdl impα6*-1 double mutant, this induction can occur after an even shorter auxin pulse if the delay is increased, similar to the increased rescue of the *bdl* phenotype by the *bdl impα3-1 impα6-1* triple mutant. Furthermore the auxin response and the rescue by a delay of the bdl import would be reduced if the level of *bdl* is increased. To confirm the latter, we used additional lines in which the rootless phenotype is more penetrant, presumably because of higher *bdl* protein levels. These lines were crossed with *impα6-1*. Quantifications of the root initiations defects confirmed that the rescue is less pronounced, as predicted by the simulations. On the other hand, a delay in MP import did not trigger a similar auxin response in the *bdl* background.

Thus the simulations of the model agree with the experimental data and even predict the behavior of the module in the presence of higher bdl levels. We conclude that fast nuclear transport in the response to auxin is important for the primary root initiation. The proposed model explains why the auxin response, which employs the constant turnover of a short-lived inhibitor, is especially sensitive to any alteration in protein transport. It further exemplifies how mathematical models can be used to descriptively summarize experimental data and support the hypothesis on the function of a gene.

The development of a sensor for the phytohormone auxin

To monitor the main auxin in plants, IAA, we used the Trp FRET-sensor published by Kaper *et al.* (2007) as a starting point. This sensor is based on the TrpR from *E. coli*. Similar to the TrpR (Marmorstein *et al.* 1987), the Trp sensor also exhibits low affinity for IAA.

The binding pocket of TrpR with bound Trp is illustrated in Figure 10a. IAA is a derivative of Trp with the amino-acid group of the latter replaced by a carboxyl group as a substituent of the mutual indole-ring (Figure 10b). We assumed a comparable binding mode for TRP and IAA regarding the indole-ring and focused our design effort on positions in the vicinity of the two substituents likely to foster their discrimination: S88, which directly faces the amino group of Trp, and T44, whose backbone oxygen stabilizes Trp-binding. This selection was later expanded by adjacent residues (Figure 10a). About 2000 variants were generated using saturation mutagenesis, and screened for IAA-affinity and -specificity, exploiting the FRET-readout of the original sensor. The structure of several variants was elucidated allowing us to refine our positional selection. In Figure 10c all the different candidates that were improved, are indicated. Candidates, which harbor similar mutations are frequently improved by similar second site mutations. Some mutations, for example several of the mutations at position S88, had a positive effect on IAA-binding. Also mutations of N87 and A91, which indirectly affect the structure of the binding pocket (Figure 10a), frequently had a positive effect on the readout. On the other hand, mutations at L41 were usually not beneficial. Notable exceptions were L41M and L41I, which improved the performance of several putative candidates. Thus small alterations at the position L41 are tolerated, and even sometimes lead to a better sensor, while large changes in the biochemical properties at

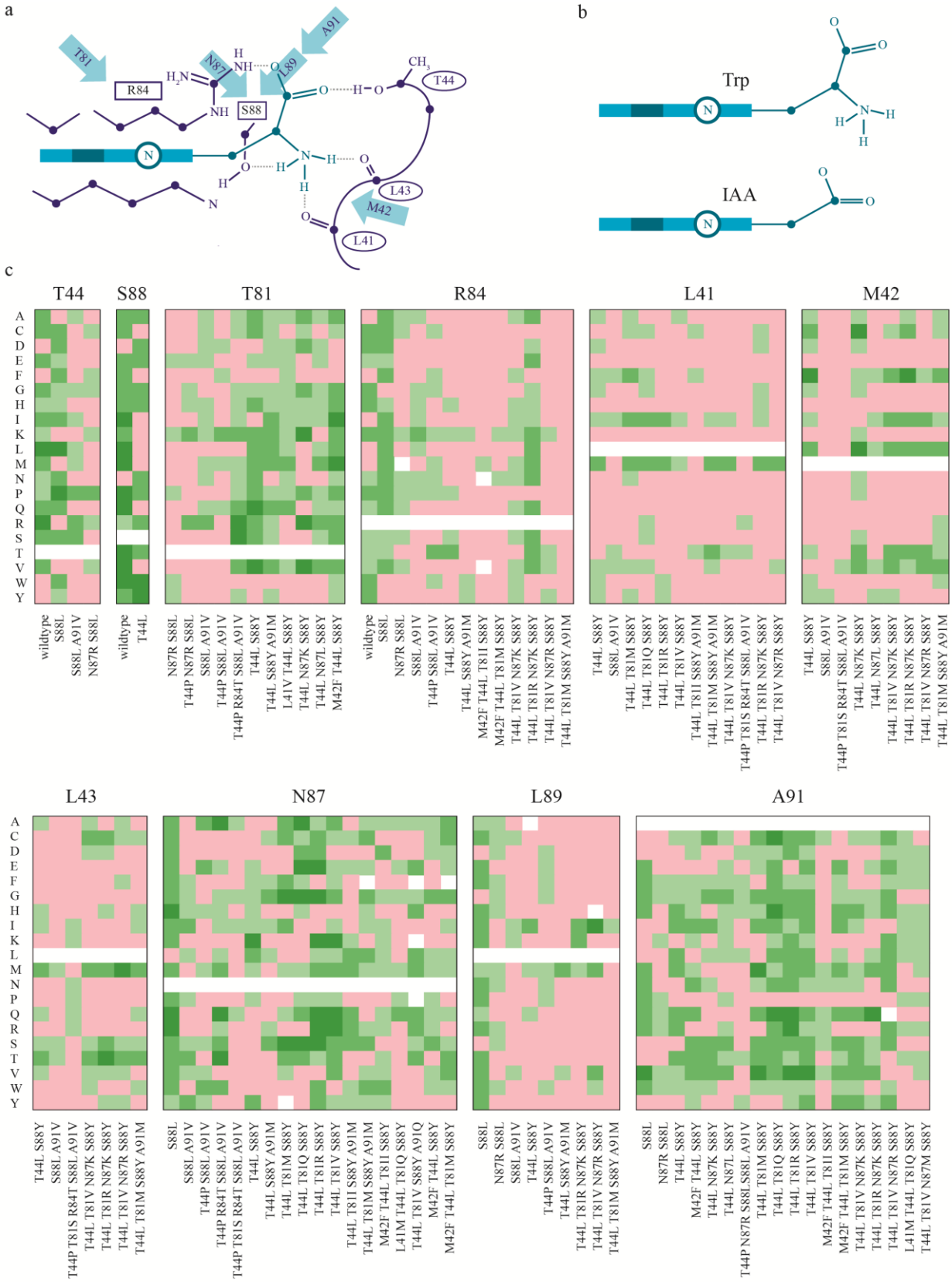
a
T81
N87
L89
A91
R84
S88
T44
L43
M42
L41
b
Trp
IAA
c
T44
S88
T81
R84
L41
M42
L43
N87
L89
A91

Figure 10: Mutations increasing the auxin binding.
a) Structure of the binding pocket of TrpR. Trp is in the middle, the indole ring is perpendicular to the plane of the paper. Residues directly binding Trp are highlighted in purple. Backbone residues mutated in this study are shown as arrows. Modified from (Marmorstein *et al.* 1987).
b) Schemes of Trp and IAA.
c) Effect of different mutations on the binding of the sensor to auxin. Each block represents the mutated residue indicated at the top, which was changed to all other possible amino acid residues (rows). Single columns represent individual mutated candidates, their mutations in comparison to the wildtype are indicated below the schematic. Variants showing auxin-binding are highlighted in green (darker green indicates stronger binding). While mutations of some original residues resulted mostly in improved auxin binding, most of the mutations of other residues did not.

this position, like a mutation to a histidine or proline, did abolish IAA binding. Another example are L89 mutations, which generally had a positive effect on the S88L variant, but seldom on other variants.

After six rounds of mutation, we obtained several variants that showed a high change in the FRET ratio upon auxin treatment. We measured the dissociation constant (K_d) of IAA and the final candidates by isothermal titration calorimetry (ITC), but noticed no correlation between the K_d and the FRET ratio change (Figure 11a).

The original sensor was designed with the blue eCFP as donor and the yellow Venus fluorophore as acceptor. The fluorescence properties of these fluorophores are far below the best fluorophores published to date; therefore, we improved the sensor by employing new FRET pairs. The results are summarized in Figure 11b. All fluorophore pairs were tested in two different orientations, located C- or N-terminally in the construct. Regardless of the fluorophore orientation, there was no close correlation between Förster distance and FRET ratio change, demonstrating that the behavior of a fluorophore is largely unpredictable. Interestingly, the blue-yellow (green circles) pairs in general performed better than the yellow-red (orange circles) pairs. We analyzed the FRET response of several highly responsive pairs with three fluorescence pairs: an eCFP-Venus, a mCerulean3-Ypet, and an Aquamarine-mNeonGreen pair. Here we observed a weak correlation between the FRET ratio change of the mCerulean3-Ypet and the Aquamarine-mNeonGreen pairs (Figure 11c).

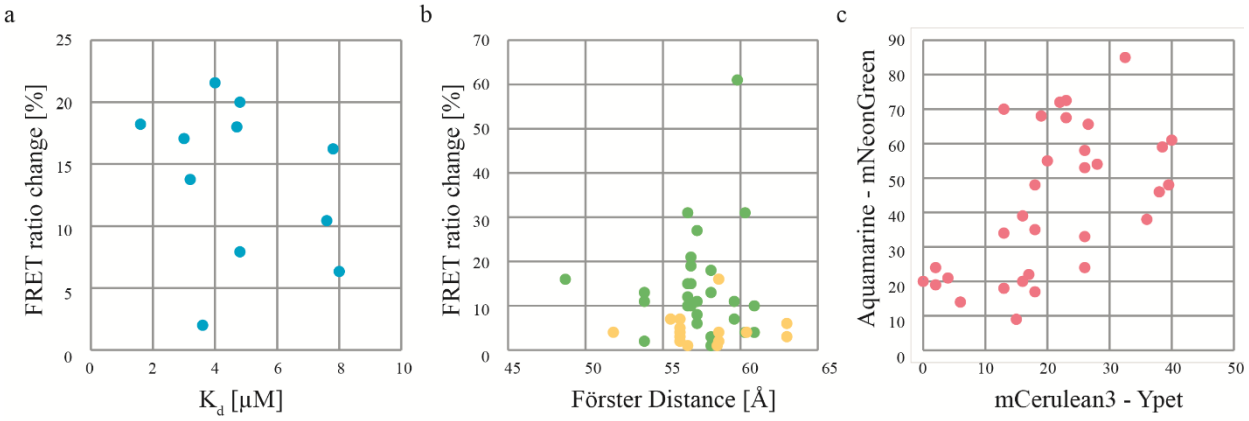

Figure 11: FRET ratio change correlations.

a) FRET ratio change upon IAA treatment plotted against the K_d of the same variant as determined by ITC.

b) FRET ratio changes do not correlate with the Förster distance. Blue-yellow pairs are marked in green, yellow-red ones in orange. Note that blue-yellow pairs in general show a higher FRET ratio change upon IAA treatment, but a similar range of Förster distances as the yellow-red ones.

c) FRET ratio changes in [%] of several variants tested with two different fluorophore pairs. Variants which show a strong response with one fluorophore pair usually also show a strong response with another pair (correlation coefficient = 0.6).

After we had improved the IAA binding, diminished the binding to IAA-related molecules and optimized the fluorophore pair, we set to improve the last important parameter of our FRET sensor, the linkers between the sensory domains and the fluorophores. TrpR is a facultative dimer (Somerville 1992), similarly the auxin sensors also bind IAA as dimers. We employed this property and designed a sensor composed of Aquamarine, the sensor domain TrpR, mNeonGreen, and a second copy of the sensor domain (Figure 12a). Other variants were tested, but proved suboptimal.

First, we mutated all linkers individually, varying the length and the amino acid composition (Figure 12b-d). Mutations in all linkers resulted in improved variants, but no pattern arose that would indicate an optimal length (Figure 12b-d). We used the variant performing best in subsequent experiments, which harbored a mutation in the linker II, and subsequently mutated the other linkers (Figure 12e-f). Still no pattern was obvious and the best candidates differed from the ones obtained in the first round, suggesting

that the optimal composition of a single linker depends on the structure of the other linkers of the sensor. This was further confirmed in the third mutation round (Figure 12g).

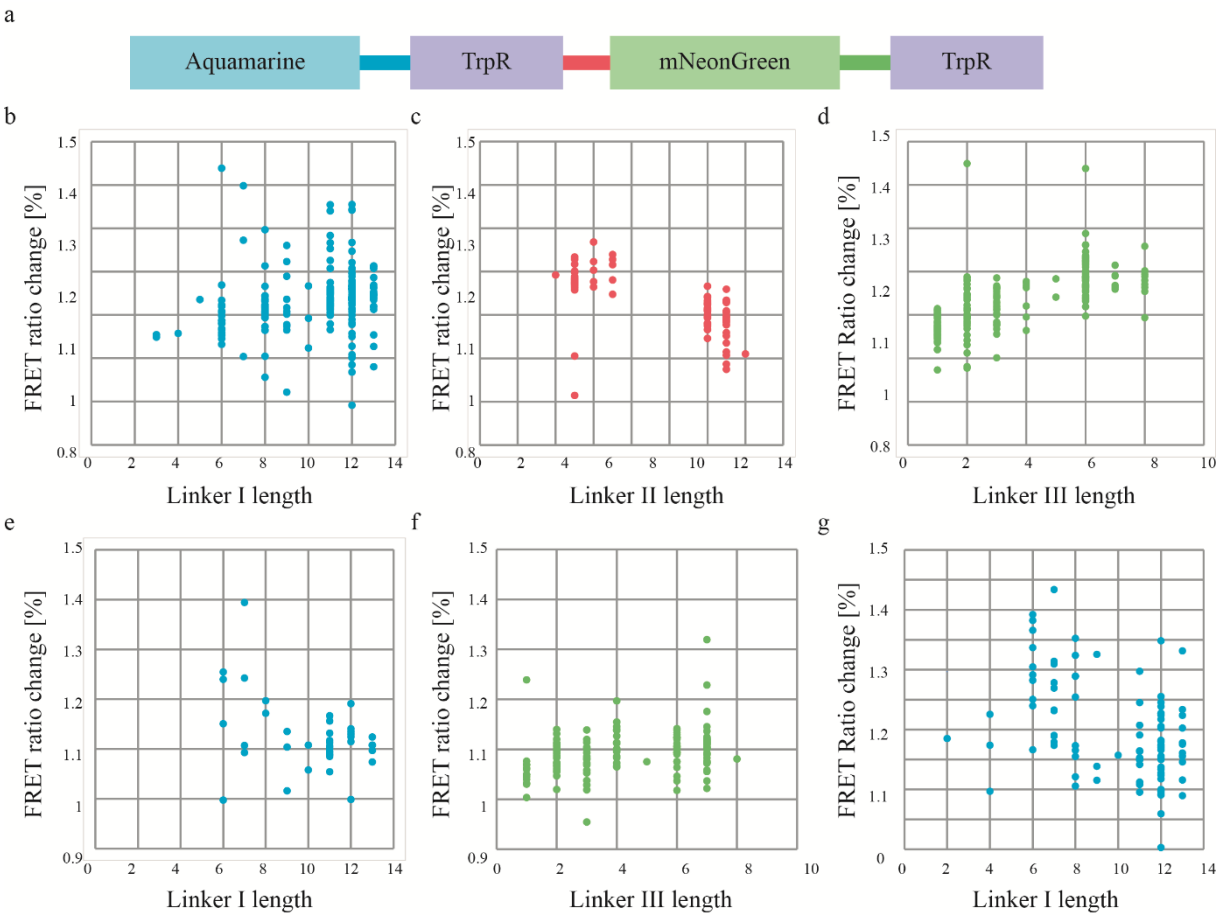

Figure 12: Effects of mutations in linkers.

a) Structure of the construct. The IAA-binding TrpR variants were cloned as tandem repeats into the construct harbouring donor and acceptor fluorophore.

b-d) First-round linker mutations. All three linkers were mutated, but no pattern for the optimal linker length could be determined. One linker II variant was chosen for further mutations.

e-f) Second round linker mutations. Linkers I and III were mutated in the variant obtained in the first round, with no changes in the optimized linker II.

g) Third round of linker mutations. Linker I was further mutated in the variant harbouring mutations in linkers II and III.

The findings are summarized in Table 2. The FRET ratio changes differ slightly between Figure 12 and Table 2, because Figure 12 shows crude measurements, which allow semi-large scale screening, and Table 2 shows measurements of purified proteins.

Linker	Original (length)	Variant Length	Best Variant (length)	Ratio change
mNeonGreen-TrpR	LESLYKKAGS (10)	3 - 13	LESLYKKAGS**TQ** (12)	70
TrpR-Aquamarine	NP**AFLYKVV**GP (11)	4-12	NP**K**GP (5)	86
Aquamarine-Trp	KL (2)	1-8	K**TAGS**L (6)	67
mNeonGreen-TrpR	L**ESLYKKAGS** (10)	6 - 13	L**ASLYTA** (7)	91
Aquamarine-Trp	KL (2)	1-8	K**VF**L (4)	143
mNeonGreen-TrpR	LESLYKKAGS (10)	2 - 13	LESLYKKAGS**NE** (12)	183

Table 2: Summary of linker mutations.

The FRET ratio change [%] indicated was caused by IAA concentrations ranging from 0 to 50 µM IAA.

The improvement of the sensor achieved by the different ways of optimization is summarized in Figure 13a. Most effective were the mutations of the binding pocket, especially the first rounds. Subsequent rounds did not improve IAA-binding much (Figure 13b), but were used to diminish the binding to IAN, an indole derivative highly abundant in *A. thaliana*.

The screen for other FRET pairs almost doubled the readout. Additionally, the new fluorophores are much brighter than the original ones, enabling easier detection *in planta*, and are also more stable to environmental disturbances. Aquamarine, for example, has a higher Q_D (0.89 vs. 0.37 for eCFP), its pKs, the pH at which half of the fluorescence is quenched, is lower (3.3 vs. 5.6) and in contrast to the multiexponential lifetime of eCFP its lifetime follows a monoexponential decay (Merola *et al.* 2014).

The best FRET pair was then tested with all other sensor domain variants, which showed a high auxin-induced FRET change. The best variants obtained with eCFP-Venus usually perform equally well in the mCerulean3-Ypet and the Aquamarine-mNeonGreen pair. Nonetheless, the best Aquamarine-mNeonGreen variant differs in 2 residues from the best eCFP-Venus pair, which increases the response by 40%.

The further improvement of the linkers increased the response tremendously, and after the third round of mutations no saturation was visible, with several variants showing a similar improvement (Figure 13c). Further screening could therefore result in even better sensors.

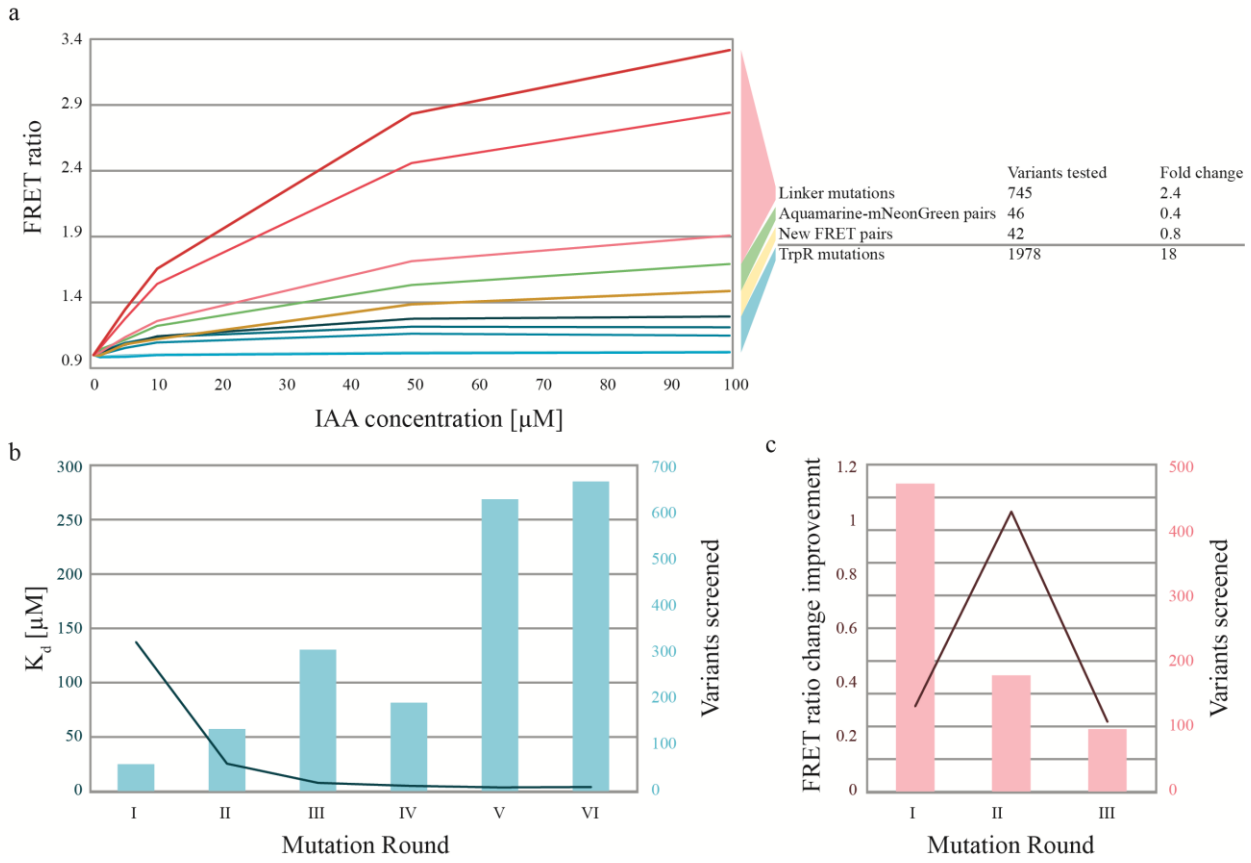

Figure 13: Summary of the different improvement steps.

a) FRET ratio change plotted against IAA concentration, and contributions of the individual steps to the final sensor. For "linker mutations", "Aquamarine-mNeonGreen pairs", and "other FRET pairs", the FRET change is shown. For "TrpR mutations," the K_d change is shown. "Aquamarine-mNeonGreen pairs" show the improvement between the TrpR variant used to screen for new FRET pairs and the variant performing best as an Aquamarine-mNeonGreen pair.

b) Improvement achieved and number of variants screened over 6 rounds of TrpR mutations. In each round 20 - 300 variants were tested (blue bars, right axis), but the K_d did not improve much in the last steps (dark blue line, left axis).

c) Improvement achieved and number of variants screened over 3 rounds of linker mutations. The number of variants screened (pink, right axis) was reduced over time, because fewer linkers were mutated. The FRET ratio change improvement (red, left axis) ranged from 25 – 100 %.

The final version exhibits a 3-fold change of the FRET ratio upon treatment with 50 µM IAA, which was shown to be the upper limit of IAA concentration in roots inferred from

root protoplasts (Petersson *et al.* 2009). Therefore, we used this version to study the FRET effect *in planta*

As a first step to confirm the functionality of the IAA sensor *in planta*, we expressed the sensor transiently under the control of the strong viral *35S* promoter in *Arabidopsis* protoplasts. Figure 14 shows the auxin response in protoplasts. Individual protoplasts differ strongly in the ratio, but populations do show clear tendencies. At low auxin concentrations, the standard deviation stays small, but it increases with higher concentrations in the medium, suggesting that IAA is not taken up by individual cells with equal efficiency (Figure 14a). Furthermore, the Aquamarine signal reaches background levels, making its quantification difficult.

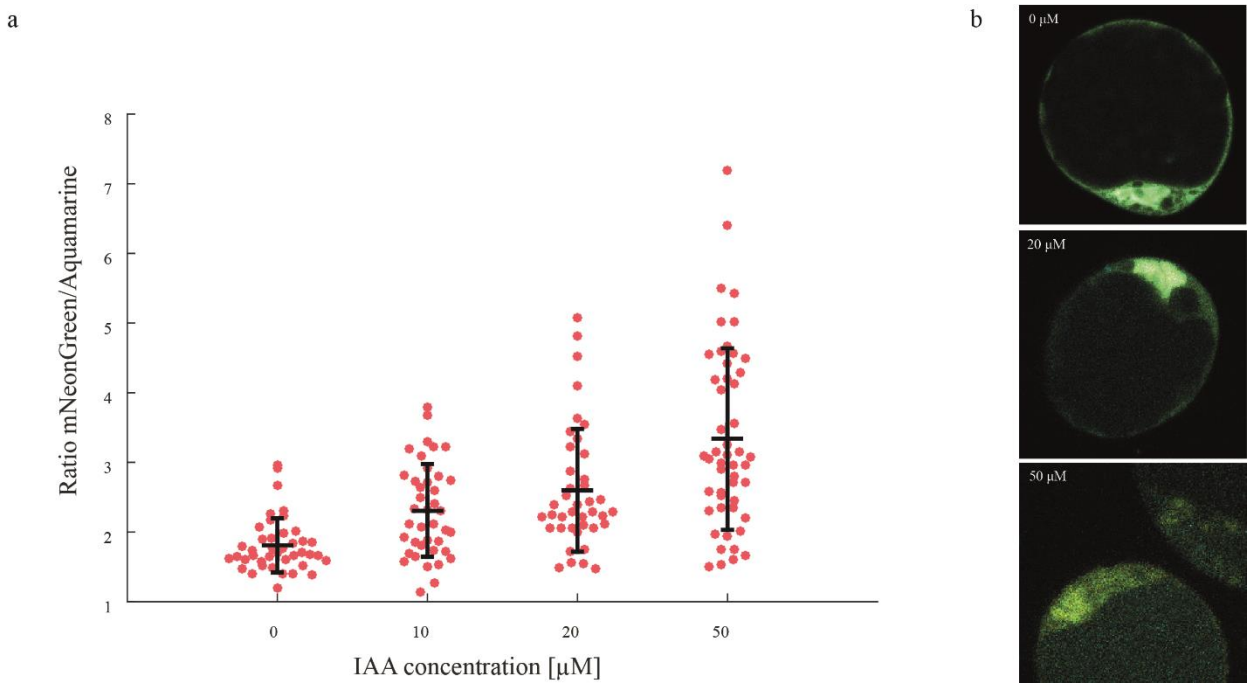

Figure 14: Auxin-sensor response in *Arabidopsis* protoplasts.

a) FRET ratio of protoplasts treated with different IAA concentrations. Each dot indicates a single protoplast. The cross shows the mean value and the standard deviation.

b) Protoplasts expressing nuclear-localized auxin sensor. The mNeonGreen signal (yellow) becomes increasingly dominant with increasing IAA concentrations.

The results of the transient expression analysis show that the sensor is functional *in planta*, but the stable expression in *Arabidopsis* seedling roots proved to be difficult for several reasons. First, the expression in plants is prone to silencing, esp. when tandem

dimers are used, second the codon usage differs between plants and bacteria. To circumvent these problems and enhance expression, we employed codon-optimized and diversified versions of the sensor domains and the fluorophores. Additionally, we used promoters with a broad range of expression strength and avoided the usage of identical terminators for the resistance gene and the sensor. Furthermore, we expressed the selection marker gene *bialaphos resistance* rather weakly and omitted the viral 35S promoter for this purpose.

To drive expression of the sensor itself we used a library of different promoters. To monitor the concentration of IAA in the range of 1 - 50 µM, the sensor should be expressed at a similar concentration (Figure 15). The percentage of sensor saturation depends on the K_d and the concentrations of IAA and the sensor. The fraction of bound sensor is plotted in Figure 15a for K_d = 4 µM. If the auxin concentration for example is in the range between 0 and 50 µM, sensor concentrations of about 25 µM would be optimal. If the sensor concentration is about 100 µM, almost all IAA will be bound by the sensor (Figure 15b). But because the affinity of the AuxIAA-SCF^{TIR1} is in the order of 10 – 75 nM for many tested pairs (Calderon Villalobos *et al.* 2012) and thereby 2-3 orders of magnitude lower than the dissociation constant of the auxin sensor, the sensor should not be able to compete with the Aux/IAA-SCF^{TIR1} co-receptor, unless the sensor concentration exceeds the Aux/IAA-SCF^{TIR1} by a similar excess.Protoplast results are plotted in Figure 15c. The protoplasts were transiently transformed with a construct containing the strong but patchy 35S promoter, resulting in a high variability of expression, as inferred from the fluorescence intensity. These results are highly encouraging, because they show that the FRET ratio does not strongly depend on the expression level of the sensor.

To find the optimal promoter for *in planta* expression, further points should be taken into account, especially how the sensor could interfere with the plant auxin response. The degradation of Aux/IAAs depends on the concentration of the Aux/IAAs as well as on the auxin concentration. Brunoud *et al.* (2012) showed that an increase in the IAA28 concentration by the 35S-driven expression does not change the auxin response. Similarly the auxin response of several AFB double mutants does not differ from the wildtype (Parry *et al.* 2009). This indicates that the plant can cope with certain

differences in the concentrations of each component. Experiments to carefully quantify any possible alteration in the auxin response of plants expressing the auxin sensor are currently under way. In addition, the K_{on} and K_{off} values will be obtained to evaluate how well the IAA bound to the sensor is accessible to other processes in the plant.

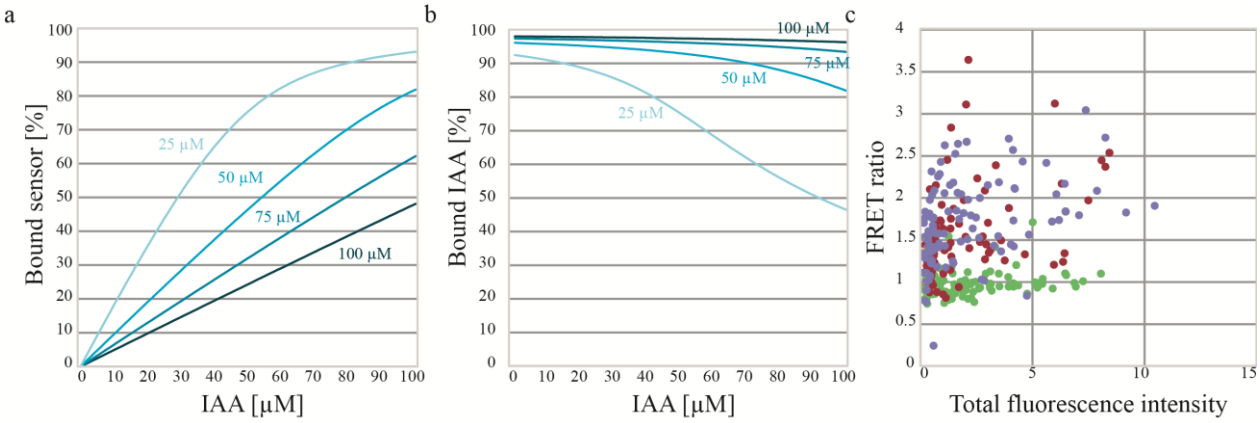

Figure 15: Concentration dependence of the sensor response.

a) Dependence of the sensor ratio on the sensor and IAA concentration. At low sensor concentration (pale blue) the sensor is 90% saturated at 79 µM IAA; if the sensor is expressed at 100 µM, more than 200 µM IAA is necessary for the same ratio of bound sensor.

b) High sensor concentrations deplete IAA from the cell. If the sensor is expressed at high levels, most IAA in the cell is bound to the sensor.

c) Ratio of sensor molecules bound to IAA plotted against the sensor concentration, inferred from the fluorescence intensity in protoplasts. No obvious correlation between fluorescence intensity and FRET ratio can be detected at any given auxin concentration (green: 0 µM, red: 25 µM, purple: 50 µM).

We used a wide variety of promoters, which are purportedly expressed relatively stable in the plant (Table 3). Some promoters are used routinely to normalize the expression of genes in RT-PCR experiments, while others were published to be more stably expressed in the plant (Czechowski *et al.* 2005, Wang *et al.* 2014). By using stably expressed promoters, we try to avoid to monitor sensor rather than ligand concentrations (Figure 15a).

Assessing the protein concentration is rather more difficult than measuring mRNA abundance, but quantifications in yeast might give a hint at the order of magnitude. In yeast, translation elongation factor 1 alpha, the homolog of TRANSLATION

ELONGATION FACTOR 1A (EF-1a) is one of the most abundant proteins and quantified to be 1 200 000 molecules per cell (Lu *et al.* 2007), the cell size is approximately 40 µm³ (Tyson *et al.* 1979), suggesting its concentration to be about 50 µM. The most abundant protein identified by Lu *et al.* (2007) is enolase 2, which reaches about 100 µM. Signaling molecules of the Ras/ERK MAPK cascade are present in much lower concentrations, ranging from 10 nM to 1 µM (Fujioka *et al.* 2006). We therefore concluded that housekeeping genes like *EF-1a* are especially well suited for driving the expression *in planta*. Additionally, we used promoters such as 35S and *UBIQUITIN 10* to drive strong or ubiquitous expression. The precise sensor concentration in plants is unknown but the 10 promoters used should provide a broad range of sensor concentrations.

Gene	Function	Expression strength	Expression stability	Reference
RIBOSOMAL PROTEIN S5A (RPS5A)	Ribosomal	N.D.	N.D.	(Weijers *et al.* 2001, Weijers *et al.* 2006)
35S	Viral	N.D.	N.D.	(Benfey *et al.* 1989)
TRANSLATION ELONGATION FACTOR 1A (EF-1a)	Translation	17.9	2.2	(Curie *et al.* 1993)
GLYCERALDEHYDE-3-PHOSPHATE DEHYDROGENASE C-2 (GAPDH)		14.9	2.5	(Wang *et al.* 2014)
UBIQUITIN 10 (UBQ10)	Ubiquitination	12.6	2.5	(Geldner *et al.* 2009, Krebs *et al.* 2012)
ACTIN 2 (ACT2)	Cytoskeleton	4.3	4.6	(An *et al.* 1996)
UBIQUITIN CONJUGATING ENZYME 9 (UBC9)	Ubiquitination	3.8	2.2	(Kraft *et al.* 2005)
YELLOW-LEAF-SPECIFIC GENE 8 (YLS8)	G2/M progression	1.8	2.0	(Yoshida *et al.* 2001)
ADAPTOR PROTEIN-2 MU-ADAPTIN (AP2M)	Clathrin Coat	1.3	1.6	(Park *et al.* 2013)
TUBULIN BETA CHAIN 4 (TUB4)	Cytoskeleton	N.D.	N.D.	(Wang *et al.* 2014)

Table 3: Promoters used in this study to drive expression of the sensor.

The expression strength is an artificial value calculated from mRNA abundance. The expression stability indicates the variability between different samples, low values indicate high stability. Normalized mean values from (Czechowski *et al.* 2005, Wang *et al.* 2014). N.D.: not determined.

We generated transgenic *Arabidopsis* lines expressing the auxin sensor from these 10 promoters. In addition, we created a construct under the control of a *UAS* promoter

multimer (effector). This artificial promoter can be induced by *GAL4:VP16*-harboring constructs (driver). We crossed 10 effector lines with 3 different driver lines, expressing *GAL4:VP16* from 2 different versions of the 35S promoter or from the *RPS5a* promoter.

The advantage of this approach is that the transformed lines can be selected without any risk of sensor expression interfering with cellular processes. Only when the lines are crossed, the GAL4 transcription factor drives expression with the help of the strong transcriptional activation domain VP16. Furthermore, this two-component system leads to very high expression levels due to amplification (Lynd and Lycett 2011).

We found that the few lines showing expression only do so when crossed with one of the *35S::GAL4:VP16* lines. When crossed with the other *35S* or the *RPS5a* driver lines, no viable seedlings were recovered. This indicates that high expression of the sensor is lethal for the developing embryo.

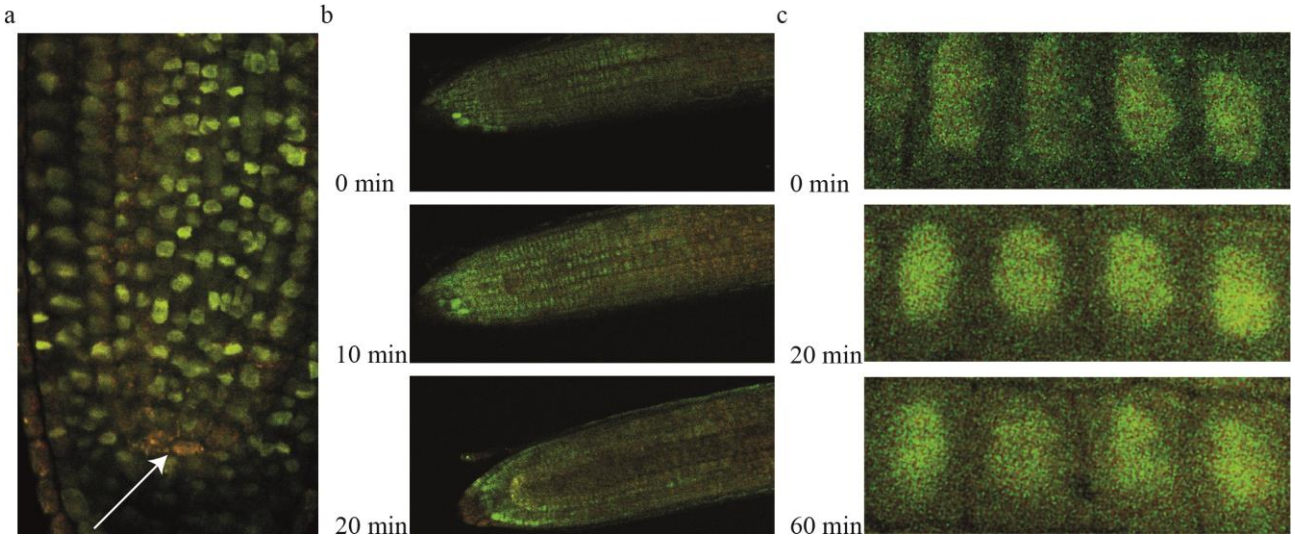

Figure 16: *pEF-1a::NLS:AuxSen* in the root. Overlay of donor (green) and acceptor (red) channels.

(a) Root tip, arrow pointing to the auxin maximum in the meristem.

(b) FRET signal over time upon treatment with 10 µM IAA.

(c) Time course of auxin concentration upon gravistimulus. Only epidermal cells of the lower root surface are shown.

Nevertheless, we obtained several lines expressing the sensor from the *EF-1a* and the ACTIN 2 promoters (Figure 16). *pEF-1a* drives detectable expression in all root tissues analyzed, including the root tip. The red signal in the quiescent center suggests an auxin

maximum in these cells (Figure 16a). This is supported by the expression of *DR5* in these cells as well as tissue-specific IAA quantifications (Sabatini *et al.* 1999, Benkova *et al.* 2003, Petersson *et al.* 2009).

Next we examined the response of *pEF-1a::NLS:AuxSen* upon variation of IAA levels *in planta.* First we treated seedlings with 10 µM IAA and observed the response over time. Within a few minutes the mNeonGreen signal increased, indicating a higher auxin concentration, especially in the basal parts of the root (Figure 16b). To further confirm the AuxSen response we studied the gravitropic response of seedling roots, which depends on the redistribution of auxin, thereby causing root-bending towards the gravitropic force. This redistribution becomes visible with AuxSen as the FRET signal increases basally within a few minutes (Figure 16c).

How well the gradient observed in roots represents the absolute auxin concentration is currently under investigation. Later, auxin gradients in other tissues and under different conditions will be studied. Nonetheless, the results obtained so far indicate that the sensor is functional in plants and can visualize auxin in living tissues in a quantitative manner.

Future perspectives

In the course of this work, we achieved a better understanding of the binding mode of tryptophan and auxin to TrpR. In addition, we generated a library of FRET pairs which will in the future reduce the screening effort in FRET sensor designs. Screening of linker libraries provided insight into the quaternary structure optimal for detection of structural changes in the helix-loop-helix domain of the tryptophan repressor.

The plant research field will also benefit from the establishment of several ubiquitous promoters suitable to drive expression at constantly high levels in all tissues.

With the developed sensor we can visualize a major patterning factor of plants for the first time directly and live. In root tissues, which are in principle accessible to cell type-specific quantifications by mass spectrometry, we were able to confirm the presence of a concentration gradient. The sensor developed here should allow us to study highly dynamic processes like the root gravitropic response. Furthermore, the unique spatial

resolution will allow us to resolve some long-standing debates in the plant development field like the possibility of an auxin gradient in the female gametophyte.

The characterization of a mutant affecting the nuclear import of the Aux/IAA protein BODENLOS showed the importance of the fast import kinetics of Aux/IAAs. The model of Lau *et al.* (2011), which was extended in this thesis, confirmed the sensitivity of the auxin-dependent *MP-BDL* module towards a delay of the activity of Aux/IAA proteins.

In summary, in this thesis, existing tools have been combined to understand the impact of *IMPα6* and new *in situ* tools have been programmed to get insights into the splicing machinery. Furthermore, the development of an auxin sensor starting from conceptual design to expression in plants provides an example of how biochemical expertise can be employed to increase our understanding of pattern formation in plants. Vice versa the knowledge gained in the design of a FRET sensor in plants will pave the way for other sensor designs in the future.

References

Abel, S., M. D. Nguyen and A. Theologis (1995). "The PS-IAA4/5-like family of early auxin-inducible mRNAs in Arabidopsis thaliana." J Mol Biol **251**(4): 533-549.

Abel, S., P. W. Oeller and A. Theologis (1994). "Early auxin-induced genes encode short-lived nuclear proteins." Proc Natl Acad Sci U S A **91**(1): 326-330.

An, Y. Q., J. M. McDowell, S. Huang, E. C. McKinney, S. Chambliss and R. B. Meagher (1996). "Strong, constitutive expression of the Arabidopsis ACT2/ACT8 actin subclass in vegetative tissues." Plant J **10**(1): 107-121.

Banas, P., M. Otyepka, P. Jerabek, M. Petrek and J. Damborsky (2006). "Mechanism of enhanced conversion of 1,2,3-trichloropropane by mutant haloalkane dehalogenase revealed by molecular modeling." J Comput Aided Mol Des **20**(6): 375-383.

Band, L. R., D. M. Wells, A. Larrieu, J. Sun, A. M. Middleton, A. P. French, G. Brunoud, E. M. Sato, M. H. Wilson, B. Peret, M. Oliva, R. Swarup, I. Sairanen, G. Parry, K. Ljung, T. Beeckman, J. M. Garibaldi, M. Estelle, M. R. Owen, K. Vissenberg, T. C. Hodgman, T. P. Pridmore, J. R. King, T. Vernoux and M. J. Bennett (2012). "Root gravitropism is regulated by a transient lateral auxin gradient controlled by a tipping-point mechanism." Proc Natl Acad Sci U S A **109**(12): 4668-4673.

Barbez, E., M. Kubes, J. Rolcik, C. Beziat, A. Pencik, B. Wang, M. R. Rosquete, J. Zhu, P. I. Dobrev, Y. Lee, E. Zazimalova, J. Petrasek, M. Geisler, J. Friml and J. Kleine-Vehn (2012). "A novel putative auxin carrier family regulates intracellular auxin homeostasis in plants." Nature **485**(7396): 119-122.

Bargmann, B. O. R., S. Vanneste, G. Krouk, T. Nawy, I. Efroni, E. Shani, G. Choe, J. Friml, D. C. Bergmann, M. Estelle and K. D. Birnbaum (2013). "A map of cell type-specific auxin responses." Molecular Systems Biology **9**(1).

Bednarek, P., M. Piślewska-Bednarek, A. Svatoš, B. Schneider, J. Doubský, M. Mansurova, M. Humphry, C. Consonni, R. Panstruga, A. Sanchez-Vallet, A. Molina and P. Schulze-Lefert (2009). "A Glucosinolate Metabolism Pathway in Living Plant Cells Mediates Broad-Spectrum Antifungal Defense." Science **323**(5910): 101-106.

Benfey, P. N., L. Ren and N. H. Chua (1989). "The CaMV 35S enhancer contains at least two domains which can confer different developmental and tissue-specific expression patterns." Embo j **8**(8): 2195-2202.

Benkova, E., M. Michniewicz, M. Sauer, T. Teichmann, D. Seifertova, G. Jürgens and J. Friml (2003). "Local, efflux-dependent auxin gradients as a common module for plant organ formation." Cell **115**(5): 591-602.

Berney, C. and G. Danuser (2003). "FRET or no FRET: a quantitative comparison." Biophys J **84**(6): 3992-4010.

Boeglin, M., A. T. Fuglsang, D. T. Luu, H. Sentenac, I. Gaillard and I. Cherel (2016). "Reduced expression of AtNUP62 nucleoporin gene affects auxin response in Arabidopsis." BMC Plant Biol **16**(1): 2.

Bornscheuer, U. T. and R. J. Kazlauskas (2004). "Catalytic promiscuity in biocatalysis: using old enzymes to form new bonds and follow new pathways." Angew Chem Int Ed Engl **43**(45): 6032-6040.

Böttcher, C., A. Chapman, F. Fellermeier, M. Choudhary, D. Scheel and E. Glawischnig (2014). "The Biosynthetic Pathway of Indole-3-Carbaldehyde and Indole-3-Carboxylic Acid Derivatives in Arabidopsis." Plant Physiol **165**(2): 841-853.

Böttcher, D. and U. T. Bornscheuer (2010). "Protein engineering of microbial enzymes." Curr Opin Microbiol **13**(3): 274-282.

Brown, P. D., J. G. Tokuhisa, M. Reichelt and J. Gershenzon (2003). "Variation of glucosinolate accumulation among different organs and developmental stages of Arabidopsis thaliana." Phytochemistry **62**(3): 471-481.

Brunoud, G., D. M. Wells, M. Oliva, A. Larrieu, V. Mirabet, A. H. Burrow, T. Beeckman, S. Kepinski, J. Traas, M. J. Bennett and T. Vernoux (2012). "A novel sensor to map auxin response and distribution at high spatio-temporal resolution." Nature **482**(7383): 103-106.

Calderon Villalobos, L. I., S. Lee, C. De Oliveira, A. Ivetac, W. Brandt, L. Armitage, L. B. Sheard, X. Tan, G. Parry, H. Mao, N. Zheng, R. Napier, S. Kepinski and M. Estelle (2012). "A combinatorial TIR1/AFB-Aux/IAA co-receptor system for differential sensing of auxin." Nat Chem Biol **8**(5): 477-485.

Caruso, J., V. Pence and L. Leverone (1995). Immunoassay Methods of Plant Hormone Analysis. Plant Hormones. P. Davies, Springer Netherlands**:** 433-447.

Chen, J., F. Wang, S. Zheng, T. Xu and Z. Yang (2015). "Pavement cells: a model system for non-transcriptional auxin signalling and crosstalks." J Exp Bot **66**(16): 4957-4970.

Cho, H., H. Ryu, S. Rho, K. Hill, S. Smith, D. Audenaert, J. Park, S. Han, T. Beeckman, M. J. Bennett, D. Hwang, I. De Smet and I. Hwang (2014). "A secreted peptide acts on BIN2-mediated phosphorylation of ARFs to potentiate auxin response during lateral root development." Nat Cell Biol **16**(1): 66-76.

Curie, C., M. Axelos, C. Bardet, R. Atanassova, N. Chaubet and B. Lescure (1993). "Modular organization and developmental activity of an Arabidopsis thaliana EF-1α gene promoter." Molecular and General Genetics MGG **238**(3): 428-436.

Czechowski, T., M. Stitt, T. Altmann, M. K. Udvardi and W. R. Scheible (2005). "Genome-wide identification and testing of superior reference genes for transcript normalization in Arabidopsis." Plant Physiol **139**(1): 5-17.

Dharmasiri, N., S. Dharmasiri, D. Weijers, E. Lechner, M. Yamada, L. Hobbie, J. S. Ehrismann, G. Jürgens and M. Estelle (2005). "Plant development is regulated by a family of auxin receptor F box proteins." Dev Cell **9**(1): 109-119.

Ferrandez-Ayela, A., M. M. Alonso-Peral, A. B. Sanchez-Garcia, R. Micol-Ponce, J. M. Perez-Perez, J. L. Micol and M. R. Ponce (2013). "Arabidopsis TRANSCURVATA1 encodes NUP58, a component of the nucleopore central channel." PLoS One **8**(6): e67661.

Friml, J., A. Vieten, M. Sauer, D. Weijers, H. Schwarz, T. Hamann, R. Offringa and G. Jürgens (2003). "Efflux-dependent auxin gradients establish the apical-basal axis of Arabidopsis." Nature **426**(6963): 147-153.

Friml, J., J. Wisniewska, E. Benkova, K. Mendgen and K. Palme (2002). "Lateral relocation of auxin efflux regulator PIN3 mediates tropism in Arabidopsis." Nature **415**(6873): 806-809.

Fujioka, A., K. Terai, R. E. Itoh, K. Aoki, T. Nakamura, S. Kuroda, E. Nishida and M. Matsuda (2006). "Dynamics of the Ras/ERK MAPK cascade as monitored by fluorescent probes." J Biol Chem **281**(13): 8917-8926.

Gao, Y., Y. Zhang, D. Zhang, X. Dai, M. Estelle and Y. Zhao (2015). "Auxin binding protein 1 (ABP1) is not required for either auxin signaling or Arabidopsis development." Proc Natl Acad Sci U S A **112**(7): 2275-2280.

Geldner, N., V. Denervaud-Tendon, D. L. Hyman, U. Mayer, Y. D. Stierhof and J. Chory (2009). "Rapid, combinatorial analysis of membrane compartments in intact plants with a multicolor marker set." Plant J **59**(1): 169-178.

Gifford, M. L., A. Dean, R. A. Gutierrez, G. M. Coruzzi and K. D. Birnbaum (2008). "Cell-specific nitrogen responses mediate developmental plasticity." Proc Natl Acad Sci U S A **105**(2): 803-808.

Grieneisen, V. A., J. Xu, A. F. Maree, P. Hogeweg and B. Scheres (2007). "Auxin transport is sufficient to generate a maximum and gradient guiding root growth." Nature **449**(7165): 1008-1013.

Grubb, C. D. and S. Abel (2006). "Glucosinolate metabolism and its control." Trends Plant Sci **11**(2): 89-100.

Grunberg, R., J. V. Burnier, T. Ferrar, V. Beltran-Sastre, F. Stricher, A. M. van der Sloot, R. Garcia-Olivas, A. Mallabiabarrena, X. Sanjuan, T. Zimmermann and L. Serrano (2013). "Engineering of weak helper interactions for high-efficiency FRET probes." Nat Methods **10**(10): 1021-1027.

Hamann, T., U. Mayer and G. Jürgens (1999). "The auxin-insensitive bodenlos mutation affects primary root formation and apical-basal patterning in the Arabidopsis embryo." Development **126**(7): 1387-1395.

Hamers, D., L. van Voorst Vader, J. W. Borst and J. Goedhart (2014). "Development of FRET biosensors for mammalian and plant systems." Protoplasma **251**(2): 333-347.

He, Y.-C., Y.-Q. He, L.-H. Qu, M.-X. Sun and H.-Y. Yang (2007). "Tobacco zygotic embryogenesis in vitro: the original cell wall of the zygote is essential for maintenance of cell polarity, the apical–basal axis and typical suspensor formation." The Plant Journal **49**(3): 515-527.

Herud, O., D. Weijers, S. Lau and G. Jürgens (2016). "Auxin responsiveness of the MONOPTEROS-BODENLOS module in primary root initiation critically depends on the nuclear import kinetics of the Aux/IAA inhibitor BODENLOS." Plant J **85**(2): 269-277.

Hough, L. E., K. Dutta, S. Sparks, D. B. Temel, A. Kamal, J. Tetenbaum-Novatt, M. P. Rout and D. Cowburn (2015). "The molecular mechanism of nuclear transport revealed by atomic-scale measurements." Elife **4**.

Jochens, H. and U. T. Bornscheuer (2010). "Natural diversity to guide focused directed evolution." Chembiochem **11**(13): 1861-1866.

Jones, A. M., J. A. Danielson, S. N. Manojkumar, V. Lanquar, G. Grossmann and W. B. Frommer (2014). "Abscisic acid dynamics in roots detected with genetically encoded FRET sensors." Elife **3**: e01741.

Jorgensen, M. E., H. H. Nour-Eldin and B. A. Halkier (2015). "Transport of defense compounds from source to sink: lessons learned from glucosinolates." Trends Plant Sci **20**(8): 508-514.

Kai, K., J. Horita, K. Wakasa and H. Miyagawa (2007). "Three oxidative metabolites of indole-3-acetic acid from Arabidopsis thaliana." Phytochemistry **68**(12): 1651-1663.

Kaper, T., L. L. Looger, H. Takanaga, M. Platten, L. Steinman and W. B. Frommer (2007). "Nanosensor detection of an immunoregulatory tryptophan influx/kynurenine efflux cycle." PLoS Biol **5**(10): e257.

Keefe, A. D. and J. W. Szostak (2001). "Functional proteins from a random-sequence library." Nature **410**(6829): 715-718.

Kim, S. H. and S. J. Roux (2003). "An Arabidopsis Ran-binding protein, AtRanBP1c, is a co-activator of Ran GTPase-activating protein and requires the C-terminus for its cytoplasmic localization." Planta **216**(6): 1047-1052.

Kimelman, D. and B. L. Martin (2012). "Anterior-posterior patterning in early development: three strategies." Wiley Interdiscip Rev Dev Biol **1**(2): 253-266.

Korasick, D. A., C. S. Westfall, S. G. Lee, M. H. Nanao, R. Dumas, G. Hagen, T. J. Guilfoyle, J. M. Jez and L. C. Strader (2014). "Molecular basis for AUXIN RESPONSE FACTOR protein interaction and the control of auxin response repression." Proc Natl Acad Sci U S A **111**(14): 5427-5432.

Kowalczyk, M. and G. Sandberg (2001). "Quantitative Analysis of Indole-3-Acetic Acid Metabolites in Arabidopsis." Plant Physiology **127**(4): 1845-1853.

Kraft, E., S. L. Stone, L. Ma, N. Su, Y. Gao, O. S. Lau, X. W. Deng and J. Callis (2005). "Genome analysis and functional characterization of the E2 and RING-type E3 ligase ubiquitination enzymes of Arabidopsis." Plant Physiol **139**(4): 1597-1611.

Kramer, E. M. and E. M. Ackelsberg (2015). "Auxin metabolism rates and implications for plant development." Front Plant Sci **6**: 150.

Krebs, M., K. Held, A. Binder, K. Hashimoto, G. Den Herder, M. Parniske, J. Kudla and K. Schumacher (2012). "FRET-based genetically encoded sensors allow high-resolution live cell imaging of Ca(2)(+) dynamics." Plant J **69**(1): 181-192.

Lakowicz, J. R. (2006). Energy Transfer. Principles of Fluorescence Spectroscopy. J. R. Lakowicz, Springer US**:** 443-475.

Lam, A. J., F. St-Pierre, Y. Gong, J. D. Marshall, P. J. Cranfill, M. A. Baird, M. R. McKeown, J. Wiedenmann, M. W. Davidson, M. J. Schnitzer, R. Y. Tsien and M. Z. Lin (2012). "Improving FRET dynamic range with bright green and red fluorescent proteins." Nat Methods **9**(10): 1005-1012.

Lane, M. C. and M. D. Sheets (2002). "Rethinking axial patterning in amphibians." Developmental Dynamics **225**(4): 434-447.

Lange, A., R. E. Mills, C. J. Lange, M. Stewart, S. E. Devine and A. H. Corbett (2007). "Classical nuclear localization signals: definition, function, and interaction with importin alpha." J Biol Chem **282**(8): 5101-5105.

Lau, S., I. De Smet, M. Kolb, H. Meinhardt and G. Jürgens (2011). "Auxin triggers a genetic switch." Nat Cell Biol **13**(5): 611-615.

Lau, S., D. Slane, O. Herud, J. Kong and G. Jürgens (2012). "Early embryogenesis in flowering plants: setting up the basic body pattern." Annu Rev Plant Biol **63**: 483-506.

Liang, G., Q. Ai and D. Yu (2015). "Uncovering miRNAs involved in crosstalk between nutrient deficiencies in Arabidopsis." Sci Rep **5**: 11813.

Liao, C. Y., W. Smet, G. Brunoud, S. Yoshida, T. Vernoux and D. Weijers (2015). "Reporters for sensitive and quantitative measurement of auxin response." Nat Methods **12**(3): 207-210, 202 p following 210.

Lituiev, D. S., N. G. Krohn, B. Müller, D. Jackson, B. Hellriegel, T. Dresselhaus and U. Grossniklaus (2013). "Theoretical and experimental evidence indicates that there is no detectable auxin gradient in the angiosperm female gametophyte." Development **140**(22): 4544-4553.

Ljung, K. (2013). "Auxin metabolism and homeostasis during plant development." Development **140**(5): 943-950.

Ljung, K., A. Ostin, L. Lioussanne and G. Sandberg (2001). "Developmental regulation of indole-3-acetic acid turnover in Scots pine seedlings." Plant Physiol **125**(1): 464-475.

Ljung, K., G. Sandberg and T. Moritz (2010). Methods of Plant Hormone Analysis. Plant Hormones, Springer Science + Business Media**:** 717-740.

Llic, N., J. Normanly and J. D. Cohen (1996). "Quantification of free plus conjugated indoleacetic acid in arabidopsis requires correction for the nonenzymatic conversion of indolic nitriles." Plant Physiol **111**(3): 781-788.

Looger, L. L., M. A. Dwyer, J. J. Smith and H. W. Hellinga (2003). "Computational design of receptor and sensor proteins with novel functions." Nature **423**(6936): 185-190.

Lu, P., C. Vogel, R. Wang, X. Yao and E. M. Marcotte (2007). "Absolute protein expression profiling estimates the relative contributions of transcriptional and translational regulation." Nat Biotechnol **25**(1): 117-124.

Ludwig-Müller, J. (2007). "Indole-3-butyric acid synthesis in ecotypes and mutants of Arabidopsis thaliana under different growth conditions." J Plant Physiol **164**(1): 47-59.

Ludwig-Müller, J. (2011). "Auxin conjugates: their role for plant development and in the evolution of land plants." J Exp Bot **62**(6): 1757-1773.

Luo, Y. and H. U. Koop (1997). "Somatic embryogenesis in cultured immature zygotic embryos and leaf protoplasts of Arabidopsis thaliana ecotypes." Planta **202**(3): 387-396.

Lynd, A. and G. J. Lycett (2011). "Optimization of the Gal4-UAS system in an Anopheles gambiae cell line." Insect Molecular Biology **20**(5): 599-608.

Maeda, H. and N. Dudareva (2012). "The shikimate pathway and aromatic amino Acid biosynthesis in plants." Annu Rev Plant Biol **63**: 73-105.

Mallory, A. C., D. P. Bartel and B. Bartel (2005). "MicroRNA-directed regulation of Arabidopsis AUXIN RESPONSE FACTOR17 is essential for proper development and modulates expression of early auxin response genes." Plant Cell **17**(5): 1360-1375.

Marmorstein, R. Q., A. Joachimiak, M. Sprinzl and P. B. Sigler (1987). "The structural basis for the interaction between L-tryptophan and the Escherichia coli trp aporepressor." J Biol Chem **262**(10): 4922-4927.

Marvin, J. S. and H. W. Hellinga (2001). "Conversion of a maltose receptor into a zinc biosensor by computational design." Proceedings of the National Academy of Sciences **98**(9): 4955-4960.

Meinhardt, H. (2015). "Models for patterning primary embryonic body axes: The role of space and time." Semin Cell Dev Biol **42**: 103-117.

Merkle, T. (2011). "Nucleo-cytoplasmic transport of proteins and RNA in plants." Plant Cell Rep **30**(2): 153-176.

Merola, F., A. Fredj, D. B. Betolngar, C. Ziegler, M. Erard and H. Pasquier (2014). "Newly engineered cyan fluorescent proteins with enhanced performances for live cell FRET imaging." Biotechnol J **9**(2): 180-191.

Miyawaki, A., J. Llopis, R. Heim, J. M. McCaffery, J. A. Adams, M. Ikura and R. Y. Tsien (1997). "Fluorescent indicators for Ca2+ based on green fluorescent proteins and calmodulin." Nature **388**(6645): 882-887.

Nakajima, K., T. Uchiumi and T. Okamoto (2010). "Positional relationship between the gamete fusion site and the first division plane in the rice zygote." J Exp Bot **61**(11): 3101-3105.

Navarro, L., P. Dunoyer, F. Jay, B. Arnold, N. Dharmasiri, M. Estelle, O. Voinnet and J. D. Jones (2006). "A plant miRNA contributes to antibacterial resistance by repressing auxin signaling." Science **312**(5772): 436-439.

Normanly, J. (2010). "Approaching cellular and molecular resolution of auxin biosynthesis and metabolism." Cold Spring Harb Perspect Biol **2**(1): a001594.

Novak, O., E. Henykova, I. Sairanen, M. Kowalczyk, T. Pospisil and K. Ljung (2012). "Tissue-specific profiling of the Arabidopsis thaliana auxin metabolome." Plant J **72**(3): 523-536.

Okada, K., J. Ueda, M. K. Komaki, C. J. Bell and Y. Shimura (1991). "Requirement of the Auxin Polar Transport System in Early Stages of Arabidopsis Floral Bud Formation." Plant Cell **3**(7): 677-684.

Okumoto, S., A. Jones and W. B. Frommer (2012). "Quantitative imaging with fluorescent biosensors." Annu Rev Plant Biol **63**: 663-706.

Ostin, A., M. Kowalyczk, R. P. Bhalerao and G. Sandberg (1998). "Metabolism of indole-3-acetic acid in Arabidopsis." Plant Physiol **118**(1): 285-296.

Pagnussat, G. C., M. Alandete-Saez, J. L. Bowman and V. Sundaresan (2009). "Auxin-dependent patterning and gamete specification in the Arabidopsis female gametophyte." Science **324**(5935): 1684-1689.

Park, M., K. Song, I. Reichardt, H. Kim, U. Mayer, Y. D. Stierhof, I. Hwang and G. Jürgens (2013). "Arabidopsis mu-adaptin subunit AP1M of adaptor protein complex 1 mediates late secretory and vacuolar traffic and is required for growth." Proc Natl Acad Sci U S A **110**(25): 10318-10323.

Parry, G., L. I. Calderon-Villalobos, M. Prigge, B. Peret, S. Dharmasiri, H. Itoh, E. Lechner, W. M. Gray, M. Bennett and M. Estelle (2009). "Complex regulation of the TIR1/AFB family of auxin receptors." Proc Natl Acad Sci U S A **106**(52): 22540-22545.

Parry, G., S. Ward, A. Cernac, S. Dharmasiri and M. Estelle (2006). "The Arabidopsis SUPPRESSOR OF AUXIN RESISTANCE proteins are nucleoporins with an important role in hormone signaling and development." Plant Cell **18**(7): 1590-1603.

Peer, W. A., Y. Cheng and A. S. Murphy (2013). "Evidence of oxidative attenuation of auxin signalling." J Exp Bot **64**(9): 2629-2639.

Pekker, I., J. P. Alvarez and Y. Eshed (2005). "Auxin response factors mediate Arabidopsis organ asymmetry via modulation of KANADI activity." Plant Cell **17**(11): 2899-2910.

Petersson, S. V., A. I. Johansson, M. Kowalczyk, A. Makoveychuk, J. Y. Wang, T. Moritz, M. Grebe, P. N. Benfey, G. Sandberg and K. Ljung (2009). "An auxin gradient and maximum in the Arabidopsis root apex shown by high-resolution cell-specific analysis of IAA distribution and synthesis." Plant Cell **21**(6): 1659-1668.

Petrasek, J. and J. Friml (2009). "Auxin transport routes in plant development." Development **136**(16): 2675-2688.

Pierre-Jerome, E., B. L. Moss and J. L. Nemhauser (2013). "Tuning the auxin transcriptional response." J Exp Bot **64**(9): 2557-2563.

Piya, S., S. K. Shrestha, B. Binder, C. N. Stewart Jr and T. Hewezi (2014). "Protein-protein interaction and gene co-expression maps of ARFs and Aux/IAAs in Arabidopsis." Frontiers in Plant Science **5**.

Rademacher, E. H., A. S. Lokerse, A. Schlereth, C. I. Llavata-Peris, M. Bayer, M. Kientz, A. Freire Rios, J. W. Borst, W. Lukowitz, G. Jürgens and D. Weijers (2012). "Different auxin response machineries control distinct cell fates in the early plant embryo." Dev Cell **22**(1): 211-222.

Rademacher, E. H., B. Moller, A. S. Lokerse, C. I. Llavata-Peris, W. van den Berg and D. Weijers (2011). "A cellular expression map of the Arabidopsis AUXIN RESPONSE FACTOR gene family." Plant J **68**(4): 597-606.

Rampey, R. A., S. LeClere, M. Kowalczyk, K. Ljung, G. Sandberg and B. Bartel (2004). "A family of auxin-conjugate hydrolases that contributes to free indole-3-acetic acid levels during Arabidopsis germination." Plant Physiol **135**(2): 978-988.

Ranocha, P., O. Dima, R. Nagy, J. Felten, C. Corratge-Faillie, O. Novak, K. Morreel, B. Lacombe, Y. Martinez, S. Pfrunder, X. Jin, J. P. Renou, J. B. Thibaud, K. Ljung, U. Fischer, E. Martinoia, W. Boerjan and D. Goffner (2013). "Arabidopsis WAT1 is a vacuolar auxin transport facilitator required for auxin homoeostasis." Nat Commun **4**: 2625.

Reeves, G. T. and A. Stathopoulos (2009). "Graded dorsal and differential gene regulation in the Drosophila embryo." Cold Spring Harb Perspect Biol **1**(4): a000836.

Sabatini, S., D. Beis, H. Wolkenfelt, J. Murfett, T. Guilfoyle, J. Malamy, P. Benfey, O. Leyser, N. Bechtold, P. Weisbeek and B. Scheres (1999). "An Auxin-Dependent Distal Organizer of Pattern and Polarity in the Arabidopsis Root." Cell **99**(5): 463-472.

Shimizu-Mitao, Y. and T. Kakimoto (2014). "Auxin sensitivities of all Arabidopsis Aux/IAAs for degradation in the presence of every TIR1/AFB." Plant Cell Physiol **55**(8): 1450-1459.

Shimozono, S., T. Iimura, T. Kitaguchi, S. Higashijima and A. Miyawaki (2013). "Visualization of an endogenous retinoic acid gradient across embryonic development." Nature **496**(7445): 363-366.

Siegel, J. B., A. Zanghellini, H. M. Lovick, G. Kiss, A. R. Lambert, J. L. St Clair, J. L. Gallaher, D. Hilvert, M. H. Gelb, B. L. Stoddard, K. N. Houk, F. E. Michael and D. Baker (2010). "Computational design of an enzyme catalyst for a stereoselective bimolecular Diels-Alder reaction." Science **329**(5989): 309-313.

Somerville, R. (1992). "The Trp repressor, a ligand-activated regulatory protein." Prog Nucleic Acid Res Mol Biol **42**: 1-38.

Spiess, G. M. and B. K. Zolman (2013). "Peroxisomes as a source of auxin signaling molecules." Subcell Biochem **69**: 257-281.

Stepanova, A. N., J. Robertson-Hoyt, J. Yun, L. M. Benavente, D. Y. Xie, K. Dolezal, A. Schlereth, G. Jürgens and J. M. Alonso (2008). "TAA1-mediated auxin biosynthesis is essential for hormone crosstalk and plant development." Cell **133**(1): 177-191.

Sugawara, S., S. Hishiyama, Y. Jikumaru, A. Hanada, T. Nishimura, T. Koshiba, Y. Zhao, Y. Kamiya and H. Kasahara (2009). "Biochemical analyses of indole-3-acetaldoxime-dependent auxin biosynthesis in Arabidopsis." Proc Natl Acad Sci U S A **106**(13): 5430-5435.

Sun, Y., Y. Yang, Z. Yuan, J. L. Muller, C. Yu, Y. Xu, X. Shao, X. Li, E. L. Decker, R. Reski and H. Huang (2010). "Overexpression of the Arabidopsis gene UPRIGHT ROSETTE reveals a homeostatic control for indole-3-acetic acid." Plant Physiol **153**(3): 1311-1320.

Szemenyei, H., M. Hannon and J. A. Long (2008). "TOPLESS mediates auxin-dependent transcriptional repression during Arabidopsis embryogenesis." Science **319**(5868): 1384-1386.

Tan, X., L. I. Calderon-Villalobos, M. Sharon, C. Zheng, C. V. Robinson, M. Estelle and N. Zheng (2007). "Mechanism of auxin perception by the TIR1 ubiquitin ligase." Nature **446**(7136): 640-645.

Tang, X., Y. Liu, Y. He, L. Ma and M. X. Sun (2013). "Exine dehiscing induces rape microspore polarity, which results in different daughter cell fate and fixes the apical-basal axis of the embryo." J Exp Bot **64**(1): 215-228.

Terrile, M. C., R. Paris, L. I. Calderon-Villalobos, M. J. Iglesias, L. Lamattina, M. Estelle and C. A. Casalongue (2012). "Nitric oxide influences auxin signaling through S-nitrosylation of the Arabidopsis TRANSPORT INHIBITOR RESPONSE 1 auxin receptor." Plant J **70**(3): 492-500.

Tyson, C. B., P. G. Lord and A. E. Wheals (1979). "Dependency of size of Saccharomyces cerevisiae cells on growth rate." J Bacteriol **138**(1): 92-98.

Ueda, M. and T. Laux (2012). "The origin of the plant body axis." Curr Opin Plant Biol **15**(6): 578-584.

Ulmasov, T., J. Murfett, G. Hagen and T. J. Guilfoyle (1997). "Aux/IAA proteins repress expression of reporter genes containing natural and highly active synthetic auxin response elements." Plant Cell **9**(11): 1963-1971.

Vandenbrink, J. P., J. Z. Kiss, R. Herranz and F. J. Medina (2014). "Light and gravity signals synergize in modulating plant development." Frontiers in Plant Science **5**.

Vert, G., C. L. Walcher, J. Chory and J. L. Nemhauser (2008). "Integration of auxin and brassinosteroid pathways by Auxin Response Factor 2." Proc Natl Acad Sci U S A **105**(28): 9829-9834.

Vinkenborg, J. L., T. H. Evers, S. W. Reulen, E. W. Meijer and M. Merkx (2007). "Enhanced sensitivity of FRET-based protease sensors by redesign of the GFP dimerization interface." Chembiochem **8**(10): 1119-1121.

Waadt, R., K. Hitomi, N. Nishimura, C. Hitomi, S. R. Adams, E. D. Getzoff and J. I. Schroeder (2014). "FRET-based reporters for the direct visualization of abscisic acid concentration changes and distribution in Arabidopsis." Elife **3**: e01739.

Wang, B., J. Chu, T. Yu, Q. Xu, X. Sun, J. Yuan, G. Xiong, G. Wang, Y. Wang and J. Li (2015). "Tryptophan-independent auxin biosynthesis contributes to early embryogenesis in Arabidopsis." Proc Natl Acad Sci U S A **112**(15): 4821-4826.

Wang, H., J. Wang, J. Jiang, S. Chen, Z. Guan, Y. Liao and F. Chen (2014). "Reference genes for normalizing transcription in diploid and tetraploid Arabidopsis." Sci Rep **4**: 6781.

Wang, J. W., L. J. Wang, Y. B. Mao, W. J. Cai, H. W. Xue and X. Y. Chen (2005). "Control of root cap formation by MicroRNA-targeted auxin response factors in Arabidopsis." Plant Cell **17**(8): 2204-2216.

Weijers, D., E. Benkova, K. E. Jäger, A. Schlereth, T. Hamann, M. Kientz, J. C. Wilmoth, J. W. Reed and G. Jürgens (2005). "Developmental specificity of auxin response by pairs of ARF and Aux/IAA transcriptional regulators." The EMBO Journal **24**(10): 1874-1885.

Weijers, D., M. Franke-van Dijk, R. J. Vencken, A. Quint, P. Hooykaas and R. Offringa (2001). "An Arabidopsis Minute-like phenotype caused by a semi-dominant mutation in a RIBOSOMAL PROTEIN S5 gene." Development **128**(21): 4289-4299.

Weijers, D., A. Schlereth, J. S. Ehrismann, G. Schwank, M. Kientz and G. Jürgens (2006). "Auxin triggers transient local signaling for cell specification in Arabidopsis embryogenesis." Dev Cell **10**(2): 265-270.

Wolpert, L. (1969). "Positional information and the spatial pattern of cellular differentiation." J Theor Biol **25**(1): 1-47.

Xuan, W., D. Audenaert, B. Parizot, B. K. Moller, M. F. Njo, B. De Rybel, G. De Rop, G. Van Isterdael, A. P. Mähönen, S. Vanneste and T. Beeckman (2015). "Root Cap-Derived Auxin Pre-patterns the Longitudinal Axis of the Arabidopsis Root." Curr Biol **25**(10): 1381-1388.

Yamaguchi, N., M. F. Wu, C. M. Winter, M. C. Berns, S. Nole-Wilson, A. Yamaguchi, G. Coupland, B. A. Krizek and D. Wagner (2013). "A molecular framework for auxin-mediated initiation of flower primordia." Dev Cell **24**(3): 271-282.

Yang, W., J. Gelles and S. M. Musser (2004). "Imaging of single-molecule translocation through nuclear pore complexes." Proc Natl Acad Sci U S A **101**(35): 12887-12892.

Yoshida, S., M. Ito, I. Nishida and A. Watanabe (2001). "Isolation and RNA gel blot analysis of genes that could serve as potential molecular markers for leaf senescence in Arabidopsis thaliana." Plant Cell Physiol **42**(2): 170-178.

Yu, P., P. Lor, J. Ludwig-Müller, A. D. Hegeman and J. D. Cohen (2015). "Quantitative evaluation of IAA conjugate pools in Arabidopsis thaliana." Planta **241**(2): 539-548.

Zadnikova, P., D. Smet, Q. Zhu, D. Van Der Straeten and E. Benkova (2015). "Strategies of seedlings to overcome their sessile nature: auxin in mobility control." Front Plant Sci **6**: 218.

Zandalinas, S. I., V. Vives-Peris, A. Gomez-Cadenas and V. Arbona (2012). "A fast and precise method to identify indolic glucosinolates and camalexin in plants by combining mass spectrometric and biological information." J Agric Food Chem **60**(35): 8648-8658.

Zhao, Y., S. Araki, J. Wu, T. Teramoto, Y. F. Chang, M. Nakano, A. S. Abdelfattah, M. Fujiwara, T. Ishihara, T. Nagai and R. E. Campbell (2011). "An expanded palette of genetically encoded Ca(2)(+) indicators." Science **333**(6051): 1888-1891.

Zhao, Y., S. K. Christensen, C. Fankhauser, J. R. Cashman, J. D. Cohen, D. Weigel and J. Chory (2001). "A role for flavin monooxygenase-like enzymes in auxin biosynthesis." Science **291**(5502): 306-309.

Zhao, Y., A. K. Hull, N. R. Gupta, K. A. Goss, J. Alonso, J. R. Ecker, J. Normanly, J. Chory and J. L. Celenza (2002). "Trp-dependent auxin biosynthesis in Arabidopsis: involvement of cytochrome P450s CYP79B2 and CYP79B3." Genes Dev **16**(23): 3100-3112.

Accepted Publications

Lau, S., D. Slane, O. Herud, J. Kong and G. Jürgens (2012). "Early embryogenesis in flowering plants: setting up the basic body pattern." Annu Rev Plant Biol **63**: 483-506.

Early Embryogenesis in Flowering Plants: Setting Up the Basic Body Pattern

Steffen Lau,[1] Daniel Slane,[1] Ole Herud,[1] Jixiang Kong,[1,2] and Gerd Jürgens[1,2]

[1]Department of Cell Biology, Max Planck Institute for Developmental Biology, D-72076 Tübingen, Germany

[2]Center for Plant Molecular Biology, University of Tübingen, D-72076 Tübingen, Germany; email: gerd.juergens@zmbp.uni-tuebingen.de

Annu. Rev. Plant Biol. 2012. 63:483–506

First published online as a Review in Advance on January 3, 2012

The *Annual Review of Plant Biology* is online at plant.annualreviews.org

This article's doi: 10.1146/annurev-arplant-042811-105507

1543-5008/12/0602-0483$20.00

Keywords

zygote, apical-basal axis, root pole initiation, radial pattern, shoot meristem initiation, cotyledon initiation

Abstract

Early embryogenesis is the critical developmental phase during which the basic features of the plant body are established: the apical-basal axis of polarity, different tissue layers, and both the root pole and the shoot pole. Polarization of the zygote correlates with the generation of apical and basal (embryonic and extraembryonic) cell fates. Whereas mechanisms of zygote polarization are still largely unknown, distinct expression domains of WOX family transcription factors as well as directional auxin transport and local auxin response are known to be involved in early apical-basal patterning. Radial patterning of tissue layers appears to be mediated by cell-cell communication involving both peptide signaling and transcription factor movement. Although the initiation of the shoot pole is still unclear, the apical organization of the embryo depends on both the proper establishment of transcription factor expression domains and, for cotyledon initiation, upward auxin flow in the protoderm. Here we focus on the essential patterning processes, drawing mainly on data from *Arabidopsis thaliana* and also including relevant data from other species if available.

Contents

INTRODUCTION 484
ZYGOTE POLARITY AND ELONGATION 485
Zygote Polarity 485
Zygote Elongation 485
ZYGOTIC GENOME ACTIVATION 487
ZYGOTE DIVISION AND SEPARATION OF APICAL AND BASAL CELL FATE 488
HYPOPHYSIS SPECIFICATION AND ROOT POLE FORMATION 490
Importance of Auxin in Hypophysis Specification and Root Pole Formation 490
Additional Factors Involved in Hypophysis Specification and Root Pole Formation 491
Positional Information During Root Initiation 491
RADIAL PATTERNING AND PROTODERM SPECIFICATION 492
Separation of Inner and Outer Fate in the Early Proembryo 492
Maintenance of Radial Patterning ... 494
SHOOT MERISTEM SPECIFICATION AND COTYLEDON INITIATION 495
The Organizing Center 495
Shoot Meristem Indeterminacy and the Shoot Meristem–Cotyledon Boundary Region 496
Meristem Establishment 496
Initiation of Cotyledon Primordia .. 497
PERSPECTIVES 498

INTRODUCTION

Zygote: fertilization product of egg and sperm cell

The basic body pattern of a multicellular organism is established from the zygote—the fertilized egg cell—during embryogenesis. In flowering plants, embryogenesis lays down the basis for a stereotyped seedling displaying a simple body organization of two superimposed patterns. Along the main apical-basal axis of polarity, the apically located shoot meristem, which is usually flanked by one or two cotyledons, is linked with the basally located root meristem via the hypocotyl and seedling root. The perpendicular radial pattern comprises a series of concentrically arranged tissue layers, from the outermost epidermal tissue via the ground tissue to the centrally located vascular tissue. Although the body organization of the seedling looks similar in different flowering plant species, its developmental origin can vary between species. For example, members of the Brassicaceae family (such as *Arabidopsis thaliana*) display distinct, nearly stereotypic cell-division patterns in early embryogenesis, whereas embryos of other flowering plant species grow by seemingly random cell divisions (62, 63, 66, 94). In the former group of species, the origin of seedling tissues and organs can thus be easily traced back to specific cells or groups of cells in the early embryo (**Figure 1**). Although this correlation might suggest a causal link between the spatial regulation of cell divisions and pattern formation in the early embryo, *A. thaliana* mutants such as *fass* (*fs*) displaying altered cell-division planes nonetheless generate a normal body organization, whereas morphogenesis is compromised (147). Thus, the stereotypic cell-division pattern seen in *A. thaliana* embryos expresses, but is not instrumental to, developmental decisions and might facilitate such decisions in the early embryo comprising very few cells.

This review covers recent studies that address molecular mechanisms underlying the origin of the apical-basal axis of polarity, the initiation of both the root meristem and the shoot meristem as well as the cotyledons, and radial patterning. It also discusses the parental contributions to gene activity in early embryogenesis in regard to their potential role in early patterning events. For ease of reference, **Table 1** lists the gene abbreviations and full names referred to in this review.

ZYGOTE POLARITY AND ELONGATION

Zygote Polarity

In flowering plants, the zygote is formed by the fusion of the egg cell with one of the two sperm cells delivered by the pollen tube (reviewed in 25). Like the egg cell, the zygote is usually polarized with respect to the relative position of nucleus and vacuole. However, egg cell polarity and zygote polarity are different in some species, suggesting that the latter might be established independently of the former.

In many species, the egg cell has its nucleus located toward the chalazal end of the ovule (i.e., apically) and usually has a large vacuole located toward the micropylar end (i.e., basally). This is, for example, the case in *A. thaliana*, *Capsella bursa-pastoris*, and *Nicotiana tabacum* (tobacco), in all of which zygote organization resembles egg cell organization (94, 95, 103, 131, 170); polarity—as inferred from nucleus and vacuole position—appears thus to be maintained after fertilization. However, this was shown not to be the case in *A. thaliana* and probably *N. tabacum*. A transient symmetric stage, in which the nucleus is located centrally and smaller vacuoles are distributed rather evenly within the cell, developmentally separates the polarized egg cell from the similarly polarized zygote (29, 103, 151, 170). In *A. thaliana*, the transcription factor WRKY DNA-BINDING PROTEIN 2 (WRKY2) is involved in the polarization of the zygote by transcriptionally activating *WUSCHEL RELATED HOMEOBOX 8* (*WOX8*) and possibly *WOX9* (151). *WRKY2* is dispensable for the establishment or maintenance of egg cell polarity, which corroborates the notion that egg cell and zygote polarity are not intimately linked (151). Even stronger effects of fertilization on zygote polarity are, for example, observed in *Oryza sativa* (rice), *Zea mays* (maize), and *Papaver nudicaule*, in all of which egg cell polarity is reversed after fertilization. Whereas the nucleus localizes to the micropylar/basal end of the egg cell and the large vacuole to the chalazal/apical end, the opposite is the case in the zygote (25, 114, 123).

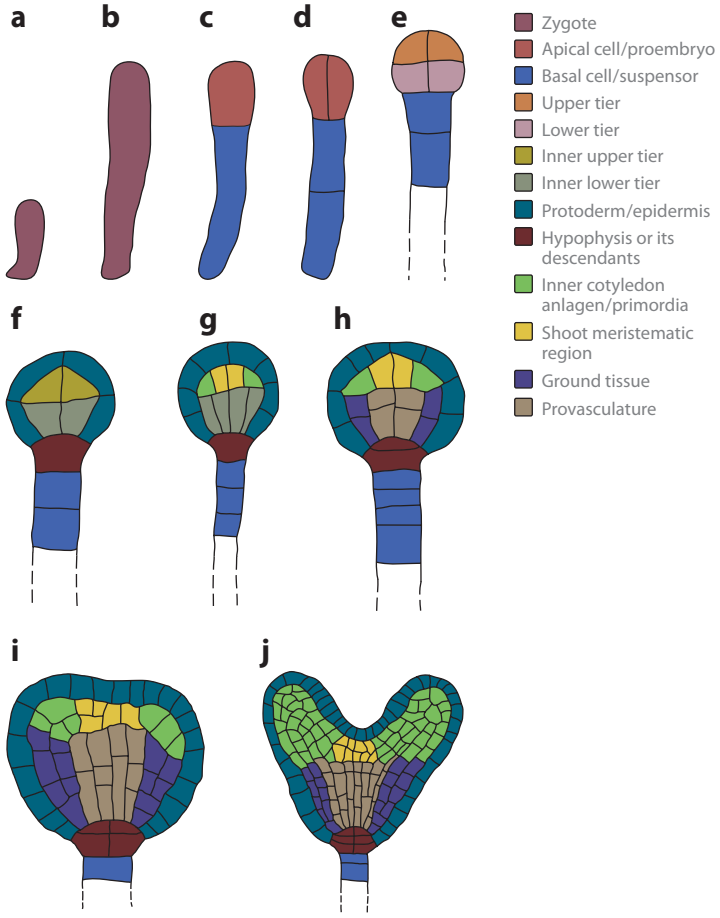

Figure 1

Early embryogenesis in *Arabidopsis thaliana*. Panels show longitudinal sections of embryos during consecutive developmental stages: (*a*) zygote, (*b*) elongated zygote, (*c*) one-cell stage, (*d*) two- or four-cell stage, (*e*) octant stage, (*f*) dermatogen stage, (*g*) early-globular stage, (*h*) mid-globular stage, (*i*) transition stage, and (*j*) heart stage. Groups of developmentally related cells are color-coded. Embryos not drawn to scale.

Zygote Elongation

The *A. thaliana* zygote not only becomes polarized but also elongates approximately threefold along its apical-basal axis before it divides. This elongation depends on the GDP/GTP exchange factor for small G proteins of the ARF class (ARF-GEF) GNOM (GN). If *GN* is knocked out, elongation and asymmetric division are compromised, but GN targets in the zygote are not known (98, 132). Zygote elongation or its asymmetric division also depends

Shoot meristem: group of self-replenishing cells at the shoot apex that sustain shoot growth and the formation of lateral organs such as leaves and flowers

Table 1 Gene abbreviations and full names used in this review

Abbreviation	Full name
ACR4	*ARABIDOPSIS CRINKLY 4*
AGO1	*ARGONAUTE 1*
ALE1/2	*ABNORMAL LEAF-SHAPE 1/2*
ARR7/15	*ARABIDOPSIS RESPONSE REGULATOR 7/15*
AS1/2	*ASYMMETRIC LEAVES 1/2*
ATDEK1	*ARABIDOPSIS THALIANA DEFECTIVE KERNEL 1*
ATH1	*ARABIDOPSIS THALIANA HOMEOBOX 1*
ATHB8/15	*ARABIDOPSIS THALIANA HOMEOBOX 8/15*
ATML1	*ARABIDOPSIS THALIANA MERISTEM LAYER 1*
BBM/PLT4	*BABY BOOM/PLETHORA 4*
BDL/IAA12	*BODENLOS/INDOLE-3-ACETIC-ACID 12*
BIM1	*BES INTERACTING MYC-LIKE PROTEIN 1*
BOP1/2	*BLADE-ON-PETIOLE 1/2*
CLE40	*CLV3/ESR-RELATED 40*
CLV3	*CLAVATA 3*
CUC1/2/3	*CUP-SHAPED COTYLEDON 1/2/3*
CUP	*CUPULIFORMIS*
DCL1	*DICER-LIKE 1*
DRN	*DORNRÖSCHEN*
DRNL	*DORNRÖSCHEN-LIKE*
ENP/MAB4	*ENHANCER OF PINOID/MACCHI-BOU 4*
FDH	*FIDDLEHEAD*
FS	*FASS*
GN	*GNOM*
GRN/RKD4	*GROUNDED/RWP-RK DOMAIN 4*
HAN	*HANABA TARANU*
KAN1	*KANADI 1*
KN1	*KNOTTED 1*
KNAT1/BP	*KNOTTED-LIKE FROM ARABIDOPSIS THALIANA 1/BREVIPEDICELLUS*
LOG	*LONELY GUY*
LTP1	*LIPID TRANSFER PROTEIN 1*
MKK4/5	*MITOGEN-ACTIVATED PROTEIN KINASE KINASE 4/5*
MP/ARF5	*MONOPTEROS/AUXIN RESPONSE FACTOR 5*
MPK3/6	*MITOGEN-ACTIVATED PROTEIN KINASE 3/6*
NAM	*NO APICAL MERISTEM*
NPH4/ARF7	*NONPHOTOTROPIC HYPOCOTYL 4/AUXIN RESPONSE FACTOR 7*
OSH1	*Oryza sativa homeobox 1*
OSTF1	*Oryza sativa transcription factor 1*
PDF1/2	*PROTODERMAL FACTOR 1/2*
PHB	*PHABULOSA*
PHV	*PHAVOLUTA*

(*Continued*)

Table 1 (*Continued*)

Abbreviation	Full name
PID	*PINOID*
PID2	*PINOID 2*
PIN1/3/4/7	*PIN-FORMED 1/3/4/7*
PLT1/2/3	*PLETHORA 1/2/3*
PNF	*POUND-FOOLISH*
PNY	*PENNYWISE*
QHB	*quiescent-center-specific homeobox*
REV	*REVOLUTA*
RPK1	*RECEPTOR-LIKE PROTEIN KINASE 1*
SCR	*SCARECROW*
SHR	*SHORT-ROOT*
SSP	*SHORT SUSPENSOR*
STM	*SHOOT MERISTEMLESS*
TAA1	*TRYPTOPHAN AMINOTRANSFERASE OF ARABIDOPSIS 1*
TAR1/2	*TRYPTOPHAN AMINOTRANSFERASE RELATED 1/2*
TMO7	*TARGET OF MONOPTEROS 7*
TOAD2	*TOADSTOOL 2*
TPL	*TOPLESS*
WAG1/2	*WAG 1/2*
WOX1/2/3/5/8/9	*WUSCHEL RELATED HOMEOBOX 1/2/3/5/8/9*
WRKY2/33	*WRKY DNA-BINDING PROTEIN 2/33*
WUS	*WUSCHEL*
YDA	*YODA*
YUC1/4/10/11	*YUCCA 1/4/10/11*
ZLL/AGO10	*ZWILLE/ARGONAUTE 10*
ZMCUC3	*Zea mays CUP-SHAPED COTYLEDON 3*
ZMNAM1/2	*Zea mays NO APICAL MERISTEM 1/2*

on the interleukin-1 receptor-associated kinase (IRAK)/Pelle-like kinase SHORT SUSPENSOR (SSP), the MAPKK kinase YODA (YDA), MITOGEN-ACTIVATED PROTEIN KINASE 3 (MPK3), MPK6, and the RWP-RK family protein GROUNDED (GRN)/RWP-RK domain 4 (RKD4), which functions as a transcriptional regulator (7, 58, 89, 154, 155). There is evidence that *SSP*, *YDA*, *MPK3*, and *MPK6* as well as MITOGEN-ACTIVATED PROTEIN KINASE KINASE 4 (MKK4) and MKK5 act in the same pathway (7, 155), but the direct targets of this hypothetical kinase pathway in the zygote remain unknown. However, it might be meaningful that a close homolog of WRKY2, WRKY33, is phosphorylated by MPK3 and MPK6 (96, 162).

ZYGOTIC GENOME ACTIVATION

Zygotic genome activation already occurs in the zygote in flowering plants. For *N. tabacum*, evidence has been presented that deposited maternal transcripts are not sufficient for zygote elongation and division, but that this process requires zygotic de novo transcription (170). In *Z. mays* and *N. tabacum*, transcripts not present in egg and sperm cells accumulate in the zygote, which indicates that these transcripts

Cotyledon: leaf formed in the developing embryo

Root meristem: group of self-replenishing cells at the root tip that sustain root growth

Ground tissue: primordium that will give rise to two tissue layers, endodermis and cortex

are made de novo in the zygote (110, 125, 170). Comparable experiments have not been done in *A. thaliana*. However, in both *A. thaliana* and *Z. mays*, genes whose expression has not been detected in pollen are expressed in the zygote from the paternal allele (130, 151), implying zygotic genome activation at the zygote stage in these species.

This de novo expression of paternal genes in the zygote also indicates that the paternal genome is not generally silenced in the zygote or early embryo. This idea has received support from other studies (120, 156, 165), although in these cases it cannot be clearly distinguished between transcripts delivered by the pollen and de novo transcription from the paternal alleles in the zygote. However, whereas *Z. mays* displays an equivalent parental contribution in the zygote and during early embryo development (101), in *A. thaliana* maternal transcripts appear to predominate during early embryogenesis (5). This maternal predominance is thought to result from the downregulation of the paternal alleles by the maternal chromatin small interfering RNA (siRNA) pathway, whereas the activation of the paternal alleles during the course of embryogenesis is thought to be mediated by maternal histone chaperone complex CAF1 (5). However, it cannot be excluded that the maternal predominance during early *A. thaliana* embryogenesis is mainly or also due to transcript carryover from the egg cell rather than specific downregulation of the paternal alleles. Hence, the two aforementioned mechanisms (the chromatin siRNA pathway and activity of the CAF1 complex) could generally be involved in zygotic genome activation. In conjunction with a supposed stronger transcript contribution of the egg cell as compared with the sperm cell, mechanisms delaying the zygotic genome activation would prolong the predominance of transcripts derived from the maternal alleles.

Some observations argue against general differences between paternal and maternal alleles in *A. thaliana*. For example, both paternal and maternal histone H3 variants are replaced by de novo synthesized H3 variants in the zygote (50, 51). And although imprinting is quite common in the angiosperm endosperm, only a few genes imprinted in the embryo have been reported so far (56, 90, 118). The maternal-to-zygotic transition thus appears to already commence in the zygote. In contrast to animals, however, because there is pronounced postmeiotic gene expression in both female and male gametophytes followed by postfertilization gene expression, the maternal-to-zygotic transition might more appropriately be called the gametophytic-to-sporophytic transition. This transition might be completed sooner or later, presumably depending mainly on species-specific velocities of development during early embryogenesis. In this view, the longer it takes for the zygote and its progeny to divide, the earlier in developmental time the gametophytic-to-sporophytic transition might occur.

ZYGOTE DIVISION AND SEPARATION OF APICAL AND BASAL CELL FATE

In the vast majority of flowering plant species, the zygote divides transversely, generating an apical daughter cell and a basal daughter cell, whereas in some species oblique or longitudinal divisions occur (62, 133). When the zygote divides transversely, the two daughter cells may be quite different in size, depending on the position of the plane of cell division. In *Ricinus communis* and *Triticum aestivum* (wheat), for example, the zygote divides "symmetrically," generating two daughter cells of equal size (74, 133). In other species, zygotes divide asymmetrically. Whereas in *Coriaria nepalensis* and *Anethum graveolens*, for example, the apical daughter cell is larger than the basal one, in *A. thaliana* the apical daughter cell of the zygote is smaller than the basal one (94, 133). There seems to be no general rule regarding the size ratio of the apical daughter cell and the basal daughter cell of angiosperm zygotes (133).

Nonetheless, the division of the zygote might still—directly or indirectly—separate apical and basal cell fate and hence might also consolidate or establish the apical-basal axis of

polarity, which is then maintained throughout plant life. Some evidence supports this view. In both *Z. mays* and *N. tabacum*, the apical daughter cell of the zygote exhibits a transcriptional profile distinct from the basal counterpart (48, 113). In *A. thaliana*, two developmental pathways, in addition to the YDA pathway mentioned above, have been linked to apical-basal axis establishment after zygote division: One involves the transcription factors WOX8, WOX9, and WOX2, whereas the other is auxin dependent, involving the auxin efflux regulator PIN-FORMED 7 (PIN7) as well as the transcriptional regulators MONOPTEROS (MP)/AUXIN RESPONSE FACTOR 5 (ARF5) and BODENLOS (BDL)/INDOLE-3-ACETIC-ACID 12 (IAA12) (see below) (**Figure 2**).

Besides *WOX8*, whose expression in the zygote is induced by WRKY2, *WOX2* is also expressed in the zygote (40, 151). After zygote division, though, these two genes are not coexpressed anymore; *WOX2* is expressed in the apical daughter cell of the zygote, and *WOX8* (together with *WOX9*) is expressed in the basal (40). *WOX9*, which is assumed to be

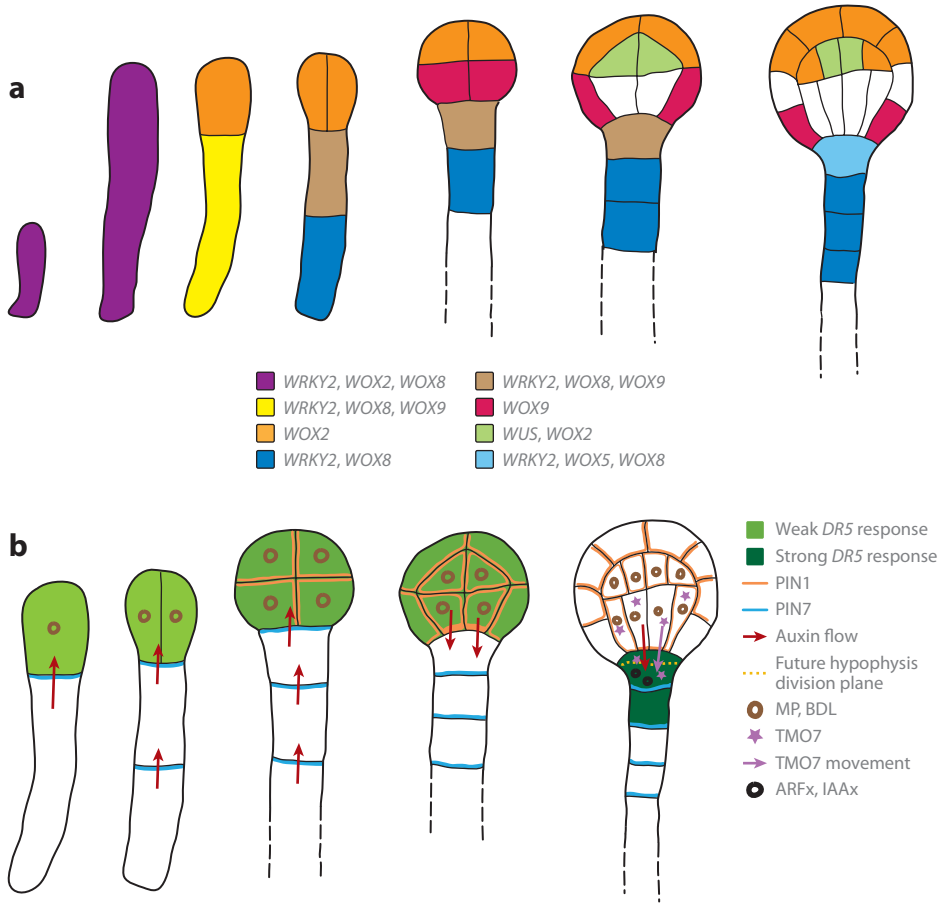

Figure 2

Apical-basal patterning and hypophysis specification in early embryogenesis of *Arabidopsis thaliana*. (*a*) Expression patterns of *WRKY2* and early-expressed *WOX* genes. (*b*) Auxin signaling and hypophysis specification. Embryos not drawn to scale.

Embryo proper: cells forming the embryo

Suspensor: extraembryonic, often filamentous structure anchoring the embryo proper to the ovule wall

Hypophysis: in *Arabidopsis thaliana*, a cell basally adjacent to the embryo proper and involved in root pole formation

a target of WRKY2 as well, might already be expressed in the zygote and possibly also in the apical daughter cell of the zygote (40, 151, 163). WOX8 and WOX9 are supposed to signal from the basal to the apical daughter cell for proper *WOX2* expression to occur (10). However, because there are stronger defects in *wox8 wox9* or *wox9* alone than there are in *wox2* mutant embryos, WOX8 and WOX9 appear to have additional, WOX2-independent functions in early development (10, 40, 163). *WRKY2* is coexpressed with *WOX8* and partially with *WOX9* during the earliest stages of embryogenesis (40, 151) (**Figure 2*a***), which could account for the early expression of these two *WOX* genes in the basal lineage. The problem of the separation of apical and basal cell fate, however, would not be solved with this extension of the WOX pathway; instead, the problem would be shifted from understanding *WOX2*, *WOX8*, and *WOX9* transcript distribution to understanding *WRKY2* transcript distribution.

The auxin-dependent pathway implicated in apical-basal axis establishment during *A. thaliana* embryogenesis becomes relevant immediately after zygote division, when auxin is transported from the basal to the apical daughter cell via PIN7 (30) (**Figure 2*b***). The auxin response in the apical descendant of the zygote triggered by this directional auxin transport might be important for its proper specification, as evidenced by its transverse instead of longitudinal division in *bdl*, *mp*, *mp bdl*, and *pin7* mutant embryos (30, 42). *MP* encodes an ARF, *BDL* encodes an AUXIN (AUX)/IAA inhibitor, and both are expressed in the apical cell lineage (41, 43); *MP* and *BDL* form a system of two interconnected feedback loops that can be modulated by auxin via the degradation of BDL protein (76). The initial transport of auxin to the apical cell(s) might thus be sufficient to establish expression of these two important developmental regulators. But, comparable to the WOX/WRKY case, the next step on the hierarchy ladder has to be taken now, and how PIN7-mediated basal-to-apical auxin transport is set up must be determined.

HYPOPHYSIS SPECIFICATION AND ROOT POLE FORMATION

Importance of Auxin in Hypophysis Specification and Root Pole Formation

The root pole is the basal end of the angiosperm embryo. In *A. thaliana*, the specification of the founder cell of the root meristem is not the result of a (spatially) isolated developmental program, but the consequence of developmental events that take place in the apically adjoining cells (157).

One of these events is the overall reversal of the above-mentioned basal-to-apical auxin flow from the dermatogen stage onward. The PIN1 auxin efflux regulator formerly nonpolarly distributed in the cells of the embryo proper starts to become localized predominantly to the basal side of the lower inner cells, and the formerly apically localized PIN7 becomes localized to the basal side of the suspensor cells. In consequence, auxin accumulates in the hypophysis and the subhypophyseal cell as indicated by the auxin response reporter *DR5* (30) (**Figure 2*b***).

This accumulation of auxin in the hypophysis appears to be crucial for its specification and subsequent root pole formation, as suggested by the fact that impairment of auxin biosynthesis and transport as well as auxin signaling interfere with these processes. The auxin-biosynthesis multiple mutants *yucca 1* (*yuc1*) *yuc4 yuc10 yuc11* and *tryptophan aminotransferase of arabidopsis 1* (*taa1*) *tryptophan aminotransferase related 1* (*tar1*) *tar2* as well as the auxin transport quadruple mutant *pin1 pin3 pin4 pin7* are rootless, just like seedlings in which the phosphorylation status-dependent polar PIN1 localization is reversed from the basal to the apical side in the inner cells of the embryo proper by the misexpression of the PIN1-phosphorylating serine/threonine kinase PINOID (PID) (19, 30, 31, 102, 139). Moreover, the regulation of *PIN1* expression involves MP and its inhibitor BDL (157). This might explain why the knockout of *MP*, or mutations causing the stabilization of BDL, lead to the non- or misspecification of the hypophysis and subsequent failure to form

a root (157). Thus, MP-BDL-dependent auxin signaling in the cells of the embryo proper indirectly ensures the accumulation of auxin in the hypophysis, where signaling through another ARF-AUX/IAA pair presumably mediates the actual specification process (157) (**Figure 2*b***). Recently, detailed expression analysis revealed several *ARF* candidates expressed in the hypophysis (117).

Additional Factors Involved in Hypophysis Specification and Root Pole Formation

In addition to auxin, other molecules likewise serve as mobile signaling cues for hypophysis specification. TARGET OF MONOPTEROS 7 (TMO7), a small transcriptional regulator whose expression is regulated by MP and BDL, also moves from the provascular cells into the hypophysis and contributes to its specification (128) (**Figure 2*b***). SHORTROOT (SHR) might also move there, as inferred from the expression of *SCARECROW* (*SCR*) in the hypophysis (106, 164). Although SCR does not appear to be necessary for hypophysis specification itself—as indicated by the apparently normal hypophysis division in the *scr* mutant—SCR is subsequently required for proper root pole formation (164). Similar considerations apply to the *PLETHORA* (*PLT*) genes *PLT1*, *PLT2*, *PLT3*, and *BABY BOOM* (*BBM*)/*PLT4* and to *WOX5*. The expression of some of them depends on *MP* and its close homolog *NONPHOTOTROPIC HYPOCOTYL 4* (*NPH4*)/*ARF7* or is initiated in the hypophysis in an *MP-BDL*-dependent fashion, but at least *WOX5* is mainly required for root organization of later developmental stages and root stem cell maintenance (3, 34, 40, 122).

Although auxin signaling is of central importance for root pole initiation, it is not the only plant hormone signaling pathway involved. The brassinosteroid signaling component *BES INTERACTING MYC-LIKE PROTEIN 1* (*BIM1*) and the AP2 transcription factors DORNRÖSCHEN (DRN) and DORNRÖSCHEN-LIKE (DRNL), which interact with BIM1, are required for proper hypophysis division and root formation, suggesting that auxin-brassinosteroid crosstalk is involved in root pole initiation (16, 17, 169). In addition, the requirement of two feedback repressors of cytokinin signaling, *ARABIDOPSIS RESPONSE REGULATOR 7* (*ARR7*) and *ARR15*, for the same process indicates the necessity to dampen cytokinin signaling (105). This dampening happens specifically in the lower derivative of the hypophysis via *ARR7* and *ARR15*, whose expression depends on auxin (105) and hence possibly also indirectly on MP-BDL-dependent signaling.

Provasculature: cells that will give rise to the vasculature (the conductive tissue)

Positional Information During Root Initiation

The fate of the hypophysis thus appears to be determined by its position at the basal end of the early embryo rather than its descent from the basal daughter cell of the zygote. Indeed, the clonal origin of the hypophysis might not be relevant for root pole initiation. In the *hanaba taranu* (*han*) mutant, expression domains of genes are shifted apically so that genes normally expressed only in the suspensor replace "apical" genes in the lower half of the embryo proper. As a consequence, it is not the histologically still-discernable hypophysis that becomes the founder cell of the future root pole, but rather cell(s) from the lower-tier descendants (108). As in the wild type, the cell(s) to be recruited for root pole formation appear to be those closest to cells with an apical cell fate.

In an even more extraordinary case of atypical embryonic root initiation, which occurs in the *topless-1* (*tpl-1*) mutant, a root is initiated not only basally but also apically and, interestingly, like in *han*, in an MP-independent fashion (87, 108). TPL, a cosuppressor that binds to BDL and probably other AUX/IAAs as well as indirectly to jasmonate ZIM-domain (JAZ) repressor proteins and directly to WUSCHEL (WUS), might recruit histone deacetylases to repress gene expression (70, 86, 115, 141; reviewed in 73). The *tpl-1* mutation is a dominant negative mutation relieving the repression

Protoderm: outermost cell layer of the embryo proper that differentiates into the epidermis

of TPL targets; especially derepression of the TPL targets *PLT1* and *PLT2* leads to the formation of a secondary root pole (135).

Many angiosperm species—including various monocots and, e.g., *Pisum sativum* (pea)—do not exhibit a cell that clearly corresponds to the *A. thaliana* hypophysis, i.e., a single uppermost derivative of the basal daughter cell of the zygote that invariably divides into a smaller upper lens-shaped and a larger lower cell to give rise to the quiescent center and the columella of the root meristem, respectively (reviewed in 59). Nevertheless, these species of course also form a root, and they may do so by employing signaling pathways similar to those in *A. thaliana*, which specify the hypophysis in a position-dependent manner. In *O. sativa*, the *WUS*-type homeobox gene *quiescent-center-specific homeobox* (*QHB*) is—similar to *WOX5* in *A. thaliana*—expressed in a few cells at the basal pole of the embryo; in *Z. mays* and *O. sativa*, an *SCR* homolog might play a role in root patterning (40, 67, 68, 82, 83). The developmental significance of the singular hypophysis in *A. thaliana* might thus mainly relate to the minimal number of cells that constitute the embryo at the very early stage when the root pole is initiated.

RADIAL PATTERNING AND PROTODERM SPECIFICATION

Separation of Inner and Outer Fate in the Early Proembryo

In *A. thaliana*, the beginning of radial patterning is marked by the tangential divisions of the cells of the embryo proper in the octant-stage embryo. The eight outer cells thus formed are the founder cells of the protoderm, and during embryogenesis the eight inner cells will give rise to, e.g., the provasculature and the ground tissue (66, 94, 126) (**Figure 1**). Like apical-basal axis establishment, these tangential divisions have been linked to the action of *WOX* genes and *MP*. In *wox2* and, with a higher penetrance, in *wox2 mp*, *wox2 wox8*, and *wox1 wox2 wox3*, some cells of the octant-stage embryo proper do not divide tangentially, so that a "continuous" protodermal layer is not formed (10, 40). How *WOX* genes and MP-dependent auxin signaling mediate the proper orientation of these cell-division planes is not known.

An early difference between protodermal and inner cells is the divergence of transcriptional activities. The GLABRA 2 (GL2) family homeodomain transcription factors *ARABIDOPSIS THALIANA MERISTEM LAYER 1* (*ATML1*) and *PROTODERMAL FACTOR 2* (*PDF2*) are initially expressed throughout the early embryo proper, but immediately after the tangential divisions have occurred their expression becomes confined to the protodermal cells (1, 88) (**Figure 3*a*,*b***). Conversely, the expression of *ZWILLE* [*ZLL*, also called *ARGONAUTE 10* (*AGO10*)], which is expressed in the apical cells from the four-cell stage on and is involved in shoot meristem maintenance, becomes confined to the inner cells (91, 104) (**Figure 3*a*,*b***). Remarkably, in *Z. mays* and *O. sativa*, where the cell-division planes after the zygotic division appear randomly oriented, the expression of *ATML1* homologs also becomes confined to the protoderm, and these homologs might serve a similar function during protoderm development as their *A. thaliana* counterparts (52–54, 167).

In *atml1 pdf2* double-mutant seedlings, cotyledons seem devoid of an epidermis and the shoot apex lacks distinct cell layers (1). The *ATML1* promoter and the *PDF2* promoter each contain a potential binding site for WUS, the founding member of the WOX family (1, 40, 143), and thus the expression of *ATML1* and *PDF2* could be directly regulated by WOX transcription factors, including those involved in the tangential divisions of the octant-stage embryo (**Figures 2*a*** and **3*c***). Furthermore, both the *ATML1* promoter and the *PDF2* promoter contain an eight-nucleotide sequence termed the L1 box, which is also present in the promoters of other epidermally expressed genes such as *PDF1*, *FIDDLEHEAD* (*FDH*), *LIPID TRANSFER PROTEIN 1* (*LTP1*), and—almost perfectly matching—the *O. sativa ATML1* homolog *Oryza sativa transcription*

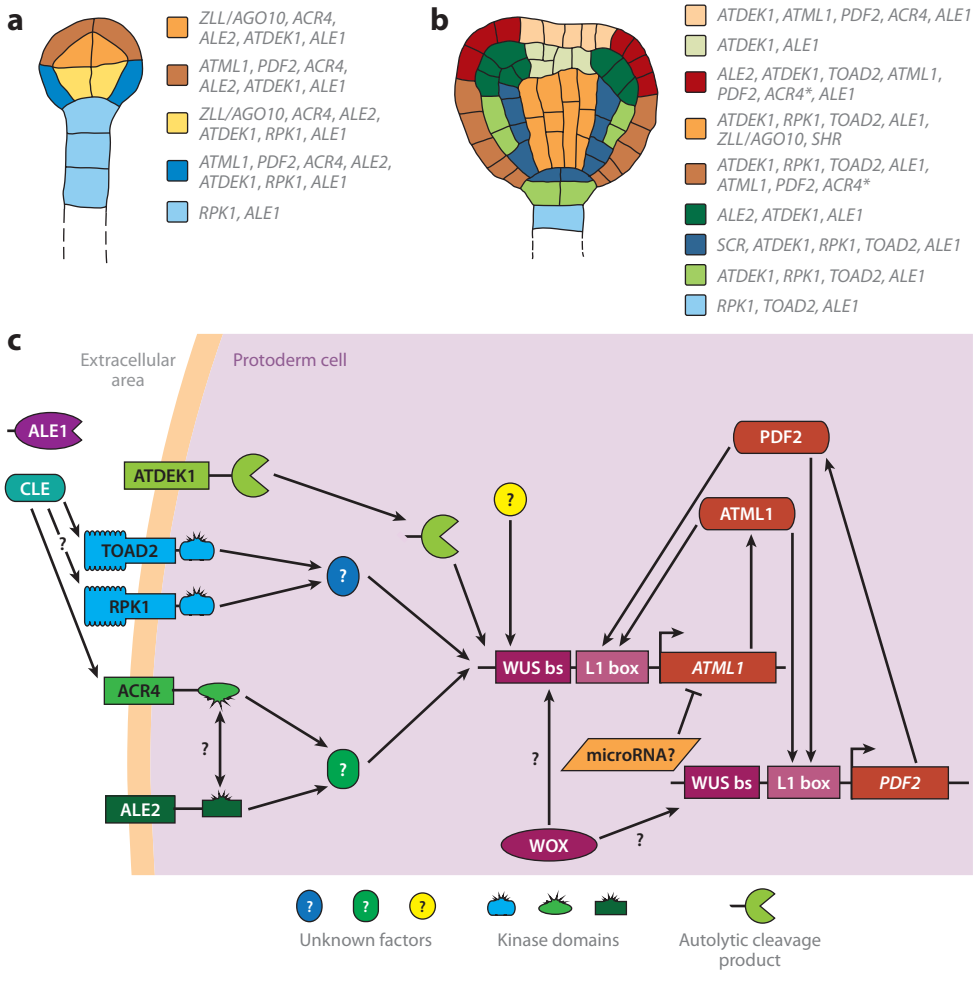

Figure 3

Radial patterning in early embryogenesis of *Arabidopsis thaliana*. (*a*,*b*) Expression patterns of genes important for radial patterning. Panel *a* shows the dermatogen stage; panel *b* shows the transition stage. Asterisk indicates that weak *ACR4* expression was detected ubiquitously in embryos. (*c*) Signaling pathways maintaining protoderm identity. Abbreviation: WUS bs, WUS binding site. Embryos not drawn to scale.

factor 1 (*OSTF1)* (1, 2, 167). Because ATML1 and PDF2 bind to the L1 box in vitro, it is conceivable that these two transcription factors establish a positive feedback loop that regulates the transcription of genes expressed in the epidermis (1, 2) (**Figure 3*c***). In the case of *ATML1*, however, the L1 box and the WUS binding site do not appear to be the only important regulatory regions. Although the L1 box is essential for the expression of *PDF1*, this is not the case for *ATML1* (2, 143). Rather, the L1 box controls expression redundantly with the WUS binding site in the *ATML1* promoter, but even when both elements are deleted, a hexameric copy of an *ATML1* promoter fragment still confers weak expression (143). In addition, *ATML1* is still expressed in the *atml1 pdf2* and *wox8 wox9* double-mutant backgrounds (10, 143). Thus, although these two "pathways" might converge on *ATML1* expression, other factors are probably involved in the regulation of this gene. Because the *ATML1* promoter

confers expression in the suspensor but the messenger RNA (mRNA) is detected there only in the *dicer-like 1* (*dcl1*) mutant, a microRNA might regulate the *ATML1* expression in the suspensor (111, 143) (**Figure 3*c***).

The inner cells of the *A. thaliana* embryo give rise to the various concentric tissue layers that have been described in the root and are laid down during embryogenesis (126, 127). The GRAS transcription factor SHR is one of the best-described players involved in radial patterning. It is expressed in the provasculature and moves out to the neighboring cell layer, where it activates the transcription of another GRAS transcription factor gene, *SCR* (46, 106). *SCR* is expressed in the ground tissue and the hypophysis at the globular stage of embryogenesis. When the cells of the ground tissue of the hypocotyl and the embryonic root pole divide periclinally between the triangular stage and the heart stage to generate the inner layer of endodermis and the outer layer of cortex cells, *SCR* continues to be expressed in the inner layer (164) (**Figure 3*b***). These periclinal cell divisions depend on both *SHR* and *SCR* (46, 164). SHR and SCR activate microRNA165/166 in the endodermis of the mature root, from where the microRNAs feed back onto the vasculature to control its patterning. Because the two microRNAs are already expressed during embryogenesis, they might contribute to embryonic patterning as well (14).

Maintenance of Radial Patterning

RECEPTOR-LIKE PROTEIN KINASE 1 (RPK1) and TOADSTOOL 2 (TOAD2), two closely related leucine-rich-repeat receptor-like kinases (LRR-RLKs), are redundantly required for the maintenance of radial patterning (112) (**Figure 3*c***). The protoderm marker *ATML1* as well as the central domain markers *ZLL/AGO10* and *SHR* are correctly expressed only initially in *rpk1 toad2* embryos, which have enlarged protoderm cells (112). At the late-globular stage of embryogenesis, the expression of *ATML1* is (almost) lost, and the expression of *ZLL/AGO10* and *SHR* extends over the entire basal domain in *rpk1 toad2*, suggesting that *RPK1* and *TOAD2* play an essential role in the maintenance but not the establishment of the radial pattern in *A. thaliana* (112).

The ligands binding to RPK1 and TOAD2 during embryogenesis are unknown, although it was recently suggested that the signaling peptide derived from CLAVATA 3 (CLV3) binds to TOAD2 (71). Because this signaling peptide is functionally similar to other signaling peptides of the CLV3/ESR-RELATED (CLE) family (109), any of these might be the endogenous ligand for RPK1 and TOAD2 (**Figure 3*c***). Hence, at least some of these signaling peptides might play a role during early embryogenesis, an assumption that receives support from the analysis of the RLK ARABIDOPSIS CRINKLY 4 (ACR4). ACR4 might bind the signaling peptide CLE40, which is the closest homolog of CLV3, and is involved in protoderm specification, where it acts together with ABNORMAL LEAF-SHAPE 2 (ALE2), another RLK (138, 145) (**Figure 3*c***). Although neither the single mutants nor the double mutant appear to show severe protodermal defects during embryo development, in mutant combinations with *ale1* the protoderm is misspecified (36, 145). Accordingly, *ale1 ale2* and *ale1 acr4* double mutants do not properly express *ATML1* (145). *ALE1* encodes a protease that is predominantly expressed in the endosperm, and thus ALE2 and ACR4 might perceive a signal from the endosperm to ensure proper protoderm specification (144, 145) (**Figure 3*c***). However, toxin-dependent endosperm ablation rather suggests that the endosperm is not involved in embryo patterning, and the feasibility of somatic embryogenesis also argues against essential peptide signals from the endosperm (158; reviewed in 168). In addition to its expression in the endosperm, *ALE1* is weakly expressed in the early embryo itself (144), and this might be relevant for embryogenesis.

Protoderm formation and *ATML1* expression are prevented in *arabidopsis thaliana defective kernel 1* (*atdek1*) mutant embryos, which arrest at the globular stage (60, 81, 150).

ATDEK1 encodes a calpain protease that undergoes autolytic cleavage (**Figure 3*c***) and is expressed in the embryo (60, 61, 81). In *ATDEK1* knockdown lines, seedlings show a transformation of epidermal to mesophyll-like cell fate in the cotyledons, similar to what has been observed in *atml1 pdf2* double mutants (1, 60). In conclusion, although a number of key players have been analyzed, the overall genetic program of setting up the radial pattern or only the protoderm is still largely unexplored.

SHOOT MERISTEM SPECIFICATION AND COTYLEDON INITIATION

The Organizing Center

The *A. thaliana* shoot meristem can be morphologically delineated for the first time during embryogenesis at the late-torpedo stage (6, 78). In the mature embryo, the shoot meristem consists of a few small cells with big nuclei and small vacuoles, and its first molecular mark is the onset of *WUS* expression in the four inner cells of the apical embryo region at the dermatogen stage (78, 97) (**Figure 2*a***). *WUS* encodes a homeodomain transcription factor, and its expression remains confined to a subset of cells close to the shoot apex during later stages of development (**Figure 4*a***), defining an organizing center that keeps the neighboring stem cells in a pluripotent state (97). The *wus* mutation results in the lack of a functional shoot meristem and the formation of a flat and enlarged shoot apex consisting of aberrant cells (78). *WUS* orthologs seem to play similar roles in dicots like *Petunia hybrida* and *Antirrhinum majus*, but possibly not in monocots like *O. sativa* and *Z. mays* (70, 107, 140).

Despite considerable efforts to identify regulators and downstream targets of this master regulator (11; reviewed in 24), our knowledge is scant about the mechanism(s) of initiation and early confinement of *WUS* expression and about the identity of the *WUS*-dependent non-cell-autonomous signal(s) maintaining stem cell fate in the shoot meristem. In postembryonic development, however, cytokinin signaling activates *WUS* expression (37). Because WUS inhibits the expression of several type-A *ARR*s that are negative regulators of cytokinin signaling, a positive feedback mechanism involving *WUS* and cytokinin signaling might thus operate in the shoot meristem to maintain

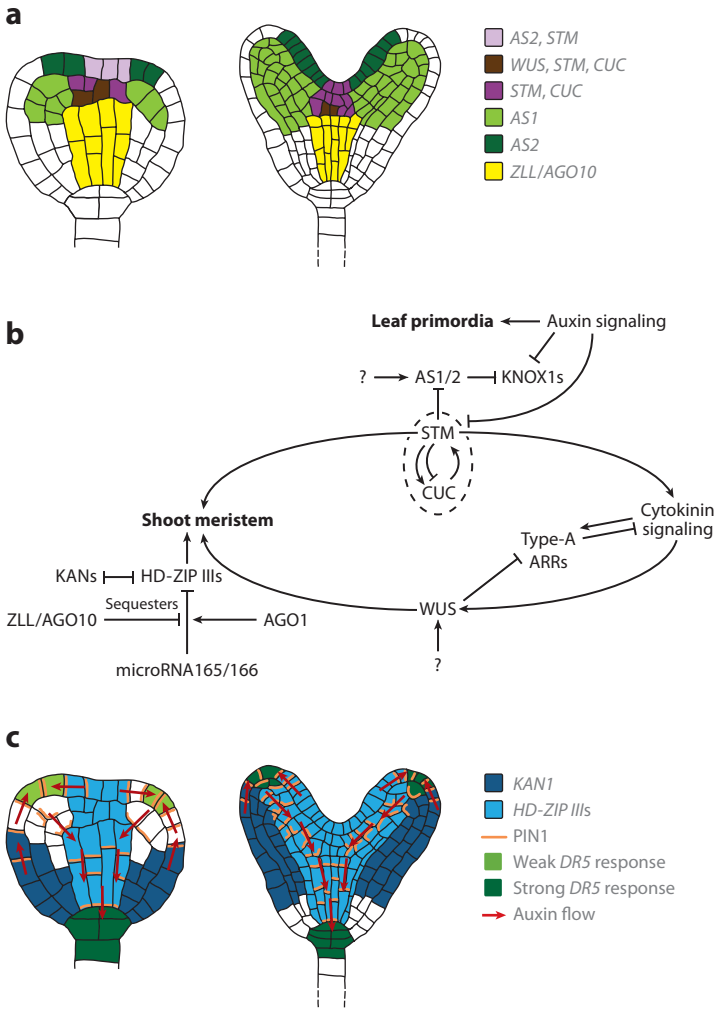

Figure 4

Shoot meristem and cotyledon initiation in *Arabidopsis thaliana*. (*a*) Expression patterns of genes important for establishment of the shoot meristem and initiation of cotyledons in *A. thaliana* during the transition stage and the heart stage. *CUC1–3* expression is generalized as *CUC*. (*b*) Pathways and hormonal regulation in shoot meristem and cotyledon initiation. (*c*) Expression patterns of *KAN1* and *HD-ZIP III* genes (exemplarily shown for *REV*, which includes domains of all other members), auxin flow mediated by PIN1 (idealized representation), and *DR5* response. Embryos not drawn to scale.

its integrity (37, 79) (**Figure 4*b***). This crosstalk may already operate during embryogenesis. In *O. sativa*, the *LONELY GUY* (*LOG*) gene, which encodes a cytokinin-activating enzyme and is specifically expressed in the shoot meristem region, is important for shoot meristem maintenance (75).

Shoot Meristem Indeterminacy and the Shoot Meristem–Cotyledon Boundary Region

The class I KNOTTED-like homeodomain transcription factor SHOOT MERISTEMLESS (STM) might indirectly activate *WUS* expression via its induction of cytokinin biosynthesis and signaling (37, 57, 85, 166) (**Figure 4*b***), and in addition to its cytokinin-related effects, it restricts gibberellic acid levels (45, 57). Similar to its *Z. mays* ortholog *KNOTTED 1* (*KN1*) and its *O. sativa* ortholog *Oryza sativa homeobox 1* (*OSH1*), *STM* is expressed in the presumptive shoot meristem from the globular stage onward (85, 124, 134) (**Figure 4*a***); in addition, in the oil palm *Elaeis guineensis* an *STM* ortholog is expressed in the shoot meristem, at least during vegetative development (64). Together with WUS, STM is required to maintain the shoot meristem: WUS acts as the instructor of the organizing center, and STM acts as a repressor of differentiation across the entire shoot meristem (80). In differentiated tissue, simultaneous expression of WUS and STM can induce meristematic activity, with WUS non-cell-autonomously triggering divisions in *STM*-expressing tissue (35).

Being a transcription factor, STM functions in the nucleus, and this localization depends on BEL1-like homeodomain transcription factors (22, 121). Shoot meristem initiation is consistently inhibited in the *stm* mutant and the *arabidopsis thaliana homeobox 1* (*ath1*) *pennywise* (*pny*) *pound-foolish* (*pnf*) triple mutant, and also in the *cup-shaped cotyledon 1* (*cuc1*) *cuc2* double mutant, which fails to express *STM* in the presumptive shoot meristem (4, 6, 121). The NAC transcription factors CUC1–3 are redundantly required for shoot meristem establishment as well as cotyledon separation. At early embryonic stages, their expression domains partially overlap with the *STM* expression domain (**Figure 4*a***), whereas *CUC1–3* expression domains in general surround the *STM* expression domain at later stages (4, 47, 142, 152). How this expression pattern evolves is not clear. However, there appears to be mutual regulation involving positive and negative feedback loops (**Figure 4*b***): Not only are the CUCs required for *STM* expression, but STM regulates the expression of *CUC1–3* and the expression of microRNA164, which in turn targets *CUC1* and *CUC2* transcripts for degradation (4, 77, 92, 137). The *P. hybrida* and *A. majus CUC* orthologs *NO APICAL MERISTEM* (*NAM*) and *CUPULIFORMIS* (*CUP*) are also expressed at organ boundaries, and they are important for both boundary establishment and shoot meristem development (136, 159). In *Z. mays*, the putative *CUC1/2* orthologs *Zea mays NO APICAL MERISTEM 1/2* (*ZmNAM1/2*) and the *CUC3* ortholog *Zea mays CUP-SHAPED COTYLEDON 3* (*ZmCUC3*) are in part initially coexpressed with a shoot meristem marker, and later in a ringlike pattern around the shoot meristem (173), hinting at a strong conservation of *CUC* gene function at least among flowering plants.

Meristem Establishment

A general prerequisite for shoot meristem identity seems to be the presence of class III HOMEODOMAIN-LEUCINE ZIPPER (HD-ZIP III) transcription factors. This family consists of PHABULOSA (PHB), PHAVOLUTA (PHV), REVOLUTA (REV), ARABIDOPSIS THALIANA HOMEOBOX 8 (ATHB8), and ATHB15. Expression of all but *ATHB8* is already detectable from early embryonic stages onward, and in part there is overlap with the future site of the shoot meristem, whereas especially *PHB*, *REV*, and *ATHB15* expression domains partially coincide with the *ZLL/AGO10* provascular expression domain as well; ATHB8 mRNA is detectable from the heart stage onward (26, 91, 100, 116). Conversely, expression domains of members of the *KANADI* (*KAN*)

gene family could be regarded as complementary to those of the *HD-ZIP III*s, which they are supposed to antagonize (26–28, 69) (**Figure 4*c***). The *phb rev* double, *phb phv rev* triple, and other loss-of-function mutant combinations involving *athb8* and *athb15* lack the embryonic shoot meristem and in severe cases fail to establish bilateral symmetry (26, 116). The dominant mutation *phb-1d* leads to ectopic meristems that express the shoot meristem marker *STM* on the lower side of leaves, and also causes an enlarged embryonic shoot meristem and partially suppresses the *stm* mutant phenotype (99). Two recent findings further support a pivotal role for HD-ZIP III transcription factors in shoot meristem formation. First, exclusion of HD-ZIP III proteins from the embryonic root pole is necessary for its proper establishment (38). Second, dominant *HD-ZIP III* mutants suppress the *tpl-1* double-root phenotype, possibly by excluding PLT1 and PLT2 from the future shoot meristem cells. Conversely, misexpression of dominant *HD-ZIP III*s can lead to (homeotic) root-pole-to-shoot-pole transformations during embryogenesis (135). It is not clear at present whether the HD-ZIP IIIs directly regulate *STM* and/or *WUS* in ectopic shoot meristem formation.

HD-ZIP III transcripts are targeted by microRNA165/166, and the dominant *HD-ZIP III* mutations reside in the microRNA pairing sites, rendering the HD-ZIP mRNAs resistant to degradation (93, 119, 146, 160, 171). The microRNA-dependent degradation involves the AGO proteins AGO1 and ZLL/AGO10, which both bind microRNA165/166 (172). It was suggested that ZLL/AGO10 and AGO1 act in an antagonistic fashion (**Figure 4*b***), with ZLL/AGO10 positively regulating HD-ZIP III transcript levels through competition with AGO1—possibly by sequestering microRNA165/166. Such a sequestration could ensure sufficiently high HD-ZIP III levels during shoot meristem establishment and maintenance (172). Given that *ZLL/AGO10* expression in the provasculature is necessary for embryonic shoot meristem maintenance, a non-cell-autonomous signal could, in principle, instruct the shoot meristem from the cells underneath (149). In this scenario, the two primary meristems of shoot and root would be initiated as WUS- and WOX5-positive cell groups, respectively, in response to inductive signals, at the opposite ends of the provasculature in early embryogenesis.

Initiation of Cotyledon Primordia

When the cotyledon primordia start to emerge in *A. thaliana*, the embryo organization shifts from radial to bilateral symmetry. The sites of cotyledon initiation correlate with auxin accumulation at subapical foci in the protoderm, as indicated by the auxin response reporter *DR5* (8) (**Figure 4*c***). Auxin might therefore directly cause cotyledon initiation in the apical margins of the globular embryo (8). In addition, *STM* and *CUC* expression have to be excluded from those sites (see below). Auxin transport toward the incipient primordia is mediated by PIN auxin efflux regulators, probably mainly by PIN1 (8) (**Figure 4*c***). PIN1 is apically localized in the protoderm, and the apical localization of PIN proteins is generally brought about by PID and its homologs PID2, WAG1, and WAG2, three of which have been shown to directly phosphorylate PINs (20, 23, 31, 49, 102). For example, the *pid wag1 wag2* triple mutant and the *pin1 pid* double mutant lack cotyledons (20, 33), as does the *pid enhancer of pinoid* (*enp*) double mutant (148). *ENP/MACCHI-BOU 4* (*MAB4*) encodes an NPH3-like protein that is involved in the regulation of PIN1 localization (32, 148). It is noteworthy that in both double mutants (*pin1 pid* and *pid enp*) the expression domains of *CUC* genes and *STM* are enlarged, and that cotyledon formation is partially restored when *CUC* genes or *STM* are knocked out in *pin1 pid* (33, 148); this highlights both the importance of directional auxin transport to the cotyledon initiation sites and the requirement to exclude specific transcripts/proteins from there. This view is supported by cotyledon formation defects in the auxin response mutants *mp* and *bdl* (9, 42). However, it might also be relevant in this context that MP directly activates the

expression of *DRN*—especially because *DRN* and *DRNL* redundantly act in cotyledon formation (16, 21). Additionally, DRN and DRNL are involved in the establishment and maintenance of boundary and shoot meristem gene expression domains, and they act together with PIN1 and PID (16, 18, 72). Auxin-related processes might be involved in cotyledon initiation in other flowering plant species as well, including monocots, but this has barely been investigated so far (reviewed in 15).

Another factor involved in cotyledon development, *ASYMMETRIC LEAVES 1* (*AS1*), which encodes a MYB domain protein and orthologs of which are present in *Z. mays* and *A. majus*, is initially expressed mainly subepidermally in the incipient cotyledon primordia, whereas *AS2*, which encodes a LATERAL ORGAN BOUNDARY (LOB) domain protein, is expressed protodermally before cotyledon outgrowth and later at the adaxial cotyledon side (12, 55, 84, 129, 153) (**Figure 4*a***). The loss of *AS1* or *AS2* makes *STM* dispensable for shoot meristem initiation and maintenance, suggesting that STM negatively regulates *AS1* and *AS2* (12, 13). Studies in primarily adult leaves suggest that *KNOX* genes are negatively regulated by AS1/2 and that AS1/2 possibly converge with auxin signaling to repress the *KNOX* member *KNOTTED-LIKE FROM ARABIDOPSIS THALIANA 1* (*KNAT1*)/*BREVIPEDICELLUS* (*BP*) (12, 39, 44) (**Figure 4*b***). The expression of *AS2* itself is negatively regulated by KAN1 and positively by BLADE-ON-PETIOLE 1/2 (BOP1/2), the expression of the latter in turn being directly or indirectly repressed by *STM* (65, 161). How exactly *AS1* and *AS2* are linked to auxin, however, has not been resolved.

PERSPECTIVES

Considerable progress has been made in the analysis of mechanisms underlying specific events in early embryogenesis, notably in *A. thaliana*. For example, we now have a clear conceptual framework for the initiation of the root meristem in the early embryo. However, although the main regulators have been identified and characterized, it is still rather obscure how these early events relate to the establishment of the molecular system for self-maintenance of the functional root meristem at the heart stage of embryogenesis. The initiation and establishment of the self-maintenance system are even less clear for the shoot meristem. Large-scale approaches combining expression profiling of specific embryo regions with functional characterization of putative developmental regulators might contribute to closing the gap.

Another unsolved problem is the origin of the apical-basal pattern. Although genes encoding developmental regulators are expressed in either the apical or the basal daughter cell of the zygote, it is not known how the expression of these regulators is ultimately established. This also relates to the mode of division of the zygote: Is it truly unequal, reflecting an intrinsic polarity of the zygote before division? Alternatively, the division might be equal, and only the two daughter cells would be exposed to different environments and thus might perceive different signals.

The contribution of the gametes to early embryogenesis still needs to be assessed. Although differentially regulated genes have been identified, their role in early patterning has not been clarified. And the significance of epigenetic regulation of patterning is still an open question.

Finally, most studies have focused on a few species, notably *A. thaliana*. Considering the differences in cell-division patterns between early embryos from different species, exploring orthologous developmental regulators might reveal to what extent their actions and regulatory networks are conserved among the flowering plant species when the cellular contexts of developmental events are not.

DISCLOSURE STATEMENT

The authors are not aware of any affiliations, memberships, funding, or financial holdings that might be perceived as affecting the objectivity of this review.

ACKNOWLEDGMENTS

We thank Martin Bayer for critical reading of the manuscript.

LITERATURE CITED

1. Abe M, Katsumata H, Komeda Y, Takahashi T. 2003. Regulation of shoot epidermal cell differentiation by a pair of homeodomain proteins in *Arabidopsis*. *Development* 130:635–43
2. Abe M, Takahashi T, Komeda Y. 2001. Identification of a *cis*-regulatory element for L1 layer-specific gene expression, which is targeted by an L1-specific homeodomain protein. *Plant J.* 26:487–94
3. Aida M, Beis D, Heidstra R, Willemsen V, Blilou I, et al. 2004. The *PLETHORA* genes mediate patterning of the *Arabidopsis* root stem cell niche. *Cell* 119:109–20
4. Aida M, Ishida T, Tasaka M. 1999. Shoot apical meristem and cotyledon formation during *Arabidopsis* embryogenesis: interaction among the *CUP-SHAPED COTYLEDON* and *SHOOT MERISTEMLESS* genes. *Development* 126:1563–70
5. Autran D, Baroux C, Raissig MT, Lenormand T, Wittig M, et al. 2011. Maternal epigenetic pathways control parental contributions to *Arabidopsis* early embryogenesis. *Cell* 145:707–19
6. Barton MK, Poethig RS. 1993. Formation of the shoot apical meristem in *Arabidopsis thaliana*: an analysis of development in the wild type and in the *shoot meristemless* mutant. *Development* 119:823–31
7. Bayer M, Nawy T, Giglione C, Galli M, Meinnel T, Lukowitz W. 2009. Paternal control of embryonic patterning in *Arabidopsis thaliana*. *Science* 323:1485–88
8. Benková E, Michniewicz M, Sauer M, Teichmann T, Seifertová D, et al. 2003. Local, efflux-dependent auxin gradients as a common module for plant organ formation. *Cell* 115:591–602
9. Berleth T, Jürgens G. 1993. The role of the *monopteros* gene in organising the basal body region of the *Arabidopsis* embryo. *Development* 118:575–87
10. Breuninger H, Rikirsch E, Hermann M, Ueda M, Laux T. 2008. Differential expression of *WOX* genes mediates apical-basal axis formation in the *Arabidopsis* embryo. *Dev. Cell* 14:867–76
11. Busch W, Miotk A, Ariel FD, Zhao Z, Forner J, et al. 2010. Transcriptional control of a plant stem cell niche. *Dev. Cell* 18:849–61
12. Byrne ME, Barley R, Curtis M, Arroyo JM, Dunham M, et al. 2000. *Asymmetric leaves1* mediates leaf patterning and stem cell function in *Arabidopsis*. *Nature* 408:967–71
13. Byrne ME, Simorowski J, Martienssen RA. 2002. *ASYMMETRIC LEAVES1* reveals *knox* gene redundancy in *Arabidopsis*. *Development* 129:1957–65
14. Carlsbecker A, Lee JY, Roberts CJ, Dettmer J, Lehesranta S, et al. 2010. Cell signalling by microRNA165/6 directs gene dose-dependent root cell fate. *Nature* 465:316–21
15. Chandler JW. 2008. Cotyledon organogenesis. *J. Exp. Bot.* 59:2917–31
16. Chandler JW, Cole M, Flier A, Grewe B, Werr W. 2007. The AP2 transcription factors DORNRÖSCHEN and DORNRÖSCHEN-LIKE redundantly control *Arabidopsis* embryo patterning via interaction with PHAVOLUTA. *Development* 134:1653–62
17. Chandler JW, Cole M, Flier A, Werr W. 2009. BIM1, a bHLH protein involved in brassinosteroid signalling, controls *Arabidopsis* embryonic patterning via interaction with DORNRÖSCHEN and DORNRÖSCHEN-LIKE. *Plant Mol. Biol.* 69:57–68
18. Chandler JW, Cole M, Jacobs B, Comelli P, Werr W. 2011. Genetic integration of *DORNRÖSCHEN* and *DORNRÖSCHEN-LIKE* reveals hierarchical interactions in auxin signalling and patterning of the *Arabidopsis* apical embryo. *Plant Mol. Biol.* 75:223–36
19. Cheng Y, Dai X, Zhao Y. 2007. Auxin synthesized by the YUCCA flavin monooxygenases is essential for embryogenesis and leaf formation in *Arabidopsis*. *Plant Cell* 19:2430–39

20. Cheng Y, Qin G, Dai X, Zhao Y. 2008. *NPY* genes and AGC kinases define two key steps in auxin-mediated organogenesis in *Arabidopsis*. *Proc. Natl. Acad. Sci. USA* 105:21017–22
21. Cole M, Chandler J, Weijers D, Jacobs B, Comelli P, Werr W. 2009. *DORNRÖSCHEN* is a direct target of the auxin response factor MONOPTEROS in the *Arabidopsis* embryo. *Development* 136:1643–51
22. Cole M, Nolte C, Werr W. 2006. Nuclear import of the transcription factor SHOOT MERISTEMLESS depends on heterodimerization with BLH proteins expressed in discrete sub-domains of the shoot apical meristem of *Arabidopsis thaliana*. *Nucleic Acids Res.* 34:1281–92
23. Dhonukshe P, Huang F, Galvan-Ampudia CS, Mahonen AP, Kleine-Vehn J, et al. 2010. Plasma membrane-bound AGC3 kinases phosphorylate PIN auxin carriers at TPRXS(N/S) motifs to direct apical PIN recycling. *Development* 137:3245–55
24. Dodsworth S. 2009. A diverse and intricate signalling network regulates stem cell fate in the shoot apical meristem. *Dev. Biol.* 336:1–9
25. Dumas C, Rogowsky P. 2008. Fertilization and early seed formation. *C. R. Biol.* 331:715–25
26. Emery JF, Floyd SK, Alvarez J, Eshed Y, Hawker NP, et al. 2003. Radial patterning of *Arabidopsis* shoots by class III HD-ZIP and KANADI genes. *Curr. Biol.* 13:1768–74
27. Eshed Y, Baum SF, Perea JV, Bowman JL. 2001. Establishment of polarity in lateral organs of plants. *Curr. Biol.* 11:1251–60
28. Eshed Y, Izhaki A, Baum SF, Floyd SK, Bowman JL. 2004. Asymmetric leaf development and blade expansion in *Arabidopsis* are mediated by KANADI and YABBY activities. *Development* 131:2997–3006
29. Faure JE, Rotman N, Fortune P, Dumas C. 2002. Fertilization in *Arabidopsis thaliana* wild type: developmental stages and time course. *Plant J.* 30:481–88
30. Friml J, Vieten A, Sauer M, Weijers D, Schwarz H, et al. 2003. Efflux-dependent auxin gradients establish the apical-basal axis of *Arabidopsis*. *Nature* 426:147–53
31. Friml J, Yang X, Michniewicz M, Weijers D, Quint A, et al. 2004. A PINOID-dependent binary switch in apical-basal PIN polar targeting directs auxin efflux. *Science* 306:862–65
32. Furutani M, Kajiwara T, Kato T, Treml BS, Stockum C, et al. 2007. The gene *MACCHI-BOU 4/ENHANCER OF PINOID* encodes a NPH3-like protein and reveals similarities between organogenesis and phototropism at the molecular level. *Development* 134:3849–59
33. Furutani M, Vernoux T, Traas J, Kato T, Tasaka M, Aida M. 2004. *PIN-FORMED1* and *PINOID* regulate boundary formation and cotyledon development in *Arabidopsis* embryogenesis. *Development* 131:5021–30
34. Galinha C, Hofhuis H, Luijten M, Willemsen V, Blilou I, et al. 2007. PLETHORA proteins as dose-dependent master regulators of *Arabidopsis* root development. *Nature* 449:1053–57
35. Gallois JL, Woodward C, Reddy GV, Sablowski R. 2002. Combined SHOOT MERISTEMLESS and WUSCHEL trigger ectopic organogenesis in *Arabidopsis*. *Development* 129:3207–17
36. Gifford ML, Dean S, Ingram GC. 2003. The *Arabidopsis ACR4* gene plays a role in cell layer organisation during ovule integument and sepal margin development. *Development* 130:4249–58
37. Gordon SP, Chickarmane VS, Ohno C, Meyerowitz EM. 2009. Multiple feedback loops through cytokinin signaling control stem cell number within the *Arabidopsis* shoot meristem. *Proc. Natl. Acad. Sci. USA* 106:16529–34
38. Grigg SP, Galinha C, Kornet N, Canales C, Scheres B, Tsiantis M. 2009. Repression of apical homeobox genes is required for embryonic root development in *Arabidopsis*. *Curr. Biol.* 19:1485–90
39. Guo M, Thomas J, Collins G, Timmermans MC. 2008. Direct repression of *KNOX* loci by the ASYMMETRIC LEAVES1 complex of *Arabidopsis*. *Plant Cell* 20:48–58
40. Haecker A, Groß-Hardt R, Geiges B, Sarkar A, Breuninger H, et al. 2004. Expression dynamics of *WOX* genes mark cell fate decisions during early embryonic patterning in *Arabidopsis thaliana*. *Development* 131:657–68
41. Hamann T, Benkova E, Bäurle I, Kientz M, Jürgens G. 2002. The *Arabidopsis BODENLOS* gene encodes an auxin response protein inhibiting MONOPTEROS-mediated embryo patterning. *Genes Dev.* 16:1610–15
42. Hamann T, Mayer U, Jürgens G. 1999. The auxin-insensitive *bodenlos* mutation affects primary root formation and apical-basal patterning in the *Arabidopsis* embryo. *Development* 126:1387–95
43. Hardtke CS, Berleth T. 1998. The *Arabidopsis* gene *MONOPTEROS* encodes a transcription factor mediating embryo axis formation and vascular development. *EMBO J.* 17:1405–11

44. Hay A, Barkoulas M, Tsiantis M. 2006. ASYMMETRIC LEAVES1 and auxin activities converge to repress *BREVIPEDICELLUS* expression and promote leaf development in *Arabidopsis*. *Development* 133:3955–61
45. Hay A, Kaur H, Phillips A, Hedden P, Hake S, Tsiantis M. 2002. The gibberellin pathway mediates KNOTTED1-type homeobox function in plants with different body plans. *Curr. Biol.* 12:1557–65
46. Helariutta Y, Fukaki H, Wysocka-Diller J, Nakajima K, Jung J, et al. 2000. The *SHORT-ROOT* gene controls radial patterning of the *Arabidopsis* root through radial signaling. *Cell* 101:555–67
47. Hibara K, Karim MR, Takada S, Taoka K, Furutani M, et al. 2006. *Arabidopsis CUP-SHAPED COTYLEDON3* regulates postembryonic shoot meristem and organ boundary formation. *Plant Cell* 18:2946–57
48. Hu TX, Yu M, Zhao J. 2010. Comparative transcriptional profiling analysis of the two daughter cells from tobacco zygote reveals the transcriptome differences in the apical and basal cells. *BMC Plant Biol.* 10:167
49. Huang F, Zago MK, Abas L, van Marion A, Galvan-Ampudia CS, Offringa R. 2010. Phosphorylation of conserved PIN motifs directs *Arabidopsis* PIN1 polarity and auxin transport. *Plant Cell* 22:1129–42
50. Ingouff M, Hamamura Y, Gourgues M, Higashiyama T, Berger F. 2007. Distinct dynamics of HISTONE3 variants between the two fertilization products in plants. *Curr. Biol.* 17:1032–37
51. Ingouff M, Rademacher S, Holec S, Soljic L, Xin N, et al. 2010. Zygotic resetting of the HISTONE 3 variant repertoire participates in epigenetic reprogramming in *Arabidopsis*. *Curr. Biol.* 20:2137–43
52. Ingram GC, Boisnard-Lorig C, Dumas C, Rogowsky PM. 2000. Expression patterns of genes encoding HD-ZipIV homeo domain proteins define specific domains in maize embryos and meristems. *Plant J.* 22:401–14
53. Ingram GC, Magnard JL, Vergne P, Dumas C, Rogowsky PM. 1999. *ZmOCL1*, an HDGL2 family homeobox gene, is expressed in the outer cell layer throughout maize development. *Plant Mol. Biol.* 40:343–54
54. Ito M, Sentoku N, Nishimura A, Hong SK, Sato Y, Matsuoka M. 2002. Position dependent expression of *GL2*-type homeobox gene, *Roc1*: significance for protoderm differentiation and radial pattern formation in early rice embryogenesis. *Plant J.* 29:497–507
55. Iwakawa H, Ueno Y, Semiarti E, Onouchi H, Kojima S, et al. 2002. The *ASYMMETRIC LEAVES2* gene of *Arabidopsis thaliana*, required for formation of a symmetric flat leaf lamina, encodes a member of a novel family of proteins characterized by cysteine repeats and a leucine zipper. *Plant Cell Physiol.* 43:467–78
56. Jahnke S, Scholten S. 2009. Epigenetic resetting of a gene imprinted in plant embryos. *Curr. Biol.* 19:1677–81
57. Jasinski S, Piazza P, Craft J, Hay A, Woolley L, et al. 2005. KNOX action in *Arabidopsis* is mediated by coordinate regulation of cytokinin and gibberellin activities. *Curr. Biol.* 15:1560–65
58. Jeong S, Palmer TM, Lukowitz W. 2011. The RWP-RK factor *GROUNDED* promotes embryonic polarity by facilitating YODA MAP kinase signaling. *Curr. Biol.* 21:1268–76
59. Jiang K, Feldman LJ. 2005. Regulation of root apical meristem development. *Annu. Rev. Cell Dev. Biol.* 21:485–509
60. Johnson KL, Degnan KA, Ross Walker J, Ingram GC. 2005. *AtDEK1* is essential for specification of embryonic epidermal cell fate. *Plant J.* 44:114–27
61. Johnson KL, Faulkner C, Jeffree CE, Ingram GC. 2008. The phytocalpain Defective Kernel 1 is a novel *Arabidopsis* growth regulator whose activity is regulated by proteolytic processing. *Plant Cell* 20:2619–30
62. Johri BM. 1984. *Embryology of Angiosperms*. Berlin: Springer-Verlag
63. Johri BM, Ambegaokar KB, Srivastava PS. 1992. *Comparative Embryology of Angiosperms*. Berlin: Springer-Verlag
64. Jouannic S, Collin M, Vidal B, Verdeil JL, Tregear JW. 2007. A class I KNOX gene from the palm species *Elaeis guineensis* (Arecaceae) is associated with meristem function and a distinct mode of leaf dissection. *New Phytol.* 174:551–68
65. Jun JH, Ha CM, Fletcher JC. 2010. BLADE-ON-PETIOLE1 coordinates organ determinacy and axial polarity in *Arabidopsis* by directly activating ASYMMETRIC LEAVES2. *Plant Cell* 22:62–76
66. Jürgens G, Mayer U. 1994. *Arabidopsis*. In *A Colour Atlas of Developing Embryos*, ed. JBL Bard, pp. 7–21. London: Wolfe

67. Kamiya N, Itoh J-I, Morikami A, Nagato Y, Matsuoka M. 2003. The *SCARECROW* gene's role in asymmetric cell divisions in rice plants. *Plant J.* 36:45–54
68. Kamiya N, Nagasaki H, Morikami A, Sato Y, Matsuoka M. 2003. Isolation and characterization of a rice *WUSCHEL*-type homeobox gene that is specifically expressed in the central cells of a quiescent center in the root apical meristem. *Plant J.* 35:429–41
69. Kerstetter RA, Bollman K, Taylor RA, Bomblies K, Poethig RS. 2001. *KANADI* regulates organ polarity in *Arabidopsis*. *Nature* 411:706–9
70. Kieffer M, Stern Y, Cook H, Clerici E, Maulbetsch C, et al. 2006. Analysis of the transcription factor WUSCHEL and its functional homologue in *Antirrhinum* reveals a potential mechanism for their roles in meristem maintenance. *Plant Cell* 18:560–73
71. Kinoshita A, Betsuyaku S, Osakabe Y, Mizuno S, Nagawa S, et al. 2010. RPK2 is an essential receptor-like kinase that transmits the CLV3 signal in *Arabidopsis*. *Development* 137:3911–20
72. Kirch T, Simon R, Grünewald M, Werr W. 2003. The *DORNRÖSCHEN/ENHANCER OF SHOOT REGENERATION1* gene of Arabidopsis acts in the control of meristem cell fate and lateral organ development. *Plant Cell* 15:694–705
73. Krogan NT, Long JA. 2009. Why so repressed? Turning off transcription during plant growth and development. *Curr. Opin. Plant Biol.* 12:628–36
74. Kumlehn J, Lörz H, Kranz E. 1999. Monitoring individual development of isolated wheat zygotes: a novel approach to study early embryogenesis. *Protoplasma* 208:156–62
75. Kurakawa T, Ueda N, Maekawa M, Kobayashi K, Kojima M, et al. 2007. Direct control of shoot meristem activity by a cytokinin-activating enzyme. *Nature* 445:652–55
76. Lau S, De Smet I, Kolb M, Meinhardt H, Jürgens G. 2011. Auxin triggers a genetic switch. *Nat. Cell Biol.* 13:611–15
77. Laufs P, Peaucelle A, Morin H, Traas J. 2004. MicroRNA regulation of the CUC genes is required for boundary size control in *Arabidopsis* meristems. *Development* 131:4311–22
78. Laux T, Mayer KFX, Berger J, Jürgens G. 1996. The *WUSCHEL* gene is required for shoot and floral meristem integrity in *Arabidopsis*. *Development* 122:87–96
79. Leibfried A, To JP, Busch W, Stehling S, Kehle A, et al. 2005. WUSCHEL controls meristem function by direct regulation of cytokinin-inducible response regulators. *Nature* 438:1172–75
80. Lenhard M, Jürgens G, Laux T. 2002. The *WUSCHEL* and *SHOOTMERISTEMLESS* genes fulfil complementary roles in *Arabidopsis* shoot meristem regulation. *Development* 129:3195–206
81. Lid SE, Olsen L, Nestestog R, Aukerman M, Brown RC, et al. 2005. Mutation in the *Arabidopisis thaliana DEK1* calpain gene perturbs endosperm and embryo development while over-expression affects organ development globally. *Planta* 221:339–51
82. Lim J, Helariutta Y, Specht CD, Jung J, Sims L, et al. 2000. Molecular analysis of the *SCARECROW* gene in maize reveals a common basis for radial patterning in diverse meristems. *Plant Cell* 12:1307–18
83. Lim J, Jung JW, Lim CE, Lee M-H, Kim BJ, et al. 2005. Conservation and diversification of *SCARECROW* in maize. *Plant Mol. Biol.* 59:619–30
84. Lin WC, Shuai B, Springer PS. 2003. The Arabidopsis *LATERAL ORGAN BOUNDARIES*–domain gene *ASYMMETRIC LEAVES2* functions in the repression of *KNOX* gene expression and in adaxial-abaxial patterning. *Plant Cell* 15:2241–52
85. Long JA, Moan EI, Medford JI, Barton MK. 1996. A member of the KNOTTED class of homeodomain proteins encoded by the *STM* gene of *Arabidopsis*. *Nature* 379:66–69
86. Long JA, Ohno C, Smith ZR, Meyerowitz EM. 2006. TOPLESS regulates apical embryonic fate in *Arabidopsis*. *Science* 312:1520–23
87. Long JA, Woody S, Poethig S, Meyerowitz EM, Barton MK. 2002. Transformation of shoots into roots in *Arabidopsis* embryos mutant at the *TOPLESS* locus. *Development* 129:2797–806
88. Lu P, Porat R, Nadeau JA, O'Neill SD. 1996. Identification of a meristem L1 layer-specific gene in Arabidopsis that is expressed during embryonic pattern formation and defines a new class of homeobox genes. *Plant Cell* 8:2155–68
89. Lukowitz W, Roeder A, Parmenter D, Somerville C. 2004. A MAPKK kinase gene regulates extra-embryonic cell fate in *Arabidopsis*. *Cell* 116:109–19

90. Luo M, Taylor JM, Spriggs A, Zhang H, Wu X, et al. 2011. A genome-wide survey of imprinted genes in rice seeds reveals imprinting primarily occurs in the endosperm. *PLoS Genet.* 7:e1002125
91. Lynn K, Fernandez A, Aida M, Sedbrook J, Tasaka M, et al. 1999. The *PINHEAD/ZWILLE* gene acts pleiotropically in *Arabidopsis* development and has overlapping functions with the *ARGONAUTE1* gene. *Development* 126:469–81
92. Mallory AC, Dugas DV, Bartel DP, Bartel B. 2004. MicroRNA regulation of NAC-domain targets is required for proper formation and separation of adjacent embryonic, vegetative, and floral organs. *Curr. Biol.* 14:1035–46
93. Mallory AC, Reinhart BJ, Jones-Rhoades MW, Tang G, Zamore PD, et al. 2004. MicroRNA control of *PHABULOSA* in leaf development: importance of pairing to the microRNA 5′ region. *EMBO J.* 23:3356–64
94. Mansfield SG, Briarty LG. 1991. Early embryogenesis in *Arabidopsis thaliana*. II. The developing embryo. *Can. J. Bot.* 69:461–76
95. Mansfield SG, Briarty LG, Erni S. 1991. Early embryogenesis in *Arabidopsis thaliana*. I. The mature embryo sack. *Can. J. Bot.* 69:447–60
96. Mao G, Meng X, Liu Y, Zheng Z, Chen Z, Zhang S. 2011. Phosphorylation of a WRKY transcription factor by two pathogen-responsive MAPKs drives phytoalexin biosynthesis in *Arabidopsis*. *Plant Cell* 23:1639–53
97. Mayer KFX, Schoof H, Haecker A, Lenhard M, Jürgens G, Laux T. 1998. Role of *WUSCHEL* in regulating stem cell fate in the *Arabidopsis* shoot meristem. *Cell* 95:805–15
98. Mayer U, Büttner G, Jürgens G. 1993. Apical-basal pattern formation in the *Arabidopsis* embryo: studies on the role of the *gnom* gene. *Development* 117:149–62
99. McConnell JR, Barton MK. 1998. Leaf polarity and meristem formation in *Arabidopsis*. *Development* 125:2935–42
100. McConnell JR, Emery J, Eshed Y, Bao N, Bowman J, Barton MK. 2001. Role of *PHABULOSA* and *PHAVOLUTA* in determining radial patterning in shoots. *Nature* 411:709–13
101. Meyer S, Scholten S. 2007. Equivalent parental contribution to early plant zygotic development. *Curr. Biol.* 17:1686–91
102. Michniewicz M, Zago MK, Abas L, Weijers D, Schweighofer A, et al. 2007. Antagonistic regulation of PIN phosphorylation by PP2A and PINOID directs auxin flux. *Cell* 130:1044–56
103. Mogensen HL, Suthar HK. 1979. Ultrastructure of the egg apparatus of *Nicotiana tabacum* (Solanaceae) before and after fertilization. *Bot. Gaz.* 140:168–79
104. Moussian B, Schoof H, Haecker A, Jürgens G, Laux T. 1998. Role of the *ZWILLE* gene in the regulation of central shoot meristem cell fate during *Arabidopsis* embryogenesis. *EMBO J.* 17:1799–809
105. Müller B, Sheen J. 2008. Cytokinin and auxin interaction in root stem-cell specification during early embryogenesis. *Nature* 453:1094–97
106. Nakajima K, Sena G, Nawy T, Benfey PN. 2001. Intercellular movement of the putative transcription factor SHR in root patterning. *Nature* 413:307–11
107. Nardmann J, Werr W. 2006. The shoot stem cell niche in angiosperms: expression patterns of *WUS* orthologues in rice and maize imply major modifications in the course of mono- and dicot evolution. *Mol. Biol. Evol.* 23:2492–504
108. Nawy T, Bayer M, Mravec J, Friml J, Birnbaum KD, Lukowitz W. 2010. The GATA factor *HANABA TARANU* is required to position the proembryo boundary in the early *Arabidopsis* embryo. *Dev. Cell* 19:103–13
109. Ni J, Clark SE. 2006. Evidence for functional conservation, sufficiency, and proteolytic processing of the CLAVATA3 CLE domain. *Plant Physiol.* 140:726–33
110. Ning J, Peng XB, Qu LH, Xin HP, Yan TT, Sun M. 2006. Differential gene expression in egg cells and zygotes suggests that the transcriptome is restructed before the first zygotic division in tobacco. *FEBS Lett.* 580:1747–52
111. Nodine MD, Bartel DP. 2010. MicroRNAs prevent precocious gene expression and enable pattern formation during plant embryogenesis. *Genes Dev.* 24:2678–92
112. Nodine MD, Yadegari R, Tax FE. 2007. *RPK1* and *TOAD2* are two receptor-like kinases redundantly required for *Arabidopsis* embryonic pattern formation. *Dev. Cell* 12:943–56

113. Okamoto T, Scholten S, Lorz H, Kranz E. 2005. Identification of genes that are up- or down-regulated in the apical or basal cell of maize two-celled embryos and monitoring their expression during zygote development by a cell manipulation- and PCR-based approach. *Plant Cell Physiol.* 46:332–38
114. Olson AR, Cass DD. 1981. Changes in megagametophyte structure in *Papaver nudicaule* L. (Papaveraceae) following in vitro placental pollination. *Am. J. Bot.* 68:1333–41
115. Pauwels L, Barbero GF, Geerinck J, Tilleman S, Grunewald W, et al. 2010. NINJA connects the co-repressor TOPLESS to jasmonate signalling. *Nature* 464:788–91
116. Prigge MJ, Otsuga D, Alonso JM, Ecker JR, Drews GN, Clark SE. 2005. Class III homeodomain-leucine zipper gene family members have overlapping, antagonistic, and distinct roles in Arabidopsis development. *Plant Cell* 17:61–76
117. Rademacher E, Möller B, Lokerse AS, Llavata-Peris CI, van den Berg W, Weijers D. 2011. A cellular expression map of the *Arabidopsis AUXIN RESPONSE FACTOR* gene family. *Plant J.* 68:597–606
118. Raissig MT, Baroux C, Grossniklaus U. 2011. Regulation and flexibility of genomic imprinting during seed development. *Plant Cell* 23:16–26
119. Rhoades MW, Reinhart BJ, Lim LP, Burge CB, Bartel B, Bartel DP. 2002. Prediction of plant microRNA targets. *Cell* 110:513–20
120. Ronceret A, Gadea-Vacas J, Guilleminot J, Lincker F, Delorme V, et al. 2008. The first zygotic division in Arabidopsis requires *de novo* transcription of thymidylate kinase. *Plant J.* 53:776–89
121. Rutjens B, Bao D, van Eck-Stouten E, Brand M, Smeekens S, Proveniers M. 2009. Shoot apical meristem function in Arabidopsis requires the combined activities of three BEL1-like homeodomain proteins. *Plant J.* 58:641–54
122. Sarkar AK, Luijten M, Miyashima S, Lenhard M, Hashimoto T, et al. 2007. Conserved factors regulate signalling in *Arabidopsis thaliana* shoot and root stem cell organizers. *Nature* 446:811–14
123. Sato A, Toyooka K, Okamoto T. 2010. Asymmetric cell division of rice zygotes located in embryo sac and produced by in vitro fertilization. *Sex. Plant Reprod.* 23:211–17
124. Sato Y, Hong SK, Tagiri A, Kitano H, Yamamoto N, et al. 1996. A rice homeobox gene, *OSH1*, is expressed before organ differentiation in a specific region during early embryogenesis. *Proc. Natl. Acad. Sci. USA* 93:8117–22
125. Sauter M, von Wiegen P, Lörz H, Kranz E. 1998. Cell cycle regulatory genes from maize are differentially controlled during fertilization and first embryonic cell division. *Sex. Plant Reprod.* 11:41–48
126. Scheres B, Di Laurenzio L, Willemsen V, Hauser MT, Janmaat K, et al. 1995. Mutations affecting the radial organisation of the *Arabidopsis* root display specific defects throughout the embryonic axis. *Development* 121:53–62
127. Scheres B, Wolkenfelt H, Willemsen V, Terlouw M, Lawson E, et al. 1994. Embryonic origin of the *Arabidopsis* primary root and root meristem initials. *Development* 120:2475–87
128. Schlereth A, Möller B, Liu W, Kientz M, Flipse J, et al. 2010. MONOPTEROS controls embryonic root initiation by regulating a mobile transcription factor. *Nature* 464:913–16
129. Schneeberger R, Tsiantis M, Freeling M, Langdale JA. 1998. The *rough sheath2* gene negatively regulates homeobox gene expression during maize leaf development. *Development* 125:2857–65
130. Scholten S, Lorz H, Kranz E. 2002. Paternal mRNA and protein synthesis coincides with male chromatin decondensation in maize zygotes. *Plant J.* 32:221–31
131. Schulz R, Jensen WA. 1968. Capsella embryogenesis: the egg, zygote, and young embryo. *Am. J. Bot.* 55:807–19
132. Shevell DE, Leu WM, Gillmor CS, Xia G, Feldmann KA, Chua NH. 1994. *EMB30* is essential for normal cell division, cell expansion, and cell adhesion in Arabidopsis and encodes a protein that has similarity to Sec7. *Cell* 77:1051–62
133. Sivaramakrishna D. 1977. Size relationships of apical cell and basal cell in two-celled embryos in angiosperms. *Can. J. Bot.* 56:1434–38
134. Smith LG, Jackson D, Hake S. 1995. Expression of *knotted1* marks shoot meristem formation during maize embryogenesis. *Dev. Genet.* 16:344–48
135. Smith ZR, Long JA. 2010. Control of *Arabidopsis* apical-basal embryo polarity by antagonistic transcription factors. *Nature* 464:423–26

136. Souer E, van Houwelingen A, Kloos D, Mol J, Koes R. 1996. The *No Apical Meristem* gene of Petunia is required for pattern formation in embryos and flowers and is expressed at meristem and primordia boundaries. *Cell* 85:159–70
137. Spinelli SV, Martin AP, Viola IL, Gonzalez DH, Palatnik JF. 2011. A mechanistic link between *STM* and *CUC1* during *Arabidopsis* development. *Plant Physiol.* 156:1894–904
138. Stahl Y, Wink RH, Ingram GC, Simon R. 2009. A signaling module controlling the stem cell niche in *Arabidopsis* root meristems. *Curr. Biol.* 19:909–14
139. Stepanova AN, Robertson-Hoyt J, Yun J, Benavente LM, Xie DY, et al. 2008. *TAA1*-mediated auxin biosynthesis is essential for hormone crosstalk and plant development. *Cell* 133:177–91
140. Stuurman J, Jaggi F, Kuhlemeier C. 2002. Shoot meristem maintenance is controlled by a *GRAS*-gene mediated signal from differentiating cells. *Genes Dev.* 16:2213–18
141. Szemenyei H, Hannon M, Long JA. 2008. TOPLESS mediates auxin-dependent transcriptional repression during *Arabidopsis* embryogenesis. *Science* 319:1384–86
142. Takada S, Hibara K, Ishida T, Tasaka M. 2001. The *CUP-SHAPED COTYLEDON1* gene of *Arabidopsis* regulates shoot apical meristem formation. *Development* 128:1127–35
143. Takada S, Jürgens G. 2007. Transcriptional regulation of epidermal cell fate in the *Arabidopsis* embryo. *Development* 134:1141–50
144. Tanaka H, Onouchi H, Kondo M, Hara-Nishimura I, Nishimura M, et al. 2001. A subtilisin-like serine protease is required for epidermal surface formation in *Arabidopsis* embryos and juvenile plants. *Development* 128:4681–89
145. Tanaka H, Watanabe M, Sasabe M, Hiroe T, Tanaka T, et al. 2007. Novel receptor-like kinase ALE2 controls shoot development by specifying epidermis in *Arabidopsis*. *Development* 134:1643–52
146. Tang G, Reinhart BJ, Bartel DP, Zamore PD. 2003. A biochemical framework for RNA silencing in plants. *Genes Dev.* 17:49–63
147. Torres-Ruiz RA, Jürgens G. 1994. Mutations in the *FASS* gene uncouple pattern formation and morphogenesis in *Arabidopsis* development. *Development* 120:2967–78
148. Treml BS, Winderl S, Radykewicz R, Herz M, Schweizer G, et al. 2005. The gene *ENHANCER OF PINOID* controls cotyledon development in the *Arabidopsis* embryo. *Development* 132:4063–74
149. Tucker MR, Hinze A, Tucker EJ, Takada S, Jürgens G, Laux T. 2008. Vascular signalling mediated by ZWILLE potentiates WUSCHEL function during shoot meristem stem cell development in the *Arabidopsis* embryo. *Development* 135:2839–43
150. Tzafrir I, Pena-Muralla R, Dickerman A, Berg M, Rogers R, et al. 2004. Identification of genes required for embryo development in Arabidopsis. *Plant Physiol.* 135:1206–20
151. Ueda M, Zhang Z, Laux T. 2011. Transcriptional activation of *Arabidopsis* axis patterning genes *WOX8/9* links zygote polarity to embryo development. *Dev. Cell* 20:264–70
152. Vroemen CW, Mordhorst AP, Albrecht C, Kwaaitaal MA, de Vries SC. 2003. The *CUP-SHAPED COTYLEDON3* gene is required for boundary and shoot meristem formation in Arabidopsis. *Plant Cell* 15:1563–77
153. Waites R, Selvadurai HR, Oliver IR, Hudson A. 1998. The *PHANTASTICA* gene encodes a MYB transcription factor involved in growth and dorsoventrality of lateral organs in *Antirrhinum*. *Cell* 93:779–89
154. Waki T, Hiki T, Watanabe R, Hashimoto T, Nakajima K. 2011. The *Arabidopsis* RWP-RK protein RKD4 triggers gene expression and pattern formation in early embryogenesis. *Curr. Biol.* 21:1277–81
155. Wang H, Ngwenyama N, Liu Y, Walker JC, Zhang S. 2007. Stomatal development and patterning are regulated by environmentally responsive mitogen-activated protein kinases in *Arabidopsis*. *Plant Cell* 19:63–73
156. Weijers D, Geldner N, Offringa R, Jürgens G. 2001. Seed development: early paternal gene activity in *Arabidopsis*. *Nature* 414:709–10
157. Weijers D, Schlereth A, Ehrismann JS, Schwank G, Kientz M, Jürgens G. 2006. Auxin triggers transient local signaling for cell specification in *Arabidopsis* embryogenesis. *Dev. Cell* 10:265–70
158. Weijers D, Van Hamburg J-P, Van Rijn E, Hooykaas PJJ, Offringa R. 2003. Diphtheria toxin-mediated cell ablation reveals interregional communication during Arabidopsis seed development. *Plant Physiol.* 133:1882–92

159. Weir I, Lu J, Cook H, Causier B, Schwarz-Sommer Z, Davies B. 2004. *CUPULIFORMIS* establishes lateral organ boundaries in *Antirrhinum*. *Development* 131:915–22
160. Williams L, Grigg SP, Xie M, Christensen S, Fletcher JC. 2005. Regulation of *Arabidopsis* shoot apical meristem and lateral organ formation by microRNA *miR166g* and its *AtHD-ZIP* target genes. *Development* 132:3657–68
161. Wu G, Lin WC, Huang T, Poethig RS, Springer PS, Kerstetter RA. 2008. KANADI1 regulates adaxial-abaxial polarity in *Arabidopsis* by directly repressing the transcription of *ASYMMETRIC LEAVES2*. *Proc. Natl. Acad. Sci. USA* 105:16392–97
162. Wu KL, Guo ZJ, Wang HH, Li J. 2005. The WRKY family of transcription factors in rice and *Arabidopsis* and their origins. *DNA Res.* 12:9–26
163. Wu X, Chory J, Weigel D. 2007. Combinations of *WOX* activities regulate tissue proliferation during *Arabidopsis* embryonic development. *Dev. Biol.* 309:306–16
164. Wysocka-Diller JW, Helariutta Y, Fukaki H, Malamy JE, Benfey PN. 2000. Molecular analysis of SCARECROW function reveals a radial patterning mechanism common to root and shoot. *Development* 127:595–603
165. Xu J, Zhang H-Y, Xie C-H, Xue H-W, Dijkhuis P, Liu C-M. 2005. *EMBRYONIC FACTOR 1* encodes an AMP deaminase and is essential for the zygote to embryo transition in Arabidopsis. *Plant J.* 42:743–56
166. Yanai O, Shani E, Dolezal K, Tarkowski P, Sablowski R, et al. 2005. *Arabidopsis* KNOXI proteins activate cytokinin biosynthesis. *Curr. Biol.* 15:1566–71
167. Yang JY, Chung MC, Tu CY, Leu WM. 2002. *OSTF1*: a HD-GL2 family homeobox gene is developmentally regulated during early embryogenesis in rice. *Plant Cell Physiol.* 43:628–38
168. Yang X, Zhang X. 2010. Regulation of somatic embryogenesis in higher plants. *Crit. Rev. Plant Sci.* 29:36–57
169. Yin Y, Vafeados D, Tao Y, Yoshida S, Asami T, Chory J. 2005. A new class of transcription factors mediates brassinosteroid-regulated gene expression in *Arabidopsis*. *Cell* 120:249–59
170. Zhao J, Xin H, Qu L, Ning J, Peng X, et al. 2011. Dynamic changes of transcript profiles after fertilization are associated with de novo transcription and maternal elimination in tobacco zygote, and mark the onset of the maternal-to-zygotic transition. *Plant J.* 65:131–45
171. Zhou G-K, Kubo M, Zhong R, Demura T, Ye Z-H. 2007. Overexpression of miR165 affects apical meristem formation, organ polarity establishment and vascular development in *Arabidopsis*. *Plant Cell Physiol.* 48:391–404
172. Zhu H, Hu F, Wang R, Zhou X, Sze SH, et al. 2011. *Arabidopsis* Argonaute10 specifically sequesters miR166/165 to regulate shoot apical meristem development. *Cell* 145:242–56
173. Zimmermann R, Werr W. 2005. Pattern formation in the monocot embryo as revealed by *NAM* and *CUC3* orthologues from *Zea mays* L. *Plant Mol. Biol.* 58:669–85

Annual Review of Plant Biology
Volume 63, 2012

Contents

There Ought to Be an Equation for That
Joseph A. Berry 1

Photorespiration and the Evolution of C_4 Photosynthesis
Rowan F. Sage, Tammy L. Sage, and Ferit Kocacinar 19

The Evolution of Flavin-Binding Photoreceptors: An Ancient Chromophore Serving Trendy Blue-Light Sensors
Aba Losi and Wolfgang Gärtner 49

The Shikimate Pathway and Aromatic Amino Acid Biosynthesis in Plants
Hiroshi Maeda and Natalia Dudareva 73

Regulation of Seed Germination and Seedling Growth by Chemical Signals from Burning Vegetation
David C. Nelson, Gavin R. Flematti, Emilio L. Ghisalberti, Kingsley W. Dixon, and Steven M. Smith 107

Iron Uptake, Translocation, and Regulation in Higher Plants
Takanori Kobayashi and Naoko K. Nishizawa 131

Plant Nitrogen Assimilation and Use Efficiency
Guohua Xu, Xiaorong Fan, and Anthony J. Miller 153

Vacuolar Transporters in Their Physiological Context
Enrico Martinoia, Stefan Meyer, Alexis De Angeli, and Réka Nagy 183

Autophagy: Pathways for Self-Eating in Plant Cells
Yimo Liu and Diane C. Bassham 215

Plasmodesmata Paradigm Shift: Regulation from Without Versus Within
Tessa M. Burch-Smith and Patricia C. Zambryski 239

Small Molecules Present Large Opportunities in Plant Biology
Glenn R. Hicks and Natasha V. Raikhel 261

Genome-Enabled Insights into Legume Biology
Nevin D. Young and Arvind K. Bharti 283

Synthetic Chromosome Platforms in Plants
Robert T. Gaeta, Rick E. Masonbrink, Lakshminarasimhan Krishnaswamy, Changzeng Zhao, and James A. Birchler 307

Epigenetic Mechanisms Underlying Genomic Imprinting in Plants
Claudia Köhler, Philip Wolff, and Charles Spillane 331

Cytokinin Signaling Networks
Ildoo Hwang, Jen Sheen, and Bruno Müller 353

Growth Control and Cell Wall Signaling in Plants
Sebastian Wolf, Kian Hématy, and Herman Höfte 381

Phosphoinositide Signaling
Wendy F. Boss and Yang Ju Im 409

Plant Defense Against Herbivores: Chemical Aspects
Axel Mithöfer and Wilhelm Boland 431

Plant Innate Immunity: Perception of Conserved Microbial Signatures
Benjamin Schwessinger and Pamela C. Ronald 451

Early Embryogenesis in Flowering Plants: Setting Up the Basic Body Pattern
Steffen Lau, Daniel Slane, Ole Herud, Jixiang Kong, and Gerd Jürgens 483

Seed Germination and Vigor
Loïc Rajjou, Manuel Duval, Karine Gallardo, Julie Catusse, Julia Bally, Claudette Job, and Dominique Job 507

A New Development: Evolving Concepts in Leaf Ontogeny
Brad T. Townsley and Neelima R. Sinha 535

Control of *Arabidopsis* Root Development
Jalean J. Petricka, Cara M. Winter, and Philip N. Benfey 563

Mechanisms of Stomatal Development
Lynn Jo Pillitteri and Keiko U. Torii 591

Plant Stem Cell Niches
Ernst Aichinger, Noortje Kornet, Thomas Friedrich, and Thomas Laux 615

The Effects of Tropospheric Ozone on Net Primary Productivity and Implications for Climate Change
Elizabeth A. Ainsworth, Craig R. Yendrek, Stephen Sitch, William J. Collins, and Lisa D. Emberson 637

Quantitative Imaging with Fluorescent Biosensors
Sakiko Okumoto, Alexander Jones, and Wolf B. Frommer 663

Herud, O., D. Weijers, S. Lau and G. Jürgens (2016). "Auxin responsiveness of the MONOPTEROS-BODENLOS module in primary root initiation critically depends on the nuclear import kinetics of the Aux/IAA inhibitor BODENLOS." Plant J. 85, 269-277.

the plant journal

SEB Society for Experimental Biology

The Plant Journal (2016) **85,** 269–277 doi: 10.1111/tpj.13108

Auxin responsiveness of the MONOPTEROS-BODENLOS module in primary root initiation critically depends on the nuclear import kinetics of the Aux/IAA inhibitor BODENLOS

Ole Herud[1], Dolf Weijers[2,†], Steffen Lau[1] and Gerd Jürgens[1,2,*]

[1]*Department of Cell Biology, Max Planck Institute for Developmental Biology, Tübingen 72076, Germany, and*

[2]*Department of Developmental Genetics, Center for Plant Molecular Biology, University of Tübingen, Tübingen 72076, Germany*

Received 27 October 2015; revised 7 December 2015; accepted 14 December 2015; published online 30 December 2015.

*For correspondence (e-mail gerd.juergens@zmbp.uni-tuebingen.de)

†Present address: Laboratory of Biochemistry, Wageningen University, Wageningen, The Netherlands.

SUMMARY

Primary root formation in early embryogenesis of *Arabidopsis thaliana* is initiated with the specification of a single cell called hypophysis. This initial step requires the auxin-dependent release of the transcription factor MONOPTEROS (MP, also known as ARF5) from its inhibition by the Aux/IAA protein BODENLOS (BDL, also known as IAA12). Auxin-insensitive *bdl* mutant embryos and *mp* loss-of-function embryos fail to specify the hypophysis, giving rise to rootless seedlings. A suppressor screen of rootless *bdl* mutant seedlings yielded a mutation in the nuclear import receptor *IMPORTIN-ALPHA 6* (*IMPα6*) that promoted primary root formation through rescue of the embryonic hypophysis defects, without causing additional phenotypic changes. Aux/IAA proteins are continually synthesized and degraded, which is essential for rapid transcriptional responses to changing auxin concentrations. Nuclear translocation of bdl:3×GFP was slowed down in *impα6* mutants as measured by fluorescence recovery after photobleaching (FRAP) analysis, which correlated with the reduced inhibition of *MP* by *bdl* in transient expression assays in *impα6* knock-down protoplasts. The MP–BDL module acts like an auxin-triggered genetic switch because MP activates its own expression as well as the expression of its inhibitor BDL. Using an established simulation model, we determined that the reduced nuclear translocation rate of BDL in *impα6* mutant embryos rendered the auxin-triggered switch unstable, impairing the fast response to changes in auxin concentration. Our results suggest that the instability of the inhibitor BDL necessitates a fast nuclear uptake in order to reach the critical threshold level required for auxin responsiveness of the MP–BDL module in primary root initiation.

Keywords: auxin, BODENLOS, MONOPTEROS, import, *Arabidopsis thaliana*, IMPORTIN-ALPHA 6.

INTRODUCTION

Initiation of the primary root meristem is the most thoroughly studied process of cell specification in *Arabidopsis thaliana* early embryogenesis (reviewed by Lau *et al.*, 2012). As a first step, the asymmetric division of the zygote gives rise to an apical lineage corresponding to the proembryo and a basal lineage generating a short file of extra-embryonic cells known as suspensor. At the 32-cell stage, the uppermost derivative of the suspensor changes cell fate to become the hypophysis, which by asymmetric division gives rise to the quiescent centre of the primary root meristem. The plant signalling molecule auxin plays a prominent role in this cell specification process.

The auxin response during primary root meristem initiation is mediated by the MONOPTEROS (MP)-BODENLOS (BDL) module as both, knock-out mutation of MP or a stabilized version of BDL, inhibit hypophysis specification (Hamann *et al.*, 1999, 2002). Auxin triggers the degradation of the Aux/IAA protein BDL (IAA12), whereby the auxin response factor MP (ARF5) gets released and in turn activates its target genes including *MP* itself and its inhibitor *BDL*. This feedback loop enables the MP–BDL module to be switched on in response to rising auxin concentration, which in turn mediates cell specification and primary root meristem initiation (Schlereth *et al.*, 2010; Lau *et al.*, 2011).

The ratio of MP to BDL appears to be critical in the auxin responsiveness of the module. A single copy of the gain-of-function *bdl* mutant allele is not sufficient to block MP action during auxin response (Hamann *et al.*, 2002).

Conversely, the root meristem initiation defect of *bdl* homozygous mutant embryos can be rescued by MP overexpression (Weijers *et al.*, 2006).

The role of the MP–BDL module during primary root meristem development is limited in space and time, mediating auxin response in inner cells of the proembryo that is required before the asymmetric division of the adjacent hypophysis (Weijers *et al.*, 2006). This local action of the module entails PIN1-dependent auxin transport to the hypophysis and also leads to the expression and subsequent movement of the non-cell-autonomously acting bHLH transcription factor TMO7 into the hypophysis (Schlereth *et al.*, 2010).

Transcriptional response to auxin occurs in the nucleus, where auxin mediates the interaction between F-box proteins TIR1 or AFBs of E3 ubiquitin ligases (SCF-TIR1/AFB) and the relevant Aux/IAA inhibitors, resulting in the ubiquitination and subsequent proteasomal degradation of the inhibitors (Salehin *et al.*, 2015). Consequently, the formerly inhibited ARF transcription factors are released and able to regulate the transcription of target genes.

Here, we report the characterization of a suppressor of the *bdl* mutant, which was isolated in a screen for EMS-induced mutants that rescue the primary root meristem initiation defect in *bdl* mutant embryos. The suppressor mutation reduced the activity of the *IMPORTIN-ALPHA 6* (*IMPα6*) gene, a component of the nuclear import machinery. The analysis of additional *impα6* mutant alleles, quantitative gene expression studies and fluorescence recovery after photobleaching (FRAP) analysis of nuclear uptake of bdl, all support the conclusion that fast nuclear import of BDL is a critical parameter of the MP–BDL module in its auxin-dependent action mediating primary root meristem initiation.

RESULTS

Screen for regulators of *bdl*

Arabidopsis plants hemizygous for a *pBDL::bdl:GUS* transgene (henceforth also referred to as *bdl:GUS* or simply *bdl*) were mutagenized with ethyl methanesulfonate (EMS) and the seedling progeny of individual plants (M2 families) was screened for the presence or absence of the primary root. We isolated several mutations that reduced the percentage of seedlings lacking the primary root. Instead of 21% in the non-mutagenized *bdl:GUS* parental line, only 7% of the progeny in line B2951 failed to establish the primary root (Figure 1a). The remaining rootless seedlings in B2951 did not differ from the rootless seedlings in the parental line. The suppressor mutation is recessive, and there were no other phenotypic differences between the parental and the B2951 line (Figures 1b and S1a).

The absence of the primary root in *bdl* mutant seedlings correlates with the failure to establish the hypophysis in early embryogenesis (Hamann *et al.*, 1999). Therefore, we

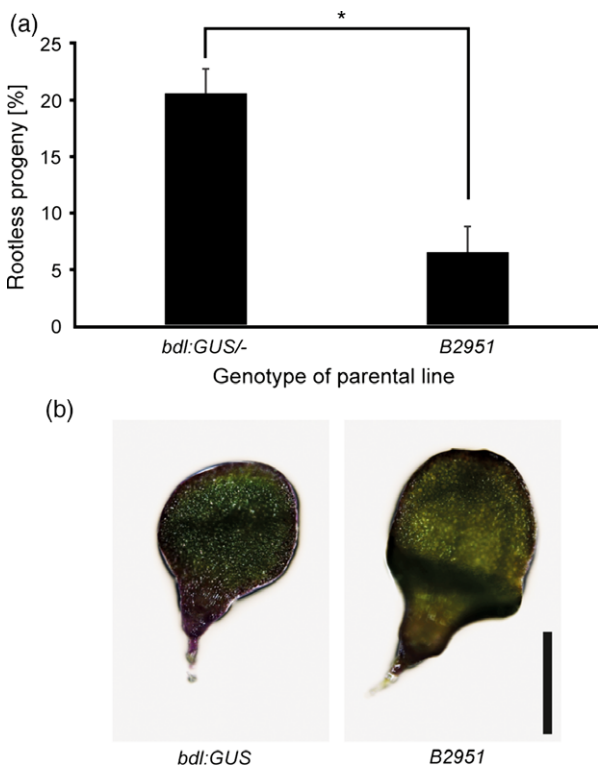

Figure 1. The *B2951* mutation rescues the *bdl* phenotype.
(a) Proportion of rootless seedlings in the progeny of *pBDL::bdl:GUS*/- and *pBDL::bdl:GUS*/- *B2951* plants. Error bars indicate standard deviation. *Indicates $P < 0.05$ according to Student's *t*-test. $N = 3293$.
(b) Seedling phenotype rootless seedling 6 days after germination. Scale bar represents 0.1 cm.

analysed the division of the uppermost suspensor cell, which normally becomes the hypophysis, in both the parental and the B2951 line. The proportion of aberrant vertical divisions of the hypophysis – a hallmark of the *bdl* mutant embryo – was reduced to a similar extent as was the proportion of rootless seedlings (Table 1 and Figure S1b). This result indicated that the specification of the hypophysis was rescued in the B2951 line, suggesting that the suppressor mutation directly affected the action of the MP–BDL module during primary root initiation (Weijers *et al.*, 2006; Schlereth *et al.*, 2010).

Primary root initiation is restored in bdl embryos by a mutation in IMPORTIN-ALPHA 6

The gene harbouring the *B2951* mutation was identified by map-based cloning. The *B2951* mutation was mapped to a 43 kilobase-pair (kb) region between the markers DNAJ

Table 1 Horizontal hypophysis divisions are rescued in B2951

	Horizontal (%)	Vertical (%)	*N*
pBDL::bdl:GUS/-	74	26	54
pBDL::bdl:GUS/- *B2951*	92	8	53

and T14P on the upper arm of chromosome 1 (Figure S2a). We sequenced all 16 open reading frames within that region and identified a mutation in the karyopherin gene *IMPORTIN-ALPHA 6* (*IMPα6*). The causative mutation was named *impα6-1* and has a single guanine-to-adenine substitution at an intron–exon junction, which likely destroys the splice acceptor site of exon 8 (Figure 2a). IMPα6 has 10 predicted Armadillo (ARM) repeats (Wirthmueller *et al.*, 2013), suggesting a similar structure and nuclear-localization sequence (NLS)-binding mode as reported for importin α proteins from mouse, yeast or rice (Conti *et al.*, 1998; Kobe, 1999; Chang *et al.*, 2012). The abnormal splicing in the mutant would delete the last four ARM repeats and thereby most likely destroys the NLS binding ability (Figure 2a). Reverse transcription (RT)-PCR revealed reduced *IMPα6* mRNA levels in *impα6-1*, suggesting that *impα6-1* is a knock-down allele (Figure S2b).

To examine whether the rescue of the rootless phenotype was caused by the dysfunctional *impα6-1* allele, we complemented the mutation with a genomic transgene including the endogenous 2.4 kb promoter (*gIMPα6*). For localization and expression studies, we additionally generated a fusion protein of IMPα6 with three copies of green fluorescent protein (3×GFP) expressed from the same promoter (*IMPα6:3×GFP*). Both constructs significantly increased the fraction of rootless seedlings in the *bdl impα6-1* mutant background, which indicated that the *impα6-1* mutation was indeed responsible for the suppression of the *bdl* mutant phenotype (Figure 2b).

In addition, we generated an artificial micro RNA (amiRNA) line targeting *IMPα6* and also analysed the T-DNA insertion allele *impα6-2* (Figure 2a). Both mutants were crossed with *pBDL::bdl:GUS*/- lines. We confirmed the absence of *IMPα6* full-length cDNA in *impα6-2* by RT-PCR (Figure S2b) and analysed the proportion of rootless seedlings in the progeny of *pBDL::bdl:GUS*/- *impα6-2* and *pBDL::bdl:GUS*/- *amiRNA* double mutants. The amiRNA did not exhibit a reduced expression in seedlings (Figure S2b), presumably because the RPS5a promoter used for this purpose is mainly active in strongly dividing tissues like embryos (Weijers *et al.*, 2001). In both cases however, the proportion of rootless *bdl:GUS* seedlings was significantly reduced (Figure 2c), providing additional evidence that reduced expression of *IMPα6* caused the rescue of the rootless phenotype of *bdl.*

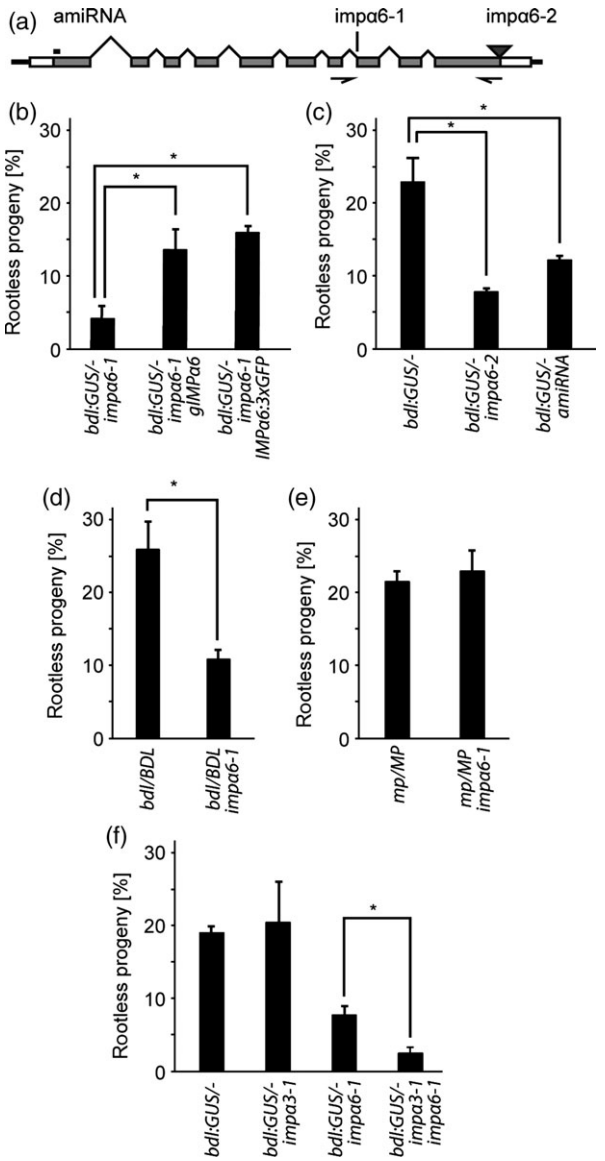

Figure 2. *impα6-1* represses the *bdl* phenotype.
(a) *IMPα6* gene model, major domains and mutated sites are indicated. Arrows indicate primer annealing for RT-PCR.
(b) Restoration of the rootless phenotype by complementation of *impα6-1*. $N = 2920$.
(c) Rescue of the rootless phenotype by additional alleles. $N = 2474$.
(d) Rescue of the original *bdl* allele by *impα6-1*. $N = 1241$.
(e) *impα6-1* does not rescue *mp*. $N = 1767$.
(f) *impα3-1* enhances the rescue of the *bdl* phenotype by *impα6-1*. $N = 2462$.
*Indicates $P < 0.05$ according to Student's *t*-test. Error bars represent standard deviation. Because of the variability of the penetrance, all quantification were compared with controls from the same experiment.

Function of IMPα6 in embryogenesis

Importin α proteins are karyopherins, which are known to facilitate import of proteins into the nucleus (Merkle, 2011). Small proteins like BDL, which is about the size of green fluorescent protein (GFP), are able to slowly diffuse into the nucleus independently of the transport machinery (Mohr *et al.*, 2009). Given that the *impa6-1* mutant was isolated in a *bdl:GUS* background, in which the size of the stabilized bdl protein is increased four-fold, an important question is if the phenotypic suppression is specific to the bdl:GUS protein. Characterization of the progeny of *impα6-1 bdl*/*BDL* plants revealed that about 11% of the seedlings lack the primary root in comparison with 26% of the progeny of *bdl*/*BDL* (Figure 2d). These data show that endoge-

nous bdl action also depends on the nuclear import machinery, specifically on the importin-α isoform *IMPα6.*

To better understand the mechanism, we intended to analyse the specificity of the rescue, confirm the expression of IMPα6 in the embryo and analyse the interaction partner(s) of IMPα6. Root initiation depends on the functionality of the MP–BDL module and its downstream targets. To examine at which step *impα6-1* compromises the auxin response pathway, we crossed *impα6-1* to the strong *mp* B4149 allele. The function of MP is impaired in *bdl*, because bdl constitutively inhibits the auxin-dependent activation of MP target genes (Hamann *et al.*, 2002). Therefore, downstream targets would be affected in a similar way in *mp* as they are in *bdl* mutants. We found no effect on the penetrance of *mp* (Figure 2e), suggesting that neither MP nor its targets are directly affected by *impα6-1.*

BDL is expressed in the inner cells of the proembryo and controls root meristem initiation non-cell-autonomously (Weijers *et al.*, 2006). To confirm that the expression of *IMPα6* overlaps with the expression of *BDL* we used the *IMPα6:3×GFP* construct, which restored the *bdl* mutant phenotype in *the impα6-1 bdl* background. Expression was detected early on in the developing embryo and the fusion protein localized to the nucleus, as expected for an importin α protein (Figure S3a). In addition, we performed RNA *in situ* hybridization with *IMPα6* probes in the embryo and detected a similar, albeit patchier, expression pattern (Figure S3b), overlapping with the expression of BDL and MP in the inner cells of the proembryo (Hamann *et al.*, 2002).

To explore the pathways depending on IMPα6, we performed mass spectrometry after immunoprecipitation of IMPα6:3×GFP. In total, 407 proteins were overrepresented in the dataset, including the importins IMPα1, IMPα2, IMPα7 and SAD2 as well as the nucleoporins nup50A and nup50B. SAD2 is the Arabidopsis importin-beta-domain protein. Vertebrate nup50 has been shown to interact with importin-α, displacing NLS, which suggests a role in importin complex disassembly and importin recycling (Matsuura and Stewart, 2005). Thus, the mass spectrometry analysis confirmed the predicted molecular function of IMP6a as an importin. However, auxin pathway components were not detected (Table S1). This shows that IMPα6 interacts with a wide range of proteins, especially with those of the nuclear transport pathway. To analyse a possible overlap of the function of IMPα6 with other importin α proteins in respect to the transport of bdl, we crossed *impα6-1* with the *impα3-1* mutant, since IMPα3 is the closest homolog of IMPα6 and is also strongly expressed in the embryo (Bhattacharjee *et al.*, 2008; Slane *et al.*, 2014). The *impα3-1* mutant alone did not rescue the root initiation defect of *bdl:GUS*, but further impairment of protein import in the double mutant *impα6-1 impα3* in the *bdl:GUS*/- background reduced the occurrence of rootless seedlings in *impα6-1 bdl:GUS*/- further to 3% (Figure 2f). This indicates that other importin α proteins can take over part of the function of *IMPα6.*

Nuclear translocation of bdl is impaired in *impα6-1* mutant cells

The *bdl* mutation causes constitutive transcriptional repression of MP target genes in the nucleus (Hamann *et al.*, 2002). This repression leads to the misspecification of the hypophysis and is abolished by a mutation in the *IMPα6* gene. The BDL protein has a putative monopartite and a bipartite NLS (Abel and Theologis, 1995), which are predicted to bind importin-α proteins (Chang *et al.*, 2012). This indicates that the nuclear uptake of bdl protein may be impaired in *impα6-1* mutant embryos. Therefore, we compared the localization of *bdl:3×GFP* expressed from the native *BDL* promoter in wild-type (wt) and *impα6-1* mutant embryos. The penetrance of the rootless phenotype of *bdl:3×GFP* transgenic seedlings was reduced from 44% to 27% by the *impα6-1* mutation (Figure S4a). However, *in vivo* confocal imaging revealed nuclear localization of bdl:3×GFP in the proembryo cells (Figure S4b). Therefore, we analysed the localization of bdl:3×GFP quantitatively in seedling root tissues. The intensity of GFP fluorescence in both nucleus and cytoplasm of root vasculature cells was slightly increased in *impα6-1* mutant seedlings (Figure 3a). This is consistent with the increased GUS staining of *impα6-1 bdl:GUS* roots (Figure S4c).

To determine the impact on the subcellular distribution of the bdl:3×GFP fusion protein, we compared the signal ratio of nucleus and cytoplasm between wild-type and *impα6-1* mutant seedlings. At steady state, the ratio of nuclear to cytoplasmic fluorescence was comparable in the two genotypes (Figure 3b). The steady-state distribution represents equilibrium and might not reflect possible differences in nuclear uptake rates. To check if the fast, presumably active, transport is affected, we measured the import speed by FRAP. We bleached the bdl:3×GFP signal in the nuclei and compared the recovery between *impα6-1* and wild-type seedlings. Recovery of the nuclear GFP signal was indeed slower in *impα6-1* (Figure 3b), suggesting that the fast nuclear import of bdl:3×GFP at least partially depends on *IMPα6.* Within the duration of our experiment (27 sec), bdl:3×GFP did not recover the original pre-bleach steady-state ratio of nuclear to cytoplasmic signal of 3.1, but only 1.9 in wild-type and 1.8 in *impα6-1* mutant seedlings (Figure 3b). Because most of the GFP signal was concentrated in the nucleus, the cytoplasmic pool was presumably not sufficient to raise the nuclear intensity again to the same level as prior to bleaching.

The reduced nuclear uptake of bdl impaired the repression of MP-dependent gene activation

To link the reduced nuclear import rate of bdl to the rescue of root initiation in *impα6-1*, we quantitatively analysed the

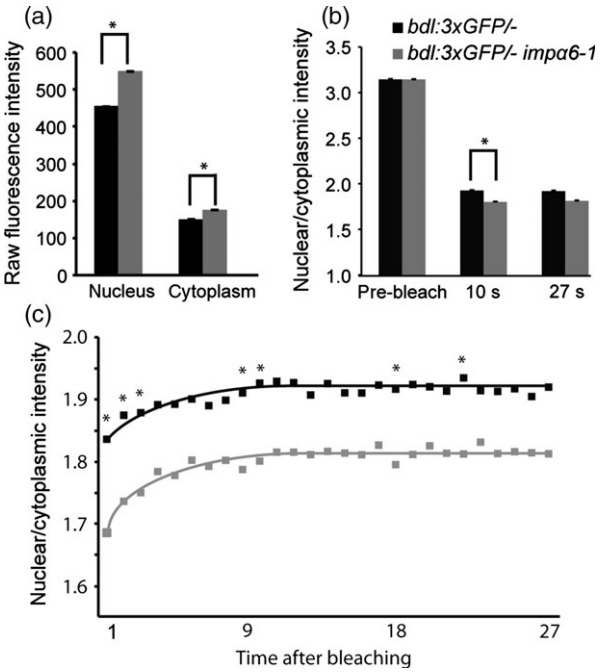

Figure 3. Fluorescence recovery after photobleaching of nucleus.
(a) Raw fluorescence intensity in wild-type (black) and *impα6-1* (grey) background.
(b) Nuclear/cytoplasmic intensity ratio before bleaching and 10 or 27 sec after bleaching.
(c) Time course of nuclear/cytoplasmic intensity ratio after bleaching (sec).
*Indicates significant difference ($P < 0.05$, Student's *t*-test). All error bars indicate standard error. $N = 183$.

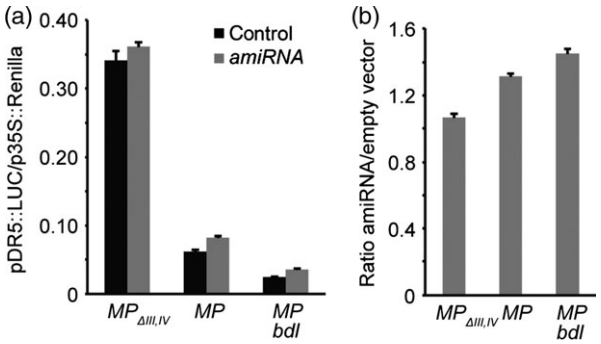

Figure 4. *pDR5::LUC* activity in response to MP and bdl.
(a) Induction of pDR5 by irrepressible $MP_{\Delta III,IV}$, MP, and the repression of MP through bdl in control and *IMPα6* knock-down protoplasts.
(b) Comparison of *pDR5::LUC* expression in protoplasts with or without amiRNA against *IMPα6* and the effect of the repression of MP.
Error bars represent standard error.

effect on the transcription of auxin-regulated genes in a transient protoplast assay (Lau *et al.*, 2011). We measured MP-dependent activation of the artificial auxin-responsive promoter *pDR5* and the repression through co-expression of bdl. To reduce the expression of *IMPα6*, we expressed *IMPα6* amiRNA, which partially rescued the root initiation defect of *bdl:GUS* seedlings (Figures 2c and 4a). The knock-down of *IMPα6* in protoplasts was confirmed by RT-PCR (Figure S2c). Furthermore, as a control for the specific contribution of MP, we expressed truncated MP protein lacking domains III and IV ($MP_{\Delta III,IV}$), which cannot interact with Aux/IAAs and is therefore independent of *bdl* (Lau *et al.*, 2011). $MP_{\Delta III,IV}$ induced the expression of *pDR5::LUC* regardless of the presence or absence of the amiRNA, indicating that $MP_{\Delta III,IV}$ is not a direct target of IMPα6 (Figure 4a, b). Full-length MP protein induced *pDR5::LUC* activity slightly more strongly with than without *IMPα6* amiRNA co-expression. The difference in *pDR5* activation between empty vector and knock-down protoplasts became stronger when bdl was also co-expressed, indicating that the nuclear uptake of bdl was impaired (Figure 4a, b). The amiRNA effect was obvious when related to the respective empty vector controls: the expression of *DR5* was almost 50% higher in protoplasts co-transformed with *bdl* and *MP* than in the protoplasts expressing $MP_{\Delta III,IV}$ (Figure 4b). The slightly higher *pDR5* expression in the protoplasts not transformed with *bdl* might be caused by the effect of IMPα6 on other inhibitory Aux/IAAs present in protoplasts.

The stable switch of the MP–BDL module depends on the fast nuclear import of BDL

To understand how IMPα6-dependent nuclear import of bdl might influence the inhibition of MP by bdl, we explored the potential impact of this additional parameter on a previously established computational model of the MP–BDL module (Lau *et al.*, 2011). We introduced an auxin-dependent degradation constant for stabilized bdl protein that was 6.5-fold smaller than the original constant used for wild-type BDL protein, which is consistent with the experimentally observed effect of a similar stabilizing mutation in IAA17 and other Aux/IAA proteins (Tiwari *et al.*, 2001). As a consequence, our model predicted that the MP–bdl module would respond more slowly to auxin, failing to activate *MP* expression after a short auxin pulse (Figure 5). As an addition, we then introduced a delay of the nuclear import of bdl, corresponding to 0.5 ‰ of the time axis, which promoted a delayed auxin response, inducing the expression of both MP and bdl similarly to a prolonged auxin treatment (Figures 5 and S5a,b). Whether and how much the response was altered depended on the extent of delay. When the time lag was short, the induction of MP became weak and might not reach the threshold needed for responsive gene activation. When a longer delay was chosen the model predicted earlier activation of MP, which might lead to oscillations of activator (MP) and inhibitor (BDL) (Figure S5c, d). Whether these oscillations be meaningful in a biological context is hard to predict since mRNA and protein stability might dampen the oscillation *in planta.* These predictions were in agreement with the observed mutant phenotype: the *impα6-1* mutation

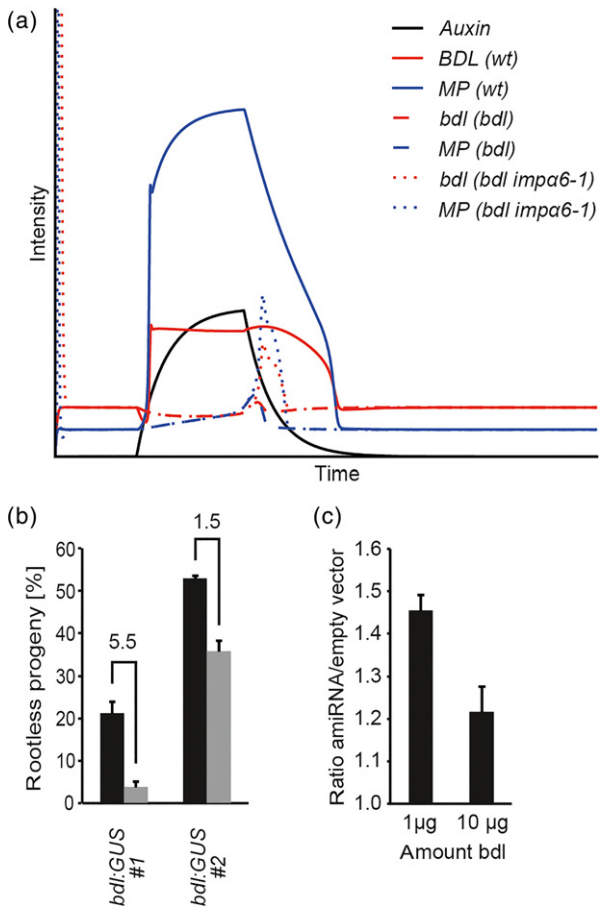

Figure 5. Model of expression of *MP* and *BDL* and the quantitative effect of *impα6-1.*

(a) Mathematical model. Solid: wild-type situation. Dashed: *bdl* situation; note that MP (blue, dashed) is not induced by auxin (black), because *bdl* (red, dashed) degradation is inhibited.

Dotted: *MP* and *bdl* expression when the import of bdl into the nucleus is inhibited. Note that in this case *MP* activity might be able to reach a threshold level, sufficient to trigger a genetic switch after a shorter auxin pulse.

(b) Proportion of rootless plants in wild-type and *impα6-1* background. Two independent lines giving rise to a different proportion of rootless plants are shown. Black: wild-type background, grey: *impα6-1* background. Error bars represent standard deviation. Numbers indicate fold change of the amount of rootless seedlings in the *impα6-1* background in comparison to wild-type.

(c) Ratio of bdl repressed MP action in protoplasts with different amounts of bdl in *IMPα6* amiRNA knock-down and empty vector control. Error bars represent standard error.

changed the proportion of rootless seedlings but did not affect other auxin responses.

To further test our model, we studied the effect of different amounts of bdl on MP activity during embryogenesis and in protoplasts. According to our model, a higher level of constitutive bdl production would reduce the induction of MP (Figure S6a). To confirm this, we analysed the effect of *impα6-1* on lines giving rise to different proportions of rootless seedlings. The *bdl* phenotype is dose dependent, only two copies of the original *bdl* are able to inhibit MP to the extent that primary root initiation fails (Hamann *et al.*, 2002). Some *bdl:GUS* lines showed a higher proportion of rootless seedlings, suggesting that hemizygous *bdl:GUS* seedlings were able to block hypophysis specification if *bdl:GUS* expression was high enough (Figure 5b). By studying the suppression of the rootless phenotype of *impα6-1* in one of those lines originally showing about 50% rootless seedlings (*bdl:GUS #2*), we noted that the rescue effect of *the impα6-1* mutation on line #2 was less pronounced than on *bdl:GUS* line #1. The proportion of rootless seedlings was reduced by a factor of 5.5 in the *bdl:GUS* line #1 used in the mutant screen. In comparison, the proportion of rootless plants was only reduced by a factor of about 1.5 in the *bdl:GUS* line #2 (Figure 5b). The same trend was observed in protoplasts, in which different amounts of *bdl* were transiently expressed. *IMPα6* amiRNA increased *DR5* induction by almost 50% in protoplasts that were transfected with 1 µg of bdl plasmid, but only by 20% when 10 µg were transfected (Figure 5c).

Like BDL, MP also localizes to the nucleus (Schlereth *et al.*, 2010). We therefore tested how a delay in MP import would affect the MP–BDL module. The model predicted no activation of MP if its translocation was reduced (Figure S6b). Also when both proteins were delayed to a similar extent, the delayed import would not result in an induction of MP (Figure S6c). This was further tested with different parameters: we reduced or increased the delay of MP and BDL import, but found no induction of the module under the conditions tested (Figure S5b, c). Unlike BDL, MP is a stable transcription factor whose activity is regulated by binding to BDL, rather than an unstable protein that is degraded in response to auxin. Therefore, the kinetics of MP import does not interfere strongly with the MP–BDL module.

Taken together, our modelling indicates that the specification of the hypophysis could be rescued by *impα6-1*, reducing nuclear import of bdl. This is in agreement with the observed early effect on division of the hypophysis as well as the different extents of *bdl* suppression.

DISCUSSION

Transcriptional auxin response is nuclear and we have shown that it depends on the kinetics of the nuclear import machinery. Besides *IMPα6*, other components are known to affect the translocation of Aux/IAAs and thereby to alter auxin response. Mutations in the nuclear-pore components SAR1 and SAR3 suppress the auxin resistance of *axr1.* In these mutants, IAA17 is not properly transported into the nucleus and is thereby not able to repress auxin target genes, which results in hypersensitivity to auxin (Parry *et al.*, 2006). The reduced import of Aux/IAAs might also be the reason for root hypersensitivity to auxin, where *AtRanBP1c*, which catalyses GTP hydrolysis of Ran, is down-regulated, and thereby the RAN-GDP/GTP gradient necessary for active nuclear transport might be impaired (Kim *et al.*, 2001).

The *impα6-1* mutation described in this study fits with these results and extends the knowledge of the pathway. Some of the proteins found in the mass spectrometry dataset have also been implicated in other hormone response pathways. Mutations in the importin-β proteins *AtKPNB1* or *SAD2* render plants hypersensitive to abscisic acid (ABA). Although the targets are not known, it has been suggested that *SAD2* is required for nuclear import of a negative regulator of ABA signalling (Verslues *et al.*, 2006; Luo *et al.*, 2013). In the auxin response pathways, Aux/IAA proteins like BDL or IAA17 presumably bind to IMPα6 and are together translocated with the importin-β-like protein SAD2 into the nucleus. Here, the nuclear-pore components SAR1 and SAR3 facilitate the import. Similarly, the function of IMPα3 is partially overlapping with IMPα6 in respect to the translocation of bdl. Previous results showed that overexpression of some, but not all, importin-α proteins can fully complement the defects in *Agrobacterium*-mediated plant transformation caused by impairment of IMPα4 Bhattacharjee *et al.* (2008). Notably, IMPα3 had a bigger effect on plant transformation than IMPα6, suggesting different primary functions of the two closely related family members.

Hormone response pathways in general and the auxin response pathways in particular might be especially sensitive to interference because they depend on the constant synthesis and turnover of Aux/IAA proteins (Abel *et al.*, 1995; Dharmasiri *et al.*, 2005b). This turnover allows fast responses to any changes in the environment, but is at the same time sensitive to kinetic interference e.g. by mutations in the import machinery (Kim *et al.*, 2001; Parry *et al.*, 2006). The developmental decision to initiate the primary root meristem in *Arabidopsis thaliana* early embryogenesis is made by the switch-like behaviour of the MP–BDL module in response to the rising intracellular auxin concentration. The MP–BDL module is a self-sustaining feedback system, with MP inducing its own expression and the expression of its inhibitor BDL (Lau *et al.*, 2011). Auxin tips the balance by causing the degradation of the inhibitor by the ubiquitin-proteasome pathway. Inhibition of MP and targeting of BDL for degradation, both take place in the nucleus (Hamann *et al.*, 2002; Dharmasiri *et al.*, 2005a). Therefore, the relative nuclear concentrations of MP and BDL critically determine the activity of the MP–BDL module. As the inhibitor BDL is short lived whereas the transcriptional activator MP is stable, uptake of BDL into the nucleus plays an important role in setting the MP–BDL balance. Like other small proteins, BDL could in principle reach the nucleus independently of the import machinery including IMPα6 (Mohr *et al.*, 2009; Bizzarri *et al.*, 2012). However, knock-down mutations in the *IMPA6* gene limit the bdl concentration below or near the threshold level required for inhibiting primary root initiation and therefore support the notion of a critical requirement of fast nuclear import for auxin response.

Functional overlaps between the individual members of the importin-alpha gene family members mask their role in the wild-type situation. Because the primary roots can only be initiated in a short timeframe, our screen allowed us to reveal the dependency of bdl on IMPα6 and provides further insights into the kinetics of the auxin response.

EXPERIMENTAL PROCEDURES

Plant material and growth conditions

If not mentioned otherwise, *Arabidopsis thaliana* ecotype Col-0 was used for all experiments.

The alleles, *bdl and mp-B4149* and the transgenic line *pBDL:: bdl:GUS* have been described previously (Hamann *et al.*, 1999; Dharmasiri *et al.*, 2005b; Weijers *et al.*, 2006). *impα6-2* (GABI_435H12, N387500, (Kleinboelting *et al.*, 2012)) and *impα3-1* (Bhattacharjee *et al.*, 2008) (Salk_025919, N525919) were obtained from the Nottingham Arabidopsis Stock Centre (NASC, Loughborough, UK). Plants were grown at 24°C, 65% relative humidity under long-day conditions (16 h illumination and 8 h dark period). Seeds were surface sterilized, stratified for 2 days at 4°C and grown on half-strength Murashige and Skoog agar plates containing 1% sucrose (½ MS + S) (SERVA, Heidelberg, Germany). After 1 week plants were transferred to soil.

Screening for suppressors of *bdl*

Seeds of a hemizygous *bdl:GUS* population were mutagenized with EMS. The phenotypic classes were quantified in the progeny of individual M2 plants grown on ½MS + S plates, supplemented with 15 mg L^{-1} phosphinothricin for transgene selection.

Mapping of *impα6-1*

The B2951 line was crossed to L*er* and the percentage of rootless plants was determined in individual F2 populations. Mapping was performed according to Lukowitz *et al.* (2000). By phenotypic characterization of 415 plants the mutation was mapped between markers F6F3 and F21 M12, and 1689 additional plants were checked for recombination events between those markers. By phenotypic characterization of 210 plants showing a recombination event between those markers, the mutation was mapped between markers DNAJ and T14P. Finally, all 16 open reading frames spanning that interval were sequenced.

Imaging

Seedlings were imaged with an AxioZoom V.16 (Carl Zeiss, Jena, Germany) and a GT-1500 scanner (Epson, Suwa (Nagano), Japan). Adult plant pictures were taken with an EOS 1000D camera (Canon, Tokyo, Japan). For confocal microscopy, the samples were mounted in 15% glycerol and imaged with an IX81 (Olympus, Tokyo, Japan). Differential interference contrast microscopy was performed with an Axio Imager Z1 (Carl Zeiss, Jena, Germany). Embryos were mounted in clearing solution containing chloral hydrate, water, and glycerol in the ratio 8:3:1. Images were processed with ImageJ (NIH, Bethesda, MD, USA), Photoshop and Illustrator software (Adobe Systems, San Jose, CA, USA).

Fluorescence recovery after photobleaching

We used seedlings expressing bdl:3×GFP from the *BDL* promoter. Seedlings were mounted in 15% glycerol and imaging was done with LSM 510 Meta confocal microscope (Carl Zeiss). over 30 sec at

1 sec intervals. The first three images were taken to assess the steady-state intensities, then the nuclear signal was bleached with the 488 nm laser line of an argon laser at maximal intensity (100 iterations, 2.51 μsec pixel dwell time), resulting in the reduction of the nuclear signal to about 50% of the pre-bleach value. Afterwards images were taken every second. The ratio of nuclear versus cytoplasmic intensity was quantified with ImageJ software.

Cloning

pGIIB pBDL::bdl:3×GFP was generated by amplification of *3×GFP* from *pGIIK NLS:3×GFP* (Schlereth *et al.*, 2010) with primers 3×GFP *Spe*l S and 3×GFP *Spe*l AS and replacement of the GUS gene *uidA* in *pGIIB pBDL::bdl:GUS* (Dharmasiri *et al.*, 2005b).

The artificial miRNA against *IMPα6* was generated according to Schwab *et al.* (2006) with the primers IMPα6 I miR-s, IMPα6 II miR-a, IMPα6 III miR*-s, IMPα6 IV miR*-a. The resulting fragment was inserted between the *Pst*I and *Bam*HI sites of *pGIIK pRPS5a* (Schlereth *et al.*, 2010) for stable transformation or *pJIT60* containing a double *CaMV 35S* promoter (Schwechheimer *et al.*, 1998) for transient protoplast assays.

Genomic fusions of *IMPα6* were amplified with IMPα6 2kbProm S [*Apa*I] and IMPα6 CDS AS (oS) [*Xho*I] and inserted between the *Apa*I and *Xho*I sites of *pGIIK 3×GFP* (Schlereth *et al.*, 2010).

RNA *in situ* hybridization

The *IMPα6* sense and antisense probes were amplified with the primers IMPα6 for inSitu F and IMPα6 for inSitu R and cloned into the pGEM-T easy vector (Promega, Fitchburg, WI, USA). Sense and antisense probes were generated with T7 or SP6 primers with the Fermentas *in vitro* transcription kit. Fixation and hybridization was performed as described previously (Mayer *et al.*, 1998; Slane *et al.*, 2014). In brief, siliques were cut and fixed in PBS buffer supplemented with 4% paraformaldehyde and 0.1% Tween 20 overnight. They were washed in PBS and dehydrated with an ethanol series, de-waxed with Roticlear® (Carl Roth, Karlsruhe, Germany) and embedded in Histowax® (Histolab, Göteborg, Sweden). 8 μm sections were placed on slides and dehydrated (Slane *et al.*, 2014).

Sections were de-waxed with Biozym Histoclear®, rehydrated with an ethanol series and proteins were digested with pronase before slides were dehydrated again. Hybridization was performed overnight at 55°C. Slides were washed and unspecific interactions were blocked by bovine serum albumin (BSA) solution before anti-digoxigenin–alkaline-phosphate-coupled antibody treatment. Samples was further washed and stained overnight. Images were taken after stoppage of the staining reaction by addition of 50% glycerol.

Transient activity assays

Bioluminescence assays were carried out as described previously (Lau *et al.*, 2011). In brief, cell suspension cultures were transformed with 10 μg of *pLucTrap pDR5*, 10 μg *pJIT60 amiRNA$_{IMPα6}$*, *pJIT60 MP* or *pJIT60 MP$_{ΔIII,IV}$*, 2 μg of *pGL4.70 2x35S::hRLuc* and 1 μg of *pJIT60 bdl* if not indicated otherwise.

After overnight incubation, protoplasts were pelleted and luminescence was determined with the Dual-Luciferase Reporter Assay System (Promega, Fitchburg, WI, USA) and an Infinite F200 plate reader (Tecan, Männedorf, Schweiz).

pLucTrap DR5, *pJIT60 MP*, *pJIT60 MP$_{ΔIII,IV}$*, *pGL4.70 2x35S::hRLuc* and *pJIT60 bdl* have been described previously (Lau *et al.*, 2011).

Modelling

The model of the impact of IMPα6 on the MP–BDL module is based on a model described previously (Lau *et al.*, 2011) with the following additions: to model the effect of the stabilizing *bdl* mutation, we reduced the auxin-dependent degradation of bdl by the factor 6.5. The impact of *impα6-1* was modelled as a time lag between production and effect of bdl by 100 time points, corresponding to 0.5 ‰ of the time axis. The expression of *MP* and *BDL*/*bdl* is determined by the concentration of MP and BDL, the regulation of auxin is not part of the model.

To account for different delays in the import of BDL and MP, we used the concentrations of BDL and MP at t = 50, t = 100, and t = 200 for [BDL] and [MP] to calculate d*MP*/d*t* and d*BDL*/d*t*.

$$\frac{dMP}{dt} = \mu_{Production\ MP} \frac{[MP]^2}{(\mu_{Km\ BDL-MP} + [BDL])(1 + \mu_{Saturation\ MP\ production}[MP]^2)} + \mu_{baseline\ MP\ production} - \mu_{degradation\ MP}[MP]$$

$$\frac{dBDL}{dt} = \beta_{Production\ BDL} \frac{[MP]^2}{(\mu_{Km\ BDL-MP} + [BDL])} + \beta_{baseline\ BDL\ production} - \beta_{degradation\ BDL}[BDL] - \beta_{auxin\ dependent\ BDL\ degradation}[auxin][BDL]$$

$$\frac{dauxin}{dt} = \alpha_{Production\ rate\ auxin} - \alpha_{Degradation\ rate\ auxin}[auxin]$$

The constants used were the same as used by Lau *et al.* (2011). In brief, the following parameters were chosen: $\mu_{Production\ MP} = 0.005$, $\mu_{Km\ BDL-MP} = 0.1$, $\mu_{saturation\ MP\ production} = 1$, $\mu_{baseline\ MP\ production} = 0.0003$, $\mu_{degradation\ MP} = 0.005$, $\beta_{Production\ BDL} = 0.001$, $\beta_{baseline\ BDL\ production} = 0.0003$, $\beta_{degradation\ BDL} = 0.002$, $\beta_{auxin\text{-}dependent\ BDL\ degradation} = 0.01$, $\alpha_{Production\ rate\ auxin} = 0.0001$. The $\alpha_{Production\ rate\ auxin}$ was changed over time to simulate an auxin pulse from 0 to 0.00005 and back to 0.

Genotyping primers

For genotyping of *impα6-1*, *mp* and *bdl* we generated dCAPs primers with dCAPS Finder 2.0. (Neff *et al.*, 2002), resulting in the primers IMPα6 dCAPS [*Bfm*I] F and IMPα6 dCAPS [*Bfm*I] R for *impα6-1* MP dCAPs [*Kpn*I] F and MP dCAPs [*Kpn*I] R for *mp* and BDL dCAPs [*Nae*I] F and BDL dCAPs [*Nae*I] R for *bdl*. The resulting fragments were digested with *Bfm*I, *Kpn*I and *Nae*I, respectively.

impα6-2 (SAIL_1220_C03) genotyping was performed with primers IMPα6-Exon 7 S and 2690R for the wild-type and At1G02690 F and LB2 (Sessions, 2002) for the T-DNA PCR.

impα3-1 (Alonso *et al.*, 2003; Bhattacharjee *et al.*, 2008) was genotyped with IMPα-3 tDNA F and IMPα-3 tDNA R (wild-type) and IMPα-3 tDNA F and LB1.3 (T-DNA).

Semi-quantitative RT-PCR

The IMPα6 fragment was amplified with the primers IMPα6-Exon 7 S and IMPα6 Exon10 AS. Actin2 was amplified with primers actin F and actin R, and Renilla Luciferase with primers Renilla Luciferase F and Renilla Luciferase R.

Mass spectrometry

For mass spectrometry, seedlings were ground in liquid nitrogen and homogenized in extraction buffer (50 mM Tri-HCl pH 7.5, 150 mM NaCl, 1 mM EDTA, 1% Triton X-100) supplemented with 1% protease inhibitor cocktail. The protein extract was incubated with magnetic beads coupled to lama anti-GFP antibody (GFP-trap®, Chromotek, Planegg-Martinsried, Germany). After washing the proteins were separated by SDS PAGE and digested in gel with trypsin. LC-MS/MS analysis was performed

with a Proxeon Easy-nLC1000 coupled to a QExactive HF, the data were processed with the MaxQuant software employing the *Arabidopsis thaliana* Uniprot database. The mass spectrometry was performed by the Proteome Centre Tübingen, Tübingen, Germany.

ACKNOWLEDGEMENTS

We thank Caterina Brancato for protoplast transfections, Mirita Franz-Wachtel and Boris Maček for performing mass spectrometry. We also thank Daniel Slane and Martin Bayer for critical reading of the manuscript.

SUPPORTING INFORMATION

Additional Supporting Information may be found in the online version of this article.

Figure S1. Phenotype of mutant plants and embryos.

Figure S2. Mapping of *impα6-1* and RT-PCR on the different alleles.

Figure S3. Expression of *IMPα6* in embryos.

Figure S4. Functionality and fluorescence signal of bdl:3×GFP and GUS signal ofbdl:GUS.

Figure S5. Model for the action of *bdl* and *MP* and the impact of auxin pulse duration and time lag.

Figure S6. Model for the action of *bdl* and *MP* in the context of increased bdl production and delayed import of MP.

Table S1. Proteins interacting with IMPα6:3×GFP.

Table S2. Primers used in this study.

REFERENCES

Abel, S. and Theologis, A. (1995) A polymorphic bipartite motif signals nuclear targeting of early auxin-inducible proteins related to PS-IAA4 from pea (*Pisum sativum*). *Plant J.* **8**, 87–96.

Abel, S., Nguyen, M.D. and Theologis, A. (1995) The PS-IAA4/5-like family of early auxin-inducible mRNAs in *Arabidopsis thaliana*. *J. Mol. Biol.* **251**, 533–549.

Alonso, J.M., Stepanova, A.N., Leisse, T.J. *et al.* (2003) Genome-wide insertional mutagenesis of *Arabidopsis thaliana*. *Science*, **301**, 653–657.

Bhattacharjee, S., Lee, L.Y., Oltmanns, H., Cao, H., Veena, Cuperus, J. and Gelvin, S.B. (2008) IMPa-4, an Arabidopsis importin alpha isoform, is preferentially involved in *Agrobacterium*-mediated plant transformation. *Plant Cell*, **20**, 2661–2680.

Bizzarri, R., Cardarelli, F., Serresi, M. and Beltram, F. (2012) Fluorescence recovery after photobleaching reveals the biochemistry of nucleocytoplasmic exchange. *Anal. Bioanal. Chem.* **403**, 2339–2351.

Chang, C.W., Counago, R.L., Williams, S.J., Boden, M. and Kobe, B. (2012) Crystal structure of rice importin-alpha and structural basis of its interaction with plant-specific nuclear localization signals. *Plant Cell*, **24**, 5074–5088.

Conti, E., Uy, M., Leighton, L., Blobel, G. and Kuriyan, J. (1998) Crystallographic analysis of the recognition of a nuclear localization signal by the nuclear import factor karyopherin alpha. *Cell*, **94**, 193–204.

Dharmasiri, N., Dharmasiri, S. and Estelle, M. (2005a) The F-box protein TIR1 is an auxin receptor. *Nature*, **435**, 441–445.

Dharmasiri, N., Dharmasiri, S., Weijers, D., Lechner, E., Yamada, M., Hobbie, L., Ehrismann, J.S., Jurgens, G. and Estelle, M. (2005b) Plant development is regulated by a family of auxin receptor F box proteins. *Dev. Cell*, **9**, 109–119.

Hamann, T., Mayer, U. and Jurgens, G. (1999) The auxin-insensitive bodenlos mutation affects primary root formation and apical-basal patterning in the Arabidopsis embryo. *Development*, **126**, 1387–1395.

Hamann, T., Benkova, E., Baurle, I., Kientz, M. and Jurgens, G. (2002) The Arabidopsis BODENLOS gene encodes an auxin response protein inhibiting MONOPTEROS-mediated embryo patterning. *Genes Dev.* **16**, 1610–1615.

Kim, S.H., Arnold, D., Lloyd, A. and Roux, S.J. (2001) Antisense expression of an Arabidopsis Ran binding protein renders transgenic roots hypersensitive to auxin and alters auxin-induced root growth and development by arresting mitotic progress. *Plant Cell*, **13**, 2619–2630.

Kleinboelting, N., Huep, G., Kloetgen, A., Viehoever, P. and Weisshaar, B. (2012) GABI-Kat SimpleSearch: new features of the *Arabidopsis thaliana* T-DNA mutant database. *Nucleic Acids Res.* **40**, D1211–D1215.

Kobe, B. (1999) Autoinhibition by an internal nuclear localization signal revealed by the crystal structure of mammalian importin alpha. *Nat. Struct. Biol.* **6**, 388–397.

Lau, S., De Smet, I., Kolb, M., Meinhardt, H. and Jurgens, G. (2011) Auxin triggers a genetic switch. *Nat. Cell Biol.* **13**, 611–615.

Lau, S., Slane, D., Herud, O., Kong, J. and Jurgens, G. (2012) Early embryogenesis in flowering plants: setting up the basic body pattern. *Annu. Rev. Plant Biol.* **63**, 483–506.

Lukowitz, W., Gillmor, C.S. and Scheible, W.R. (2000) Positional cloning in Arabidopsis. Why it feels good to have a genome initiative working for you. *Plant Physiol.* **123**, 795–805.

Luo, Y., Wang, Z., Ji, H., Fang, H., Wang, S., Tian, L. and Li, X. (2013) An Arabidopsis homolog of importin beta1 is required for ABA response and drought tolerance. *Plant J.* **75**, 377–389.

Matsuura, Y. and Stewart, M. (2005) Nup50/Npap60 function in nuclear protein import complex disassembly and importin recycling. *EMBO J.* **24**, 3681–3689.

Mayer, K.F., Schoof, H., Haecker, A., Lenhard, M., Jurgens, G. and Laux, T. (1998) Role of WUSCHEL in regulating stem cell fate in the Arabidopsis shoot meristem. *Cell*, **95**, 805–815.

Merkle, T. (2011) Nucleo-cytoplasmic transport of proteins and RNA in plants. *Plant Cell Rep.* **30**, 153–176.

Mohr, D., Frey, S., Fischer, T., Guttler, T. and Gorlich, D. (2009) Characterisation of the passive permeability barrier of nuclear pore complexes. *EMBO J.* **28**, 2541–2553.

Neff, M.M., Turk, E. and Kalishman, M. (2002) Web-based primer design for single nucleotide polymorphism analysis. *Trends Genet.* **18**, 613–615.

Parry, G., Ward, S., Cernac, A., Dharmasiri, S. and Estelle, M. (2006) The Arabidopsis SUPPRESSOR OF AUXIN RESISTANCE proteins are nucleoporins with an important role in hormone signaling and development. *Plant Cell*, **18**, 1590–1603.

Salehin, M., Bagchi, R. and Estelle, M. (2015) SCFTIR1/AFB-based auxin perception: mechanism and role in plant growth and development. *Plant Cell*, **27**, 9–19.

Schlereth, A., Moller, B., Liu, W., Kientz, M., Flipse, J., Rademacher, E.H., Schmid, M., Jurgens, G. and Weijers, D. (2010) MONOPTEROS controls embryonic root initiation by regulating a mobile transcription factor. *Nature*, **464**, 913–916.

Schwab, R., Ossowski, S., Riester, M., Warthmann, N. and Weigel, D. (2006) Highly specific gene silencing by artificial microRNAs in Arabidopsis. *Plant Cell*, **18**, 1121–1133.

Schwechheimer, C., Smith, C. and Bevan, M.W. (1998) The activities of acidic and glutamine-rich transcriptional activation domains in plant cells: design of modular transcription factors for high-level expression. *Plant Mol. Biol.* **36**, 195–204.

Sessions, A. (2002) A high-throughput Arabidopsis reverse genetics system. *The Plant Cell Online*, **14**, 2985–2994.

Slane, D., Kong, J., Berendzen, K.W. *et al.* (2014) Cell type-specific transcriptome analysis in the early *Arabidopsis thaliana* embryo. *Development*, **141**, 4831–4840.

Tiwari, S.B., Wang, X.J., Hagen, G. and Guilfoyle, T.J. (2001) AUX/IAA proteins are active repressors, and their stability and activity are modulated by auxin. *Plant Cell*, **13**, 2809–2822.

Verslues, P.E., Guo, Y., Dong, C.H., Ma, W. and Zhu, J.K. (2006) Mutation of SAD2, an importin beta-domain protein in Arabidopsis, alters abscisic acid sensitivity. *Plant J.* **47**, 776–787.

Weijers, D., Franke-van Dijk, M., Vencken, R.J., Quint, A., Hooykaas, P. and Offringa, R. (2001) An Arabidopsis Minute-like phenotype caused by a semi-dominant mutation in a RIBOSOMAL PROTEIN S5 gene. *Development*, **128**, 4289–4299.

Weijers, D., Schlereth, A., Ehrismann, J.S., Schwank, G., Kientz, M. and Jurgens, G. (2006) Auxin triggers transient local signaling for cell specification in Arabidopsis embryogenesis. *Dev. Cell*, **10**, 265–270.

Wirthmueller, L., Roth, C., Banfield, M.J. and Wiermer, M. (2013) Hop-on hop-off: importin-alpha-guided tours to the nucleus in innate immune signaling. *Front. Plant Sci.* **4**, 149.

Supporting Information Legends

Figure S1. Phenotype of mutant plants and embryos.
(a) Adult phenotype of 6 week old plants. Scale bar 10 cm.
(b) Embryo phenotype. Scale bar 50 µm.
Arrows indicate the hypophysis division plane.

Figure S2: Mapping of *impα6-1* and RT-PCR on the different alleles.
(a) *impα6-1* mapped to the upper arm of chromosome 1 between markers DNAJ and T14P.
(b) The full length IMPα6 product was downregulated in *impα6-1* and undetectable in the *impα6-2* line. The amiRNA line did not show a transcript reduction in seedlings.
(c) IMPα6 was downregulated by the amiRNA in protoplasts. Renilla Luciferase mRNA was used as transfection control.

Figure S3: Expression of *IMPα6* in embryos.
(a) Localization of *pIMPα6::IMPα6:3xGFP* in embryos. The expression was detectable early on, the protein localized mainly to the nucleus. Scale bars 10 µm.
(b) *In situ* hybridization of IMPα6 in embryos. The expression was patchy and from transition stage onwards, stronger in the vasculature than in other tissues (AS: antisense probe, S: sense probe). Scale bars 10 µm.

Figure S4. Functionality and fluorescence signal of bdl:3xGFP and GUS signal of bdl:GUS.
(a) Rescue of rootless seedling phenotype of *bdl:3xGFP* by *impα6-1*. * indicates $p<0.05$ according to student's t-test. Error bars indicate standard error. N = 4 194.
(b) Nuclear localization of bdl:3xGFP in *impα6-1* embryos. Scale bar 20 µm.
(c) GUS staining of roots 6 days after germination. Scale bar 0.1 cm.
(d) FRAP example. Circle, nucleus corresponding to bleached area; polygon, cytoplasm.

Figure S5. Model for the action of *bdl* and *MP* and the impact of auxin pulse duration and time lag.
(a,b) Model of the auxin response if the auxin pulse is prolonged. Note that also in this case the threshold is reached, independent of a delay in bdl uptake. Tick marks (a) highlight the excerpt shown in (b).
(b) Detail view of (a) at the time point when the threshold is reached. The general behaviour of *bdl* (dashed) and *bdl impα6-1* (dotted) is similar; however, the mutant reacts slightly faster. The continuous line show the wild-type situation.

(c,d) Model of the auxin response with different time lags. Tick marks (c) highlight the excerpt shown in (d).
(d) Detail view of (c) at the time point when the threshold is reached. A short time lag weakened the induction of MP which might not reach the threshold needed (dotted), a prolonged time lag caused earlier activation of MP (dashed). The continuous line show the intermediate time lag used for the model in Figure 5.

Figure S6. Model for the action of *bdl* and *MP* in the context of increased bdl production and delayed import of MP.
(a) Model for increased bdl production. The peak of MP induction is smaller and would diminish if the amount of bdl would be further increased (arrow). MP did not reach the threshold or would need longer to reach it.
(b) Model of the auxin response when the import of MP was inhibited with different time lags. The model did not predict any induction of the MP-BDL module when only MP import was delayed. Note that the outcome is very similar for the two time lags chosen (dashed and dotted lines).
(c) Model of the auxin response when the import of both MP and bdl was delayed different. The model did not predict any induction of the MP-BDL module when the import of both MP and bdl was delayed to the same extent. Note that the outcome is very similar for the two time lags chosen (dashed and dotted lines).

Table S1: Proteins interacting with IMPα6:3xGFP. The table only show proteins at least 2-fold enriched in comparison to other GFP tagged datasets.

Table S2: Primers used in this study.

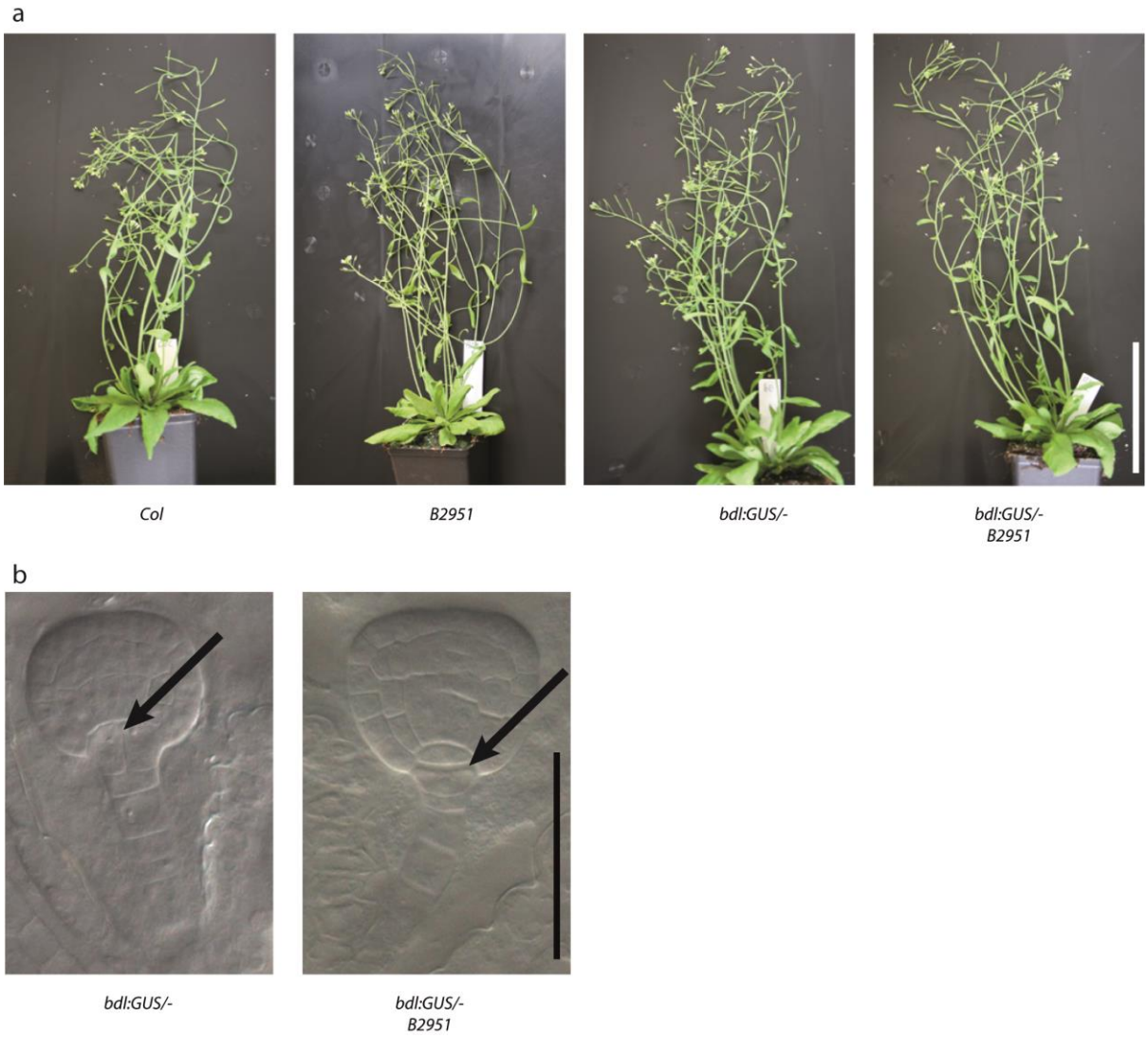

Figure S1. Phenotype of mutant plants and embryos.

(a) Adult phenotype of 6 week old plants. Scale bar 10 cm.

(b) Embryo phenotype. Scale bar 50 µm.

Arrows indicate the hypophysis division plane.

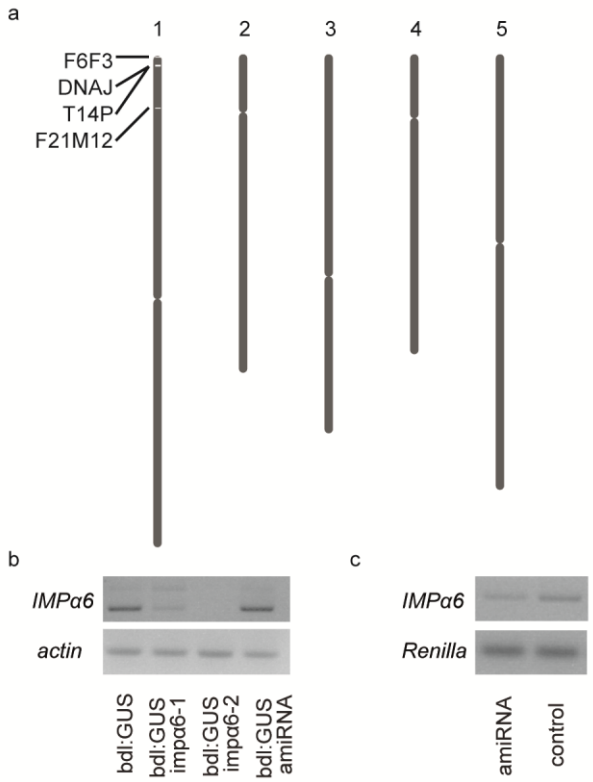

Figure S2: Mapping of *impα6-1* and RT-PCR on the different alleles.

(a) *impα6-1* mapped to the upper arm of chromosome 1 between markers DNAJ and T14P.

(b) The full length IMPα6 product was downregulated in *impα6-1* and undetectable in the *impα6-2* line. The amiRNA line did not show a transcript reduction in seedlings.

(c) IMPα6 was downregulated by the amiRNA in protoplasts. Renilla Luciferase mRNA was used as transfection control.

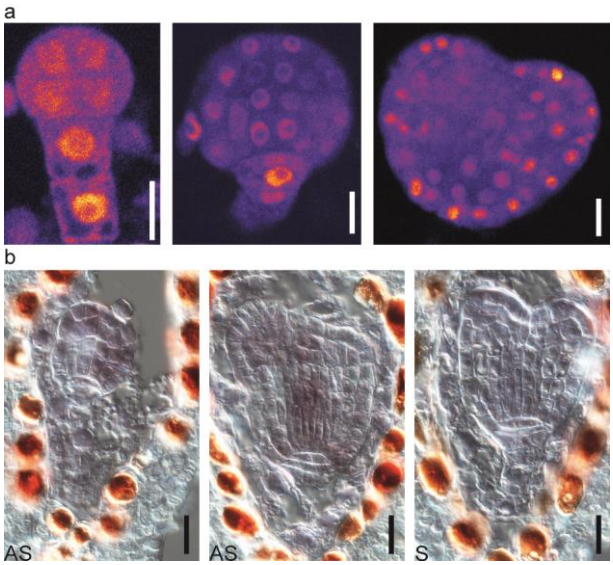

Figure S3: Expression of *IMPα6* in embryos.

(a) Localization of *pIMPα6::IMPα6:3xGFP* in embryos. The expression was detectable early on, the protein localized mainly to the nucleus. Scale bars 10 µm.

(b) *In situ* hybridization of IMPα6 in embryos. The expression was patchy and from transition stage onwards, stronger in the vasculature than in other tissues (AS: antisense probe, S: sense probe). Scale bars 10 µm.

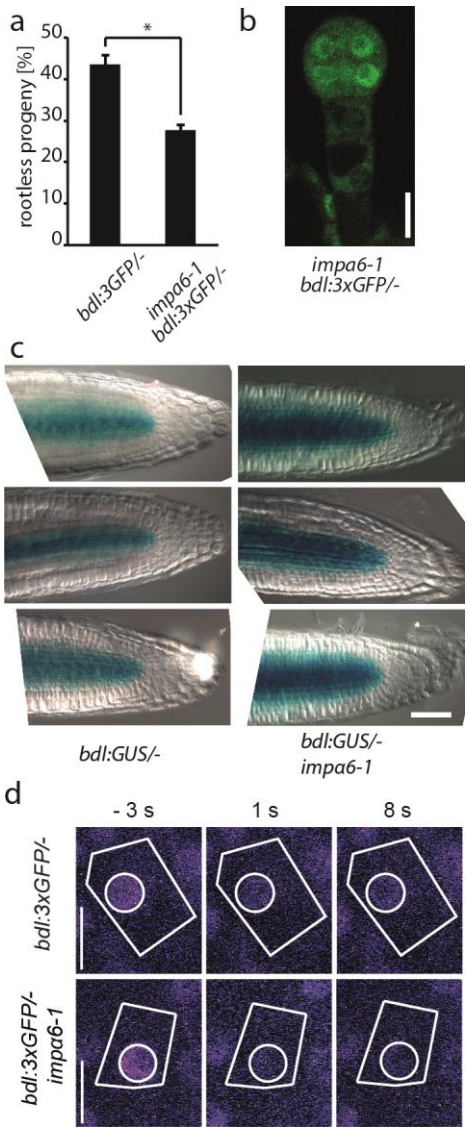

Figure S4. Functionality and fluorescence signal of bdl:3xGFP and GUS signal of bdl:GUS.

(a) Rescue of rootless seedling phenotype of *bdl:3xGFP* by *impα6-1*. * indicates p<0.05 according to student's t-test. Error bars indicate standard error. N = 4 194.

(b) Nuclear localization of bdl:3xGFP in *impα6-1* embryos. Scale bar 20 µm.

(c) GUS staining of roots 6 days after germination. Scale bar 0.1 cm.

(d) FRAP example. Circle, nucleus corresponding to bleached area; polygon, cytoplasm.

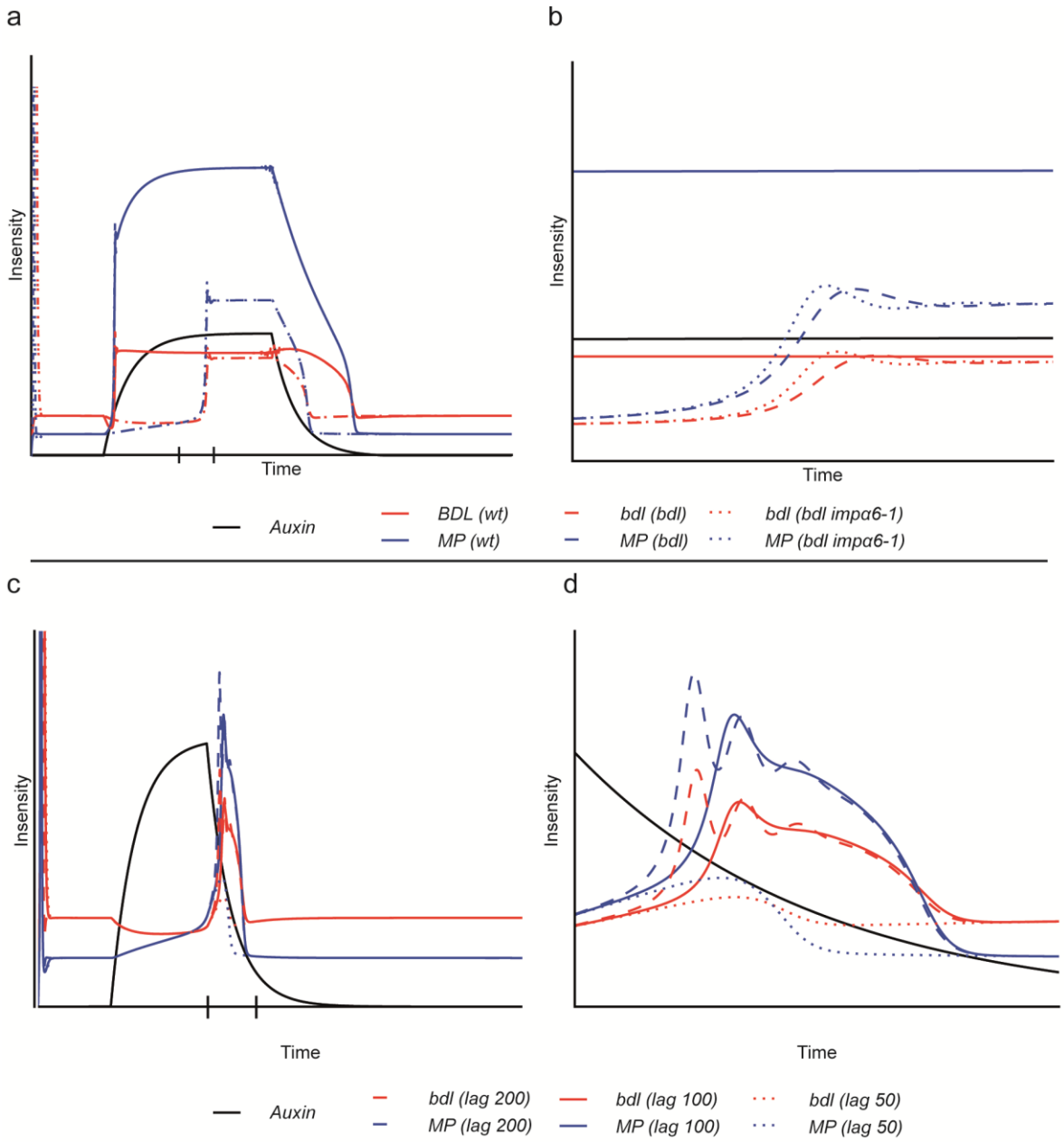

Figure S5. Model for the action of *bdl* and *MP* and the impact of auxin pulse duration and time lag.

(a,b) Model of the auxin response if the auxin pulse is prolonged. Note that also in this case the threshold is reached, independent of a delay in bdl uptake. Tick marks (a) highlight the excerpt shown in (b).

(b) Detail view of (a) at the time point when the threshold is reached. The general behaviour of *bdl* (dashed) and *bdl impα6-1* (dotted) is similar; however, the mutant reacts slightly faster. The continuous line show the wild-type situation.

(c,d) Model of the auxin response with different time lags. Tick marks (c) highlight the excerpt shown in (d).

(d) Detail view of (c) at the time point when the threshold is reached. A short time lag weakened the induction of MP which might not reach the threshold needed (dotted), a

prolonged time lag caused earlier activation of MP (dashed). The continuous line show the intermediate time lag used for the model in Figure 5.

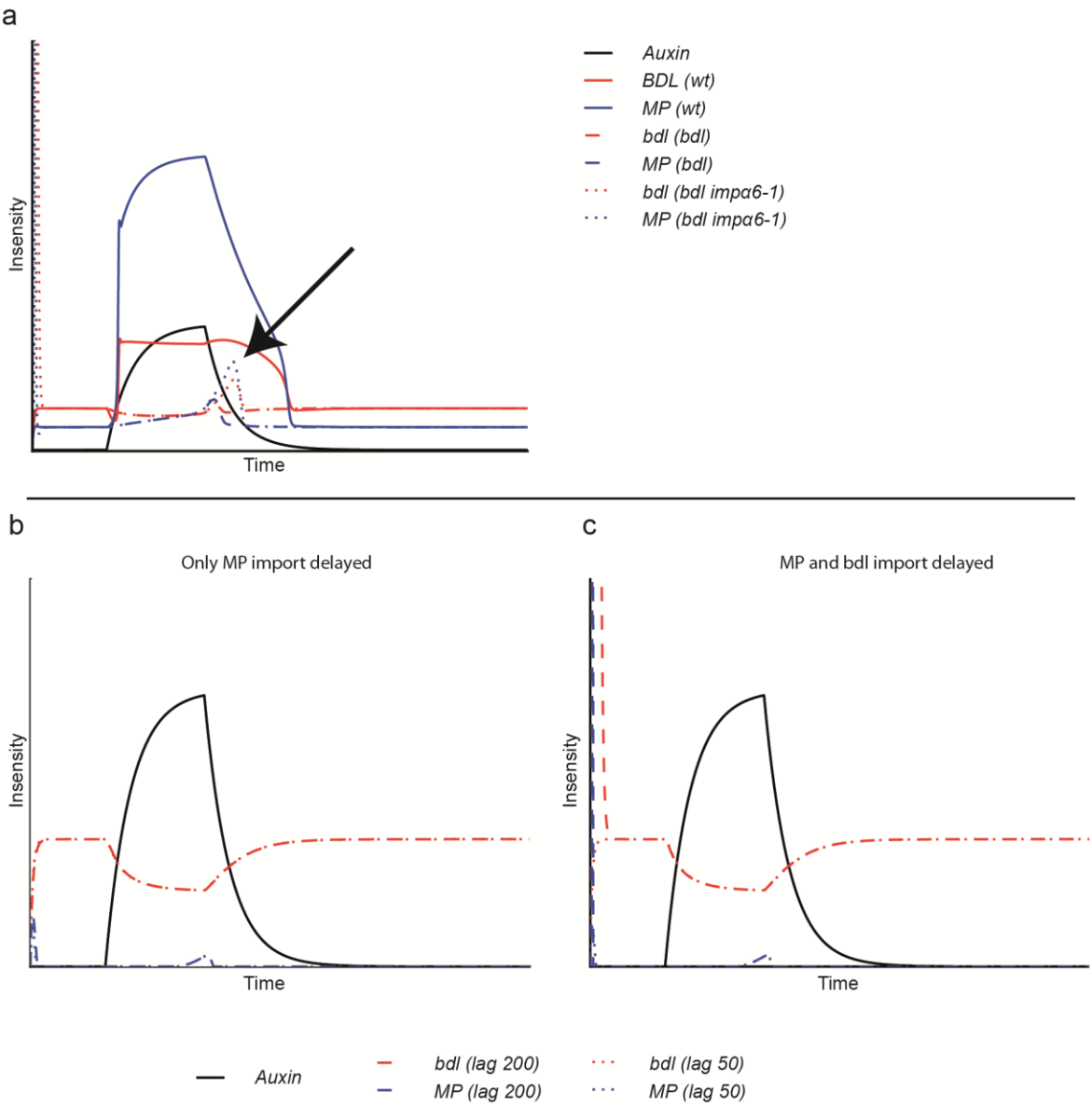

Figure S6. Model for the action of *bdl* and *MP* in the context of increased bdl production and delayed import of MP.

(a) Model for increased bdl production. The peak of MP induction is smaller and would diminish if the amount of bdl would be further increased (arrow). MP did not reach the threshold or would need longer to reach it.

(b) Model of the auxin response when the import of MP was inhibited with different time lags. The model did not predict any induction of the MP-BDL module when only MP import was delayed. Note that the outcome is very similar for the two time lags chosen (dashed and dotted lines).

(c) Model of the auxin response when the import of both MP and bdl was delayed different. The model did not predict any induction of the MP-BDL module when the import of both MP and bdl was delayed to the same extent. Note that the outcome is very similar for the two time lags chosen (dashed and dotted lines).

Table S1: Proteins interacting with IMPα6:3xGFP. The table only show proteins at least 2-fold enriched in comparison to other GFP tagged datasets.

AtG Number	Name
At1g02690	**Importin subunit alpha-6 (IMPa-6)**
At3g14240	Subtilase family protein (Subtilisin proteinase-like protein)
At5g67360	Subtilisin-like protease SBT1.7 (EC 3.4.21.-) (Cucumisin-like serine protease) (Subtilase subfamily 1 member 7) (AtSBT1.7) (Subtilisin-like serine protease 1) (At-SLP1)
At5g26742	DEAD-box ATP-dependent RNA helicase 3, chloroplastic (EC 3.6.4.13) (Protein EMBRYO DEFECTIVE 1138)
At1g06950	Protein TIC110, chloroplastic (Translocon at the inner envelope membrane of chloroplasts 110) (AtTIC110)
At3g09630	60S ribosomal protein L4-1 (L1)
AtCg00780	50S ribosomal protein L14, chloroplastic
At1g52380	**Nuclear pore complex protein NUP50A (Nucleoporin 50A)**
At5g48300	Glucose-1-phosphate adenylyltransferase small subunit, chloroplastic (EC 2.7.7.27) (ADP-glucose pyrophosphorylase) (ADP-glucose synthase) (AGPase B) (Alpha-D-glucose-1-phosphate adenyl transferase)
At1g15500	ADP,ATP carrier protein 2, chloroplastic (ADP/ATP translocase 2) (Adenine nucleotide translocase 2)
At4g17330	G2484-1 protein
At1g27400	60S ribosomal protein L17-1
At3g15970	**Nuclear pore complex protein NUP50B (Nucleoporin 50B)**
At5g47010	Regulator of nonsense transcripts 1 homolog (EC 3.6.4.-) (ATP-dependent helicase UPF1)
At2g43030	50S ribosomal protein L3-1, chloroplastic
At2g31660	**Importin beta-like SAD2 (Protein ENHANCED MIRNA ACTIVITY 1) (Protein SUPER SENSITIVE TO ABA AND DROUGHT 2) (Protein UNARMED 9)**
AtCg00810	50S ribosomal protein L22, chloroplastic
At5g27850	60S ribosomal protein L18-3
At2g25730	Uncharacterized protein
At4g29040	26S proteasome regulatory subunit 4 homolog A (26S proteasome AAA-ATPase subunit RPT2a) (26S proteasome subunit 4 homolog A) (Protein HALTED ROOT) (Regulatory particle triple-A ATPase subunit 2a)
At4g39420	Uncharacterized protein
At2g19730	60S ribosomal protein L28-1
At5g53170	ATP-dependent zinc metalloprotease FTSH 11, chloroplastic/mitochondrial (AtFTSH11) (EC 3.4.24.-)
At3g04840	40S ribosomal protein S3a-1
At1g80480	At1g80480 (Plastid transcriptionally active 17 protein) (Putative uncharacterized protein T21F11.27)
At3g04400	60S ribosomal protein L23
At1g78630	50S ribosomal protein L13, chloroplastic (CL13) (Protein EMBRYO DEFECTIVE 1473)
At2g44120	60S ribosomal protein L7-3
At5g02870	60S ribosomal protein L4-2 (L1)

AtG Number	Name
At3g05720	**Importin subunit alpha-7 (IMPa-7)**
At1g35680	50S ribosomal protein L21, chloroplastic (CL21)
At3g11940	40S ribosomal protein S5-2
At5g45930	Magnesium-chelatase subunit ChlI-2, chloroplastic (Mg-chelatase subunit I-2) (EC 6.6.1.1) (Mg-protoporphyrin IX chelatase subunit ChlI-2)
At1g04270	40S ribosomal protein S15-1
At5g47190	50S ribosomal protein L19-2, chloroplastic
At1g43170	60S ribosomal protein L3-1
At3g24830	60S ribosomal protein L13a-2
At1g22530	Patellin-2
At5g18190	Casein kinase-like protein (Protein kinase)
At1g59870	ABC transporter G family member 36 (ABC transporter ABCG.36) (AtABCG36) (Pleiotropic drug resistance protein 8) (Protein PENETRATION 3)
AT1G01610	GPAT4/ GLYCEROL-3-PHOSPHATE SN-2-ACYLTRANSFERASE 4
At4g39980	Phospho-2-dehydro-3-deoxyheptonate aldolase 1, chloroplastic (EC 2.5.1.54) (3-deoxy-D-arabino-heptulosonate 7-phosphate synthase 1) (DAHP synthase 1) (Phospho-2-keto-3-deoxyheptonate aldolase 1)
At3g10610	40S ribosomal protein S17-3
At1g79920	Heat shock protein 70
AT3G06720	**IMPORTIN ALPHA ISOFORM 1**
At3g62530	E-Z type HEAT repeat-containing protein (Putative uncharacterized protein At3g62530)
At1g11650	Polyadenylate-binding protein RBP45B (Poly(A)-binding protein RBP45B) (RNA-binding protein 45B) (AtRBP45B)
AtCg00840	50S ribosomal protein L23, chloroplastic
At5g61050	Histone deacetylase-like protein
At1g08520	Magnesium-chelatase subunit ChlD, chloroplastic (Mg-chelatase subunit D) (EC 6.6.1.1) (Mg-protoporphyrin IX chelatase subunit ChlD) (Protein ALBINA 1) (Protein PIGMENT DEFECTIVE EMBRYO 166)
At2g30490	Trans-cinnamate 4-monooxygenase (EC 1.14.13.11) (Cinnamic acid 4-hydroxylase) (C4H) (CA4H) (Cytochrome P450 73) (Cytochrome P450C4H)
At5g19940	Plastid-lipid associated protein PAP / fibrillin family protein
At3g25920	50S ribosomal protein L15, chloroplastic (CL15)
At4g29410	60S ribosomal protein L28-2
At5g56710	60S ribosomal protein L31-3
At1g57660	60S ribosomal protein L21-2
At4g17560	50S ribosomal protein L19-1, chloroplastic
At2g20790	AP-5 complex subunit mu (Adaptor protein complex AP-5 subunit mu) (Adaptor protein-5 mu-adaptin) (Adaptor-related protein complex 5 subunit mu) (Mu5-adaptin)
At2g39190	ATH subfamily protein ATH8 (Putative ABC transporter; alternative splicing isoform gene prediction data combined with cDNA alignment data to generate this model)
At5g19990	26S protease regulatory subunit 8 homolog A (26S proteasome AAA-ATPase subunit RPT6a) (26S proteasome subunit 8 homolog A) (Regulatory particle triple-A ATPase subunit 6a)
At1g02150	Pentatricopeptide repeat-containing protein At1g02150
At4g36130	60S ribosomal protein L8-3

AtG Number	Name
AtCg00520	Photosystem I assembly protein Ycf4
At1g14320	60S ribosomal protein L10-1
At3g46740	Protein TOC75-3, chloroplastic (75 kDa translocon at the outer-envelope-membrane of chloroplasts 3) (AtTOC75-III)
At2g27530	60S ribosomal protein L10a-2
At3g18000	Phosphoethanolamine N-methyltransferase 1 (AtNMT1) (PEAMT 1) (EC 2.1.1.103) (Protein XIPOTL 1)
At1g74060	60S ribosomal protein L6-2
At4g36250	Aldehyde dehydrogenase family 3 member F1 (EC 1.2.1.3)
At4g28080	Tetratricopeptide repeat domain protein
At2g26280	Polyadenylate-binding protein-interacting protein 7 (PABP-interacting protein 7) (Poly(A)-binding protein-interacting protein 7) (PAM2-containing protein CID7) (Protein CTC-INTERACTING DOMAIN 7)
AtMg00480	ATP synthase protein YMF19 (EC 3.6.3.14) (Mitochondrial protein YMF19)
At4g15000	60S ribosomal protein L27-3
At5g65220	50S ribosomal protein L29, chloroplastic (CL29)
At2g40590	40S ribosomal protein S26-1
At3g49010	60S ribosomal protein L13-1
At2g26250	3-ketoacyl-CoA synthase 10 (KCS-10) (EC 2.3.1.199) (Protein FIDDLEHEAD) (Very long-chain fatty acid condensing enzyme 10) (VLCFA condensing enzyme 10)
At2g44640	Expressed protein (Uncharacterized protein)
At2g43460	60S ribosomal protein L38
At5g08650	Translation factor GUF1 homolog, chloroplastic (EC 3.6.5.-) (Elongation factor 4 homolog) (EF-4) (GTPase GUF1 homolog) (Ribosomal back-translocase)
At1g20330	24-methylenesterol C-methyltransferase 2 (24-sterol C-methyltransferase 2) (Sterol-C-methyltransferase 2) (EC 2.1.1.143) (Protein COTYLEDON VASCULAR PATTERN 1)
At4g01690	Protoporphyrinogen oxidase 1, chloroplastic (PPO1) (EC 1.3.3.4)
At3g19870	Uncharacterized protein
At4g18100	60S ribosomal protein L32-1
At3g48870	Clp ATPase
At3g09500	60S ribosomal protein L35-1
At1g63660	At1g63660 (GMP synthase; 61700-64653) (GMP-synthase-C and glutamine amidotransferase domain-containing protein)
At3g15160	Putative uncharacterized protein At3g15160 (Uncharacterized protein)
At5g13110	Glucose-6-phosphate 1-dehydrogenase 2, chloroplastic (G6PD2) (G6PDH2) (EC 1.1.1.49)
At2g36160	40S ribosomal protein S14-1
At5g17170	Putative uncharacterized protein At5g17170 (Rubredoxin family protein)
At3g58610	Ketol-acid reductoisomerase, chloroplastic (EC 1.1.1.86) (Acetohydroxy-acid reductoisomerase) (Alpha-keto-beta-hydroxylacyl reductoisomerase)
AtCg01120	30S ribosomal protein S15, chloroplastic
AtCg00900	30S ribosomal protein S7, chloroplastic
At1g76010	Alba DNA/RNA-binding protein (At1g76010/T4O12_22)
At2g28800	Inner membrane protein ALBINO3

AtG Number	Name
At1g20200	26S proteasome non-ATPase regulatory subunit 3 homolog A (26S proteasome regulatory subunit RPN3a) (AtRPN3a) (26S proteasome regulatory subunit S3 homolog A) (Protein EMBRYO DEFECTIVE 2719) (Protein HAPLESS 15)
At5g62390	BAG family molecular chaperone regulator 7 (Bcl-2-associated athanogene 7)
At5g66470	GTP-binding protein Era (GTP-binding protein-like)
At4g36220	Cytochrome P450 84A1 (EC 1.14.-.-) (Ferulate-5-hydroxylase) (F5H)
At3g09680	40S ribosomal protein S23-1 (S12)
At5g51110	Transcriptional coactivator/pterin dehydratase
At2g37970	SOUL heme-binding-like protein
At5g58420	40S ribosomal protein S4-3
At1g48630	Guanine nucleotide-binding protein subunit beta-like protein B (Receptor for activated C kinase 1B)
At4g25550	Pre-mRNA cleavage factor Im 25 kDa subunit 2
At4g30950	Omega-6 fatty acid desaturase, chloroplastic (EC 1.14.19.-)
At4g02510	Translocase of chloroplast 159, chloroplastic (AtToc159) (EC 3.6.5.-) (159 kDa chloroplast outer envelope protein) (Plastid protein import 2) (Translocase of chloroplast 160, chloroplastic) (AtToc160) (Translocase of chloroplast 86, chloroplastic) (AtToc86)
At4g34670	40S ribosomal protein S3a-2
At2g40890	Cytochrome P450 98A3 (EC 1.14.-.-) (Protein REDUCED EPIDERMAL FLUORESCENCE 8) (p-coumaroylshikimate/quinate 3'-hydrolxylase) (C3'H)
At1g26230	Chaperonin 60 subunit beta 4, chloroplastic (CPN-60 beta 4)
At3g13460	CIPK1 interacting protein ECT2
At4g22010	At4g22010 (Pectinesterase like protein) (Pectinesterase-like protein) (Protein SKU5 similar 4)
At2g20990	Synaptotagmin-1 (NTMC2T1.1) (Synaptotagmin A)
At5g19370	Rhodanese-like/PpiC domain-containing protein 12 (Sulfurtransferase 12) (AtStr12)
At2g38280	AMP deaminase (AtAMPD) (EC 3.5.4.6) (Protein EMBRYONIC FACTOR 1)
At1g30360	CSC1-like protein ERD4 (Protein EARLY-RESPONSIVE TO DEHYDRATION STRESS 4)
At5g33320	Phosphoenolpyruvate/phosphate translocator 1, chloroplastic (AtPPT1) (Protein CAB UNDEREXPRESSED 1)
At3g13470	Chaperonin 60 subunit beta 2, chloroplastic (CPN-60 beta 2)
At1g47490	Polyadenylate-binding protein RBP47C (Poly(A)-binding protein RBP47C) (RNA-binding protein 47C) (AtRBP47C)
At3g15610	Expressed protein (Putative uncharacterized protein At3g15610) (Transducin/WD40 domain-containing protein) (WD-40 repeat protein-like)
AT3G04870	ZDS/ ZETA-CAROTENE DESATURASE
At1g52220	Protein CURVATURE THYLAKOID 1C, chloroplastic
At3g14110	Protein flourescent in blue light
At5g42080	Dynamin-related protein 1A
At4g34620	AT4g34620/T4L20_200 (At4g34620/T4L20_200) (Putative ribosomal protein S16) (Small subunit ribosomal protein 16)
At1g10510	Putative uncharacterized protein At1g10510 (RNI-like superfamily protein)
At3g02560	40S ribosomal protein S7-2

AtG Number	Name
At1g32080	Plastidal glycolate/glycerate translocator 1, chloroplastic (Bacterial membrane protein LrgB-like protein) (AtLrgB)
At1g27430	GYF domain-containing protein
At3g13120	30S ribosomal protein S10, chloroplastic
At3g48750	Cyclin-dependent kinase A-1 (CDKA;1) (EC 2.7.11.22) (EC 2.7.11.23) (Cell division control protein 2 homolog A)
At1g18500	2-isopropylmalate synthase 1, chloroplastic (EC 2.3.3.13) (Methylthioalkylmalate synthase-like 4)
At5g27540	Mitochondrial Rho GTPase 1 (AtMIRO1) (EC 3.6.5.-) (Miro-related GTPase 1)
At3g58570	DEAD-box ATP-dependent RNA helicase 52 (EC 3.6.4.13)
At5g67030	Zeaxanthin epoxidase, chloroplastic (AtZEP) (EC 1.14.13.90) (Protein ABA DEFICIENT 1) (AtABA1) (Protein IMPAIRED IN BABA-INDUCED STERILITY 3) (Protein LOW EXPRESSION OF OSMOTIC STRESS-RESPONSIVE GENES 6) (Protein NON-PHOTOCHEMICAL QUENCHING 2)
At3g61690	Nucleotidyltransferase
At5g67560	ADP-ribosylation factor-like A1D (ADP-ribosylation factor-like protein)
At1g49970	ATP-dependent Clp protease proteolytic subunit-related protein 1, chloroplastic (ClpR1) (nClpP5)
At4g15560	1-deoxy-D-xylulose-5-phosphate synthase, chloroplastic (1-deoxyxylulose-5-phosphate synthase) (DXP synthase) (DXPS) (EC 2.2.1.7) (Protein CLOROPLASTOS ALTERADOS 1)
At1g80300	ADP,ATP carrier protein 1, chloroplastic (ADP/ATP translocase 1) (Adenine nucleotide translocase 1)
At2g31410	Expressed protein (Putative uncharacterized protein At2g31410) (Uncharacterized protein)
At2g27530	60S ribosomal protein L10a-2
At5g15270	Putative uncharacterized protein At5g15270 (RNA-binding KH domain-containing protein)
At2g29200	Pumilio homolog 1 (APUM-1) (AtPUM1)
At1g17370	Oligouridylate binding protein 1B
At3g48560	Acetolactate synthase, chloroplastic (AtALS) (EC 2.2.1.6) (Acetohydroxy-acid synthase) (Protein CHLORSULFURON RESISTANT 1)
At1g77490	L-ascorbate peroxidase T, chloroplastic (EC 1.11.1.11) (Thylakoid-bound ascorbate peroxidase) (AtAPx06) (tAPX)
At5g09510	40S ribosomal protein S15-4
At2g19520	WD-40 repeat-containing protein MSI4 (Altered cold-responsive gene 1 protein)
At3g13670	Casein kinase-like protein (Protein kinase family protein) (Putative casein kinase)
At5g59250	D-xylose-proton symporter-like 3, chloroplastic
At1g30680	Twinkle homolog protein, chloroplastic/mitochondrial (DNA helicase) (EC 3.6.4.12) (DNA primase) (EC 2.7.7.-)
At5g41520	40S ribosomal protein S10-2
At3g25520	60S ribosomal protein L5-1
At3g54760	Dentin sialophosphoprotein-related protein
At4g19210	ABC transporter E family member 2 (ABC transporter ABCE.2) (AtABCE2) (RNase L inhibitor-like protein 2) (AtRLI2) (AthaRLI2)
At3g51820	Chlorophyll synthase, chloroplastic (EC 2.5.1.62) (Polyprenyl transferase) (Protein G4) (AtG4)

AtG Number	Name
At5g20090	Uncharacterized protein
At1g09130	ATP-dependent Clp protease proteolytic subunit-related protein 3, chloroplastic (ClpR3) (nClpP8)
At1g09130	ATP-dependent Clp protease proteolytic subunit-related protein 3, chloroplastic (ClpR3) (nClpP8)
At3g51140	Putative uncharacterized protein At3g51140 (Uncharacterized protein)
At5g24690	AT5g24690/MXC17_8 (Putative uncharacterized protein At5g24690) (Putative uncharacterized protein At5g24700) (Uncharacterized protein)
At5g13630	Magnesium chelatase subunit H
At1g18450	Actin-related protein 4
AtCg00830	50S ribosomal protein L2, chloroplastic
At1g07320	50S ribosomal protein L4 (AT1G07320 protein)
At1g14345	NAD(P)-linked oxidoreductase-like protein (Putative uncharacterized protein At1g14345)
At5g01590	Protein TIC 56, chloroplastic (Translocon at the inner envelope membrane of chloroplasts 56) (AtTIC56)
AtMg01170	ATP synthase subunit a-2 (F-ATPase protein 6) (P6-2)
At3g12345	FKBP-type peptidyl-prolyl cis-trans isomerase, putative (Genomic DNA, chromosome 3, P1 clone: MQC3) (Putative uncharacterized protein At3g12340) (Stress-enhanced protein 4) (Uncharacterized protein)
At3g60770	40S ribosomal protein S13-1
At1g35620	Protein disulfide-isomerase 5-2 (AtPDIL5-2) (Protein disulfide-isomerase 7-1) (AtPDIL7-1) (Protein disulfide-isomerase 8) (PDI8)
At5g10480	Very-long-chain (3R)-3-hydroxyacyl-CoA dehydratase PASTICCINO 2 (EC 4.2.1.134) (3-hydroxyacyl-CoA dehydratase PASTICCINO 2) (AtPAS2) (HACD) (HCD) (Protein PEPINO) (PEP) (Protein tyrosine phosphatase-like protein)
At5g04530	3-ketoacyl-CoA synthase 21 (KCS-21) (EC 2.3.1.199) (Very long-chain fatty acid condensing enzyme 21) (VLCFA condensing enzyme 21)
At3g49910	60S ribosomal protein L26-1
At1g04820	Tubulin alpha-4 chain
At4g38630	26S proteasome non-ATPase regulatory subunit 4 homolog (26S proteasome regulatory subunit RPN10) (AtRPN10) (26S proteasome regulatory subunit S5A homolog) (Multiubiquitin chain-binding protein 1) (AtMCB1)
AtCg00820	30S ribosomal protein S19, chloroplastic
At3g26570	Inorganic phosphate transporter 2-1, chloroplastic (H(+)/Pi cotransporter) (AtPht2;1)
At1g10950	Transmembrane 9 superfamily member 1 (Endomembrane protein 12) (Transmembrane nine protein 1) (AtTMN1)
At2g39010	Probable aquaporin PIP2-6 (Plasma membrane intrinsic protein 2-6) (AtPIP2;6) (Plasma membrane intrinsic protein 2e) (PIP2e) [Cleaved into: Probable aquaporin PIP2-6, N-terminally processed]
At1g23290	60S ribosomal protein L27a-2
At1g64550	ABC transporter F family member 3 (ABC transporter ABCF.3) (AtABCF3) (GCN20-type ATP-binding cassette protein GCN3)
At3g52750	Cell division protein FtsZ homolog 2-2, chloroplastic (AtFtsZ2-2) (Plastid division protein FTSZ2-2)
At3g06980	DEAD-box ATP-dependent RNA helicase 50 (EC 3.6.4.13)

AtG Number	Name
At1g31790	Pentatricopeptide repeat-containing protein At1g31790
At2g21580	40S ribosomal protein S25-2
At5g55610	Uncharacterized protein
At3g54470	Uridine 5'-monophosphate synthase (UMP synthase) [Includes: Orotate phosphoribosyltransferase (OPRTase) (EC 2.4.2.10); Orotidine 5'-phosphate decarboxylase (EC 4.1.1.23) (OMPdecase)]
At1g54520	Putative uncharacterized protein At1g54520 (Uncharacterized protein)
At4g27990	Putative uncharacterized protein AT4g27990 (Putative uncharacterized protein At4g27990) (Putative uncharacterized protein T13J8.100) (YGGT family protein)
At1g01320	Tetratricopeptide repeat-containing protein
At5g50000	Protein kinase
At1g56050	Obg-like ATPase 1
At1g75140	Uncharacterized membrane protein At1g75140
At1g48950	C3HC zinc finger-like protein
At5g09870	Cellulose synthase A catalytic subunit 5 [UDP-forming] (AtCesA5) (EC 2.4.1.12)
At3g57010	Protein STRICTOSIDINE SYNTHASE-LIKE 8 (AtSSL8) (Strictosidine synthase 5) (AtSS5)
At1g06700	PTI1-like tyrosine-protein kinase 1 (PTI1-1) (EC 2.7.10.2)
At1g67730	Very-long-chain 3-oxoacyl-CoA reductase 1 (EC 1.1.1.330) (Beta-ketoacyl reductase 1) (AtKCR1) (Protein GLOSSY 8) (gl8At)
AT3G57020	Merged into Q9M1J6.
At3g11945	Homogentisate solanesyltransferase, chloroplastic (AtHST) (EC 2.5.1.117) (Homogentisate phytyltransferase 2) (AtHPT2) (Vitamin E pathway gene 2-2 protein) (AtVTE2-2)
At3g53020	60S ribosomal protein L24-2 (Protein SHORT VALVE 1)
At1g64090	Reticulon-like protein B3 (AtRTNLB3)
At1g63710	Cytochrome P450 86A7 (EC 1.14.14.1)
At1g03880	12S seed storage protein CRB (Cruciferin 2) (AtCRU2) (Cruciferin B) (Legumin-type globulin storage protein CRU2) [Cleaved into: 12S seed storage protein CRB alpha chain (12S seed storage protein CRB acidic chain); 12S seed storage protein CRB beta chain (12S seed storage protein CRB basic chain)]
At3g50370	Uncharacterized protein
At3g55360	Very-long-chain enoyl-CoA reductase (EC 1.3.1.93) (Enoyl-CoA reductase) (AtECR) (Protein ECERIFERUM 10) (Synaptic glycoprotein SC2-like protein)
At5g49220	Putative uncharacterized protein At5g49220 (Uncharacterized protein)
At3g61870	Uncharacterized protein
At1g70730	Probable phosphoglucomutase, cytoplasmic 2 (PGM 2) (EC 5.4.2.2) (Glucose phosphomutase 2)
At5g42820	Splicing factor U2af small subunit B (U2 auxiliary factor 35 kDa subunit B) (U2 small nuclear ribonucleoprotein auxiliary factor small subunit B) (U2 snRNP auxiliary factor small subunit B) (Zinc finger CCCH domain-containing protein 60) (AtC3H60)
At5g63970	Putative uncharacterized protein At5g63970 (Ring domain ligase 3)
At4g04770	UPF0051 protein ABCI8, chloroplastic (ABC transporter I family member 8) (ABC transporter ABCI.8) (AtABCI8) (Non-intrinsic ABC protein 1) (Protein ABC1) (Plastid sufB-like protein) (Protein LONG AFTER FAR-RED 6)
At2g32480	Serine protease

AtG Number	Name
AT5G47040	ABERRANT PEROXISOME MORPHOLOGY 10
At3g54210	50S ribosomal protein L17, chloroplastic (CL17)
At3g08510	Phosphoinositide phospholipase C (EC 3.1.4.11)
At4g33650	Dynamin-related protein 3A (Dynamin-like protein 2) (Dynamin-like protein 2a)
At5g48810	Cytochrome B5 isoform D (AtCb5-D) (Cytochrome b5 isoform B) (AtCb5-B)
At1g78620	Putative uncharacterized protein At1g78620 (T30F21.5 protein) (Uncharacterized transmembrane protein)
At2g33450	50S ribosomal protein L28, chloroplastic (CL28)
At2g35840	Probable sucrose-phosphatase 2 (AtSPP2) (EC 3.1.3.24)
At3g13580	60S ribosomal protein L7-4
AtCg00330	30S ribosomal protein S14, chloroplastic
At4g36480	Long chain base biosynthesis protein 1 (AtLCB1) (EC 2.3.1.50) (Protein EMBRYO DEFECTIVE 2779) (Protein FUMONISIN B1 RESISTANT 11)
At5g19750	Mpv17/PMP22 family protein
At3g57470	Insulysin
At3g49560	At3g49560 (Mitochondrial import inner membrane translocase subunit Tim17/Tim22/Tim23 family protein) (Putative uncharacterized protein At3g49560) (Putative uncharacterized protein T9C5.150)
At2g14720	Vacuolar-sorting receptor 4 (AtVSR4) (BP80-like protein a) (AtBP80a) (Epidermal growth factor receptor-like protein 2b) (AtELP2b)
At3g27570	Sucrase/ferredoxin-like protein
At5g47200	Ras-related protein RABD2b (AtRABD2b) (Ras-related protein Rab1A) (AtRab1A)
At3g25860	Dihydrolipoyllysine-residue acetyltransferase component 4 of pyruvate dehydrogenase complex, chloroplastic (EC 2.3.1.12) (Dihydrolipoamide S-acetyltransferase component 4 of pyruvate dehydrogenase complex) (Pyruvate dehydrogenase complex component E2 4) (PDC-E2 4) (PDCE2 4) (plE2)
At2g47000	ABC transporter B family member 4 (ABC transporter ABCB.4) (AtABCB4) (Multidrug resistance protein 4) (P-glycoprotein 4)
At1g18060	AT1g18060/T10F20.23 (Putative uncharacterized protein At1g18060) (T10O22.3) (Uncharacterized protein)
At3g14600	60S ribosomal protein L18a-3
At3g12080	GTP-binding protein
At1g15730	At1g15730/F7H2_7 (Cobalamin biosynthesis CobW-like protein) (F7H2.7 protein) (Putative PRLI-interacting factor L)
At1g76090	24-methylenesterol C-methyltransferase 3 (24-sterol C-methyltransferase 3) (Sterol-C-methyltransferase 3) (EC 2.1.1.143)
At1g02280	Translocase of chloroplast 33, chloroplastic (AtToc33) (EC 3.6.5.-) (33 kDa chloroplast outer envelope protein) (Plastid protein import 1)
At5g65020	Annexin
At4g12390	Pectin methylesterase inhibitor 1 (Putative uncharacterized protein AT4g12390) (Putative uncharacterized protein At4g12390) (Putative uncharacterized protein At4g12390; T4C9.230) (Putative uncharacterized protein T4C9.230)
At5g14640	Shaggy-related protein kinase epsilon (EC 2.7.11.1) (ASK-epsilon)
At5g27390	Mog1/PsbP/DUF1795-like photosystem II reaction center PsbP family protein
At5g05780	Probable 26S proteasome non-ATPase regulatory subunit 8A

AtG Number	Name
At2g24765	ADP-ribosylation factor 3 (AtARF3) (Protein ARF-LIKE 1) (AtARL1)
At1g17840	ABC transporter G family member 11 (ABC transporter ABCG.11) (AtABCG11) (Protein CUTICULAR DEFECT AND ORGAN FUSION 1) (Protein DESPERADO) (Protein PERMEABLE LEAVES 1) (White-brown complex homolog protein 11) (AtWBC11)
At1g51500	ABC transporter G family member 12 (ABC transporter ABCG.12) (AtABCG12) (Protein ECERIFERUM 5) (White-brown complex homolog protein 12) (AtWBC12)
At2g39470	Photosynthetic NDH subunit of lumenal location 1, chloroplastic (PsbP-like protein 2)
At5g64940	ABC transporter-like (Putative ABC transporter) (Putative ABC transporter protein)
At4g27720	AT4g27720/T29A15_210 (At4g27720/T29A15_210) (Major facilitator protein) (Putative transporter) (Putative uncharacterized protein T29A15.210)
At1g09940	Glutamyl-tRNA reductase 2, chloroplastic (GluTR) (EC 1.2.1.70)
AtCg01090	NAD(P)H-quinone oxidoreductase subunit I, chloroplastic (EC 1.6.5.-) (NAD(P)H dehydrogenase subunit I) (NDH subunit I) (NADH-plastoquinone oxidoreductase subunit I)
At2g37410	Mitochondrial import inner membrane translocase subunit TIM17-2
At4g35060	At4g35060 (Farnesylated protein (ATFP6)) (Heavy metal transport/detoxification domain-containing protein) (Putative uncharacterized protein AT4g35060) (Putative uncharacterized protein M4E13.120)
At2g47610	60S ribosomal protein L7a-1
At1g08640	Chloroplast J-like domain 1-containing protein (Putative uncharacterized protein At1g08640)
At4g39150	AT4g39150/T22F8_50 (DNAJ heat shock N-terminal domain-containing protein) (DnaJ-like protein)
At2g34470	Urease accessory protein G (AtUREG)
At5g39410	Probable mitochondrial saccharopine dehydrogenase-like oxidoreductase At5g39410 (SDH) (EC 1.-.-.-)
At1g72750	Mitochondrial import inner membrane translocase subunit TIM23-2
At2g36885	Uncharacterized protein
At5g53060	At5g53060 (RNA-binding KH domain-containing protein) (RNA-binding protein-like)
At5g18660	Divinyl chlorophyllide a 8-vinyl-reductase, chloroplastic (EC 1.3.1.75) (Protein PALE-GREEN AND CHLOROPHYLL B REDUCED 2)
At4g16630	DEAD-box ATP-dependent RNA helicase 28 (EC 3.6.4.13)
At1g17850	Rhodanese homology domain-containing protein
At1g48860	3-phosphoshikimate 1-carboxyvinyltransferase (EC 2.5.1.19)
At1g11680	Sterol 14-demethylase (EC 1.14.13.70) (Cytochrome P450 51A2) (Cytochrome P450 51G1) (AtCYP51) (Obtusifoliol 14-demethylase) (Protein EMBRYO DEFECTIVE 1738)
At4g34240	Aldehyde dehydrogenase family 3 member I1, chloroplastic (AtALDH3) (Ath-ALDH3) (EC 1.2.1.3)
At1g20050	Probable 3-beta-hydroxysteroid-Delta(8),Delta(7)-isomerase (EC 5.3.3.5) (Cholestenol Delta-isomerase) (Delta(8)-Delta(7) sterol isomerase) (D8-D7 sterol isomerase)
At3g18680	Genomic DNA, chromosome 3, P1 clone: MVE11 (Putative uridylate kinase) (Uridylate kinase-like protein)
At2g19860	Hexokinase-2 (EC 2.7.1.1)
At3g04340	FtsH extracellular protease family protein

AtG Number	Name
At5g18570	GTP-binding protein OBGC, chloroplastic (AtOBGC) (GTP-binding protein OBG-like) (AtOBGL) (Protein CHLOROPLASTIC SAR1) (CPSAR1) (Protein EMBRYO DEFECTIVE 269) (Protein EMBRYO DEFECTIVE 3138)
AT4G16143	**IMPA-2/ IMPORTIN ALPHA ISOFORM 2**
At2g48070	Expressed protein (Putative uncharacterized protein At2g48070) (Resistance to phytophthora 1 protein)
AT5G58260	Merged into Q9LVM2.
At2g05830	Methylthioribose-1-phosphate isomerase (M1Pi) (MTR-1-P isomerase) (EC 5.3.1.23) (S-methyl-5-thioribose-1-phosphate isomerase) (Translation initiation factor eIF-2B subunit alpha/beta/delta-like protein)
At1g76810	Eukaryotic translation initiation factor 2 (EIF-2) family protein
At4g00090	AT4g00090/F6N15_8 (At4g00090/F6N15_8) (Transducin/WD40 domain-containing protein)
At1g37130	Nitrate reductase [NADH] 2 (NR2) (EC 1.7.1.1)
At1g58290	Glutamyl-tRNA reductase 1, chloroplastic (GluTR) (EC 1.2.1.70)
At4g26870	Asx tRNA synthetase (AspRS/AsnRS) class II core domain-contating protein (Putative aspartate-tRNA ligase)
At5g24650	AT5g24650/K18P6_19 (At5g24650) (At5g24650/K18P6_19) (Emb|CAB62460.1) (Mitochondrial import inner membrane translocase subunit Tim17/Tim22/Tim23 family protein)
At5g55670	RNA recognition motif-containing protein
At4g34430	SWI/SNF complex subunit SWI3D (AtSWI3D) (Transcription regulatory protein SWI3D)
At1g42960	Chloroplast inner membrane localized protein (Putative uncharacterized protein At1g42960) (Putative uncharacterized protein F13A11.2)
At2g43950	Outer envelope pore protein 37, chloroplastic (Chloroplastic outer envelope pore protein of 37 kDa) (AtOEP37)
At5g60250	C3H4 type zinc finger protein (Emb|CAB75487.1)
AtCg00670	ATP-dependent Clp protease proteolytic subunit 1 (EC 3.4.21.92) (Endopeptidase ClpP1) (pClpP)
At3g17970	Outer envelope protein 64, chloroplastic (Translocon at the outer membrane of chloroplasts 64-III)
At1g08470	Protein STRICTOSIDINE SYNTHASE-LIKE 3 (AtSSL3) (Strictosidine synthase 9) (AtSS9)
At2g25610	V-type proton ATPase subunit c"2 (V-ATPase subunit c"2) (Vacuolar H(+)-ATPase subunit c" isoform 2) (Vacuolar proton pump subunit c"2)
At4g36390	CDK5RAP1-like protein
At4g19640	Ras-related protein RABF2b (AtRABF2b) (Ras-related protein Ara-7) (Ras-related protein Rab5B) (AtRab5B)
At5g18110	Eukaryotic translation initiation factor NCBP (Novel cap-binding protein) (nCBP) (mRNA cap-binding protein)
At5g64330	Root phototropism protein 3 (BTB/POZ domain-containing protein RPT3) (Non-phototropic hypocotyl protein 3)
At1g55850	Cellulose synthase-like protein E1 (AtCslE1) (EC 2.4.1.-)
At3g21690	At3g21690 (Genomic DNA, chromosome 3, P1 clone: MIL23) (MATE efflux family protein)
At1g50450	At1g50450/F11F12_20 (Saccharopine dehydrogenase)

AtG Number	Name
At5g55280	Cell division protein FtsZ homolog 1, chloroplastic (AtFtsZ1) (AtFtsZ1-1) (Chloroplast FtsZ) (CpFtsZ) (Protein ACCUMULATION AND REPLICATION OF CHLOROPLASTS 10) (Protein PLASTID MOVEMENT IMPAIRED4)
At3g13062	At3g13062 (Polyketide cyclase/dehydrase and lipid transport superfamily protein)
At2g47840	Protein TIC 20-II, chloroplastic (Translocon at the inner envelope membrane of chloroplasts 20-II) (AtTIC20-II)
At4g14210	Phytoene desaturase 3
At4g27080	Protein disulfide-isomerase 5-4 (AtPDIL5-4) (Protein disulfide-isomerase 7) (PDI7) (Protein disulfide-isomerase 8-2) (AtPDIL8-2)
At4g19710	Bifunctional aspartokinase/homoserine dehydrogenase 2, chloroplastic (AK-HD 2) (AK-HSDH 2) (Beta-aspartyl phosphate homoserine 2) [Includes: Aspartokinase (EC 2.7.2.4); Homoserine dehydrogenase (EC 1.1.1.3)]
At3g27820	Probable monodehydroascorbate reductase, cytoplasmic isoform 2 (MDAR 2) (EC 1.6.5.4)
At1g30890	Integral membrane HRF1-like protein (Putative uncharacterized protein At1g30890)
AtMg00990	NADH-ubiquinone oxidoreductase chain 3 (EC 1.6.5.3) (NADH dehydrogenase subunit 3)
At3g16240	Aquaporin TIP2-1 (Delta-tonoplast intrinsic protein) (Delta-TIP) (Tonoplast intrinsic protein 2-1) (AtTIP2;1) [Cleaved into: Aquaporin TIP2-1, N-terminally processed]
At1g79560	ATP-dependent zinc metalloprotease FTSH 12, chloroplastic (AtFTSH12) (EC 3.4.24.-)
At5g47110	At5g47110 (Chlorophyll A-B binding family protein)
AT1G50250	FTSH PROTEASE 1
At5g46580	Pentatricopeptide repeat-containing protein At5g46580, chloroplastic
At5g16715	ATP binding/valine-tRNA ligase/aminoacyl-tRNA ligase
At3g16000	MAR-binding filament-like protein 1
At3g05590	60S ribosomal protein L18-2
At5g42980	Thioredoxin H3 (AtTrxh3) (Thioredoxin 3) (AtTRX3)
At5g40890	Chloride channel protein
At2g27710	60S acidic ribosomal protein P2-2
At5g05740	S2P-like putative metalloprotease
At5g02450	60S ribosomal protein L36-3
At1g05010	1-aminocyclopropane-1-carboxylate oxidase 4 (ACC oxidase) (EC 1.14.17.4) (Ethylene-forming enzyme) (EFE)
At1g21130	At1g21130 (Indole glucosinolate O-methyltransferase 4)
At3g62700	ABC transporter C family member 14 (ABC transporter ABCC.14) (AtABCC14) (EC 3.6.3.44) (ATP-energized glutathione S-conjugate pump 10) (Glutathione S-conjugate-transporting ATPase 10) (Multidrug resistance-associated protein 10)
At3g25480	Rhodanese-like domain-containing protein 4A, chloroplastic (Sulfurtransferase 4A) (AtStr4a)
At1g11260	Sugar transport protein 1 (Glucose transporter) (Hexose transporter 1)
At1g06190	Rho-N domain-containing protein 1, chloroplastic
At5g64840	ABC transporter F family member 5 (ABC transporter ABCF.5) (AtABCF5) (GCN20-type ATP-binding cassette protein GCN5)
At1g48920	Nucleolin 1 (Protein NUCLEOLIN LIKE 1) (AtNUC-L1) (Protein PARALLEL 1) (AtPARL1)

AtG Number	Name
At4g10060	Non-lysosomal glucosylceramidase (NLGase) (EC 3.2.1.45)
At3g06480	DEAD-box ATP-dependent RNA helicase 40 (EC 3.6.4.13)
At5g60170	RNA binding (RRM/RBD/RNP motifs) family protein
At3g04790	Probable ribose-5-phosphate isomerase 3, chloroplastic (EC 5.3.1.6) (Phosphoriboisomerase 3) (Protein EMBRYO DEFECTIVE 3119)
AT5G05000	ARABIDOPSIS THALIANA TRANSLOCON AT THE OUTER ENVELOPE MEMBRANE OF CHLOROPLASTS 34
At5g18400	Anamorsin homolog (Fe-S cluster assembly protein DRE2 homolog)
At1g59990	DEAD-box ATP-dependent RNA helicase 22 (EC 3.6.4.13)
At5g19690	Dolichyl-diphosphooligosaccharide--protein glycosyltransferase subunit STT3A (Oligosaccharyl transferase subunit STT3A) (STT3-A) (EC 2.4.99.18) (Integral membrane protein 1) (Protein STAUROSPORIN AND TEMPERATURE SENSITIVE 3-LIKE A)
At2g47450	Signal recognition particle 43 kDa protein, chloroplastic (Chromo protein SRP43) (CpSRP43)
At2g41560	Calcium-transporting ATPase 4, plasma membrane-type (EC 3.6.3.8) (Ca(2+)-ATPase isoform 4)
At5g62670	ATPase 11, plasma membrane-type (EC 3.6.3.6) (Proton pump 11)
At2g30930	Expressed protein (Putative uncharacterized protein At2g30930) (Putative uncharacterized protein At2g30930; F7F1.14) (Uncharacterized protein)
At2g40100	Chlorophyll a-b binding protein CP29.3, chloroplastic (LHCB4.3) (LHCII protein 4.3)
At1g51690	Serine/threonine protein phosphatase 2A 55 kDa regulatory subunit B alpha isoform (AtB alpha) (PP2A, subunit B, alpha isoform)
At2g30200	[acyl-carrier-protein] S-malonyltransferase
At5g14170	SWI/SNF complex component SNF12 homolog
At3g23820	UDP-glucuronate 4-epimerase 6 (EC 5.1.3.6) (UDP-glucuronic acid epimerase 6) (AtUGlcAE2)
At1g06460	Alpha-crystallin domain 32.1 (At1g06460) (Peroxisomal small heat shock protein Acd31.2)
At3g48930	40S ribosomal protein S11-1 (Protein EMBRYO DEFECTIVE 1080)
At5g12130	Protein pigment defective 149
At4g17090	Beta-amylase 3, chloroplastic (EC 3.2.1.2) (1,4-alpha-D-glucan maltohydrolase) (Beta-amylase 8) (Chloroplast beta-amylase) (CT-BMY)
At3g49870	ADP-RIBOSYLATION FACTOR-like protein (ADP-ribosylation factor-like A1C) (ADP-ribosylation factor-like protein)
At3g48890	Membrane steroid-binding protein 2 (AtMP2) (Membrane-associated progesterone-binding protein 3) (AtMAPR3)
At2g20230	Tetraspanin-18 (TOM2A homologous protein 2)
At2g17290	Calcium-dependent protein kinase 6 (EC 2.7.11.1) (Calcium-dependent protein kinase isoform CDPK3) (AtCDPK3) (Calmodulin-domain protein kinase CDPK isoform 6)
At3g52190	SEC12-like protein 1 (Protein PHOSPHATE TRANSPORTER TRAFFIC FACILITATOR 1) (PHF-1)
At5g20250	Probable galactinol--sucrose galactosyltransferase 6 (EC 2.4.1.82) (Protein DARK INDUCIBLE 10) (Raffinose synthase 6)

AtG Number	Name
At3g47450	NO-associated protein 1, chloroplastic/mitochondrial (AtNOA1) (Dubious mitochondrial nitric oxide synthase 1) (AtNOS1) (EC 1.14.13.39) (GTPase NOA1) (Protein RESISTANT TO INHIBITION BY FOSMIDOMYCIN 1)
At3g45780	Phototropin-1 (EC 2.7.11.1) (Non-phototropic hypocotyl protein 1) (Root phototropism protein 1)
At2g21340	MATE efflux family protein
At1g55900	Mitochondrial import inner membrane translocase subunit TIM50
At3g16060	AT3g16060/MSL1_10 (ATP binding microtubule motor family protein)
At4g31120	Protein arginine N-methyltransferase 1.5 (AtPMRT15) (AtPMRT5) (EC 2.1.1.-) (EC 2.1.1.125) (Shk1 kinase-binding protein 1 homolog)
At4g31500	Cytochrome P450 83B1 (EC 1.14.-.-) (Protein ALTERED TRYPTOPHAN REGULATION 4) (Protein RED ELONGATED 1) (Protein SUPERROOT 2)
At2g32700	WD40 repeat protein MUCILAGE-MODIFIED 1
At1g19740	ATP-dependent protease La domain-containing protein (F6F9.20 protein) (Putative uncharacterized protein At1g19740)
At5g01750	Protein LURP-one-related 15
At3g27120	P-loop containing nucleoside triphosphate hydrolases superfamily protein
At2g47710	Adenine nucleotide alpha hydrolases-like protein (Expressed protein) (Putative uncharacterized protein At2g47710) (Putative uncharacterized protein At2g47710; F17A22.10)
At4g30210	NADPH--cytochrome P450 reductase 2 (EC 1.6.2.4)
At3g07810	AT3g07810/F17A17_15 (Putative RNA-binding protein) (RNA recognition motif-containing protein)
At5g23040	AT5g23040/MYJ24_3 (At5g23040/MYJ24_3) (Cell growth defect factor) (Cell growth defect factor 1) (Emb|CAB62636.1)
At1g52510	Putative hydrolase
At3g15110	At3g15110 (Uncharacterized protein)
At5g06680	Gamma-tubulin complex component 3 (AtGCP3) (GCP-3) (Spindle pole body component 98) (AtSPC98)
At1g16820	V-ATPase-related protein
At1g29470	Probable methyltransferase PMT24 (EC 2.1.1.-)
At3g15450	Aluminum induced protein with YGL and LRDR motif
At1g54990	Protein AUXIN RESPONSE 4
At1g79050	DNA repair protein recA homolog 1, chloroplastic (Recombinase A homolog 1)
At4g03560	Two pore calcium channel protein 1 (Calcium channel protein 1) (AtCCH1) (Fatty acid oxygenation up-regulated protein 2) (Voltage-dependent calcium channel protein TPC1) (AtTPC1)
At1g10290	Dynamin-2A (EC 3.6.5.5) (Dynamin-like protein 6) (Dynamin-related protein 2A)
At3g43520	AT3g43520/T18D12_90 (At3g43520/T18D12_90) (Transmembrane protein 14C)
At2g43910	Thiocyanate methyltransferase 1 (EC 2.1.1.n4) (Protein HARMLESS TO OZONE LAYER 1) (AtHOL1)
At5g03520	Ras-related protein RABE1d (AtRABE1d) (Ras-related protein Rab8C) (AtRab8C)
At5g57110	Calcium-transporting ATPase 8, plasma membrane-type (EC 3.6.3.8) (Ca(2+)-ATPase isoform 8)
At1g01620	Aquaporin PIP1-3 (AtPIP1;3) (Plasma membrane intrinsic protein 1c) (PIP1c) (Transmembrane protein B) (TMP-B)

AtG Number	Name
AtCg00170	DNA-directed RNA polymerase subunit beta'' (EC 2.7.7.6) (PEP) (Plastid-encoded RNA polymerase subunit beta'') (RNA polymerase subunit beta'')
At1g31230	Bifunctional aspartokinase/homoserine dehydrogenase 1, chloroplastic (AK-HD 1) (AK-HSDH 1) (Beta-aspartyl phosphate homoserine 1) [Includes: Aspartokinase (EC 2.7.2.4); Homoserine dehydrogenase (EC 1.1.1.3)]
At5g07290	Protein MEI2-like 4 (AML4) (MEI2-like protein 4)
At4g33360	Rossmann-fold NAD(P)-binding domain-containing protein
At4g35760	Thiol-disulfide oxidoreductase LTO1 (EC 1.1.4.-) (Protein LUMEN THIOL OXIDOREDUCTASE 1) (Vitamin K reductase)
At3g57090	Mitochondrial fission 1 protein A (FIS1 homolog A) (AtFIS1a) (Protein BIGYIN 1)
At3g22230	60S ribosomal protein L27-2
At5g56290	Peroxisome biogenesis protein 5 (Peroxin-5) (AtPEX5) (Peroxisomal targeting signal type 1 receptor) (Pex5p)
At4g16990	Resistance to leptosphaeria maculans 3 protein
At3g49490	Putative uncharacterized protein T9C5.90 (Uncharacterized protein)
At1g12310	Probable calcium-binding protein CML13 (Calmodulin-like protein 13)
At5g21326	CBL-interacting serine/threonine-protein kinase 26 (EC 2.7.11.1) (SNF1-related kinase 3.26) (SOS2-like protein kinase PKS26)
At1g58110	BZIP transcription factor-like protein
At4g00730	Homeobox-leucine zipper protein ANTHOCYANINLESS 2
At1g13730	At1g13730 (At1g13730/F21F23_12) (Expressed protein) (F21F23.16 protein) (Nuclear transport factor 2 and RNA recognition motif domain-containing protein)
At5g48880	3-ketoacyl-CoA thiolase 5, peroxisomal (EC 2.3.1.16) (Acetyl-CoA acyltransferase 5) (Beta-ketothiolase 5) (Peroxisomal 3-oxoacyl-CoA thiolase 5)
At1g21480	Exostosin family protein
At3g10840	Alpha/beta-hydrolase domain-containing protein (At3g10840)

Table S2: Primers used in this study.

F6F3 S [SapI]	GAATATACCGAATTAACAAAAATTCTGAAGCTCTT
F6F3 AS [SapI]	GCATTGTTGCTGTCTTCATATATCAACAC
F21M12 S	GGCTTTCTCGAAATCTGTCC
F21M12 AS	TTACTTTTTGCCTCTTGTCATTG
DNAJ[XbaI] F	CTCAGCCACAACCAATCACCGAATTCTAG
DNAJ[XbaI] R	GTTGCAATCGGCGATGGAATCC
T14P S [-14/14]	GCTATGACGCTCCGACATAATCAAC
T14P AS [-14/14]	GGTTGAGAATGATCAATATTACTCGG
3xGFP SpeI S	CAAAGAAGAAGAGAACTAGTATGGTGAGCAAG
3xGFP SpeI AS	GATCGGGGATCGGAACTAGTCTTGTACAGCTC
IMPα6 I miR-s	GATATACTTTATACCTGTTCCGTTCTCTCTTTTGTATTCC
IMPα6 II miR-a	GAACGGAACAGGTATAAAGTATATCAAAGAGAATCAATGA
IMPα6 III miR*-s	GAACAGAACAGGTATTAAGTATTTCACAGGTCGTGATATG
IMPα6 IV miR*-a	GAAATACTTAATACCTGTTCTGTTCTACATATATATTCCT
IMPα6 2kbProm S [ApaI]	CCGGGCCCGCAAATAAACAACACGAGC
IMPα6 CDS AS (oS) [XhoI]	ACCTCGAGACCAAAGTTGAATCCACCC
IMPα6 for inSitu F	AAGCAGTCAAAATCCTGG
IMPα6 for inSitu R	ATTCACTCAAAACATGACCC
IMPα6 dCAPS [BfmI] F	AAATCATCTCTGTTTTCTCCACTACA
IMPα6 dCAPS [BfmI] R	GAATTTGACTTGTGTTCCCAG
MP dCAPs [KpnI] F	GATCCCTCTAGCTAAGTACCGTAA
MP dCAPs [KpnI] R	CTGATTCCAACAATAGTTCCCAGGTAC
BDL dCAPs [NaeI] F	TGGCAGTCAAGTGGTAGGCCGG
BDL dCAPs [NaeI] R	ACCCTAAGCCCTGAACTTTC
At1G02690 F	CTTTTGTAGACGTTGCGA
At1G02690 R	CCTTCTTATTTTGTCACGC
IMPα6-Exon 7 S	CTCCGTACAATTGGTAACAT
LB2	GCTTCCTATTATATCTTCCCAAATTACCAATACA
IMPα-3 tDNA F	CTGCAGTCGTTTTTTTTTGG
IMPα-3 tDNA R	GATAACATAATCATGCCTGG
LB1.3	ATTTTGCCGATTTCGGAAC
IMPα6 Exon10 AS	CCACCCGTAGGAGCATTA
actin F	TGAGCAAAGAAATCACAGCACTTGC
actin R	TCTGTGAACGATTCCTGGACCTG
Renilla Luciferase F	CCTACGAGCACCAAGACAAGA
Renilla Luciferase R	TGTCAGGCCACTCGTCCCAGGA

Manuscripts in Preparation

Herud, O., A. Stiel, B. Höcker and G. Jürgens (In preparation). "Direct visualization of the phytohormone auxin via semi-rational design of a biosensor."

Title (75 characters)

Direct visualization of the phytohormone auxin via semi-rational design of a biosensor

Abstract (150 words)

Pattern formation is frequently governed by small molecules. Despite their relevance during development, scientists usually have to rely on indirect readouts to study their activities. The small molecule auxin is the main morphogen in plants. It is indispensable for organ initiation, tropic growth responses and cell cycle control.

Here we report the engineering of a FRET-based biosensor for auxin by redesign of the binding pocket of the *E. coli* tryptophan repressor. This biosensor allows the direct and dynamic measurement of the main developmental regulator during the life-cycle of the plant at subcellular resolution.

Introduction (500 max)

Small molecules play a pivotal role in most regulatory processes, in single cells and on the level of whole organisms. The study of their temporal and spatial distribution is therefore a hallmark of many topics in life sciences with an outreach to medical diagnostics. However, visualization of small molecules *in vivo* without significant perturbation of the system often proofs difficult. Genetically encodable molecular sensors providing readout of small molecule concentrations *in vivo* are therefore tools of high demand.

In plants the most important regulative small molecule is the phytohormone auxin, mainly indole-3-acetic acid (IAA) (Simon and Petrasek 2011). Auxin concentration gradients play a role in virtually every aspect of plant life: it controls organogenesis, photo- and gravitropism, and regulates cell shape and division (Teale *et al.* 2006, Perrot-Rechenmann 2010). Plants with defects in auxin distribution fail to establish a correct embryonic axis, subsequently lacking the root and leaves (Friml *et al.* 2003).

The auxin dependent degradation of Aux/IAA proteins and thereby induction of expression of auxin response genes have been studied to address the action of auxin in *Arabidopsis thaliana* (*A. th*.) and other plants (Ulmasov *et al.* 1997, Sabatini *et al.* 1999, Zhou *et al.* 2014). Auxin response maxima are usually visualized with the artificial auxin response promoter DR5 (Ulmasov *et al.* 1997) which is induced by IAA (Sabatini *et al.* 1999 and reference therein). However, the transcriptional auxin response pathway is heavily regulated on all levels of the signaling cascade: transcriptionally (Parry *et al.* 2009, Rademacher *et al.* 2011), post-transcriptionally (Mallory *et al.* 2005, Wang *et al.* 2005, Navarro *et al.* 2006, Liu *et al.* 2007), and post-translationally (Vert *et al.* 2008, Terrile *et al.* 2012, Cho *et al.* 2014). This allows for cross-talk between the plant hormone pathways and fine-tuning of the response (Nakamura *et al.* 2003), but for quantification purposes precludes an accurate measurement of the auxin concentration. To reduce the regulatory leverage points, another approach uses the degradation of the Aux/IAA protein IAA28 fused to the fluorescent reporter Venus to infer auxin levels from the absence of the Venus signal (Brunoud *et al.* 2012). In both cases the response is based on parts of the auxin pathway itself and not on a dedicated measurement of an auxin molecule.

Here we describe the generation of a genetically encoded fluorescent sensor for the major auxin IAA. For the first time, this sensor allows to directly follow concentration gradients of IAA in plant cells and their fate determining effects. Our engineering is based on the semi-rational redesign of the binding pocket of a tryptophan repressor (TrpR) based sensor (Kaper *et al.* 2007) aiming at an affinity swap from the IAA related tryptophan (TRP) to auxin. Along with our design strategy we elucidated a number of x-ray

structures providing insight into the steps leading to the affinity switch and discrimination against other ligands in molecular detail.

Main text (<=6 Subheadings, 2500 words)

Semi-rational design of AuxSen

IAA is a derivative of tryptophan (TRP) with the amino-acid group of the latter replaced by a carboxyl as a substituent of the mutual indole-ring. We assumed a comparable binding mode for TRP and IAA regarding the indole-ring and focused our design effort on positions in the vicinity of the two substituents likely to foster their discrimination. This selection was later expanded to adjacent residues. About 2000 variants were generated using saturation mutagenesis and screened for both IAA-affinity as well as –specificity, exploiting the FRET-readout of the original sensor (Kaper *et al.* 2007). In later rounds screening for discrimination against TRP was expanded by discrimination against indole-3-acetonitrile (IAN), which is the only indole-based compound highly similar to IAA and abundant in *A. th.* (Novak *et al.* 2012). To exclude false-positives based on interaction of the ligands with the FRET-pairs and to provide accurate binding data, selected variants were analyzed by isothermal titration calorimetry (ITC). Furthermore, the structure of several variants was elucidated allowing us to refine our positional selection based on structural findings [Supp Material].

After several rounds of design, the affinity for IAA could not be improved further. While the affinity for TRP was completely diminished already in early stages of the design-approach, affinity for the alternative ligand IAN mirrored the improvements made for IAA. Consequently our final variant was chosen based upon IAA affinity (X µM) and most beneficial discrimination against IAN (Y µM).

The sensor binds auxin as a facultative dimer, and therefore we cloned it into tandem-dimer configurations with one fluorophore placed N-terminally and one between the two auxin binding domains. We screened a library of 16 fluorophores in different combinations and different configurations, resulting in 52 different sensors. The variant performing best, an Aquamarine - mNeonGreen pair, was used for further optimization. We varied the length and amino acid compositions of all linkers individually, chose the best and repeated this process for two more rounds until all linkers were optimized, resulting in the final sensor (“AuxSen”).

in vitro and *in vivo* characterization of AuxSen

AuxSen has a $Kd_{[IAA]}$ of X µM and a fast Kon/Koff rate (? µM/s) and *in vitro* it exhibits a FRET ratio change by the factor of 3 after treatment with 50 µM IAA, which is in the same range as the auxin concentration expected within cells (Petersson *et al.* 2009). The signal is stable around the cytoplasmic pH of 7.3 (Shen *et al.* 2013) and resistant to reducing and oxidizing environments (Extended Data – pH, H2O2, DTT, Salt).

Specificity of AuxSen for IAA was tested against other indole-derivatives published to be present in *A.th.*. Beside IAN no other component caused a significant response at concentrations present in plants (Extended Data – Indole derivatives). Whole plant IAN levels are reported to be higher (Novak *et al.* 2012), but plants show growth responses at IAN concentrations below the detection limit of AuxSen (Extended Data – IAN; DR5::RFP reference), indicating that cytosolic IAN would not interfere with the measurements.

As a first step to confirm the functionality *in planta*, we expressed the sensor transiently under the control of the strong viral *35S* promoter in protoplasts. Figure 2 shows the auxin response in protoplasts. Individual protoplasts differ strongly in the ratio, but populations show clear tendencies. Under low auxin concentrations, the standard deviation stays small, but it increases with higher concentrations in the medium, suggesting that IAA in not taken up by the cells with equal efficiency (Figure 2a).

To quantify AuxSen responses *in vivo*, we generated lines expressing AuxSen under a variety of promoters. To enhance the contrast we fused it to a nuclear localization sequence (NLS). Overall, the ubiquitous ELONGATION FACOTOR 1 a promoter (pEF1a) proved to perform the best. Ectopic expression in the plant did not interfere with auxin signaling as exemplified by root growth responses and lateral root initiation (Figure Extended data – Root growth).

The auxin maximum in the root tip was confirmed by many independent studies. Tissue specific mass spectrometry (Petersson *et al.* 2009), antibody staining against cross-linked (Leverone *et al.* 1991, Benkova *et al.* 2003), *DII-Venus* (Brunoud *et al.* 2012) and *DR5* (Sabatini *et al.* 1999) all indicate an auxin maximum around the meristem. Confocal imaging of AuxSen in seedling roots exhibited maximal FRET signal intensity in the vascular tissue adjacent to the meristem (Figure AuxSen in the root).

Next we examined the response of pEF-1a::NLS:AuxSen upon variation of IAA levels *in planta*. First we treated seedlings with 10 µM IAA and observed the response over time. Within a few minutes the AuxSen signal increased (Figure AuxSen in the root). To further confirm the AuxSen response, we studied the gravitropic response of seedling roots, which depends on the redistribution of auxin causing root-bending towards the gravitropic force. This redistribution becomes visible with AuxSen, the FRET signal increases basally within a few minutes Figure AuxSen in the root). Because this process depends on the redistribution of IAA, it is inhibited by the auxin transport inhibitor naphthylphthalamic acid (NPA) (Extended data).

These experiments establish AuxSen as a reliable tool in plant biology, for the first time enabling scientists to visualize the dynamics of the main plant hormone directly.

Structural Understanding

Next to improving our design approach we employed the structural data of several variants to gather a comprehensive understanding of the redesign of a binding pocket as well as factors governing specificity in general. As expected, comparison of the binding pocket of Trp-Wt with the native ligand TRP and with bound IAA shows in both cases that the indole-ring is buried in the hydrophobic pocket. However, in the case of IAA the position of the ligand is flipped by 180° compared to the native ligand with its carboxyl group now facing towards the guanidino-group of Arg84 without clear interaction ([Supp Material, smeared density, loop stabilization, crystallography]).

The different substituent positions facilitate a major discriminatory effect introduced by the early variant T44L+S88Y. Designs with bulky side-chains at position 88 showed a markedly increase in affinity and specificity towards IAA (KD). Structural data of this variant with IAA as ligand indicate that the large side-chain effectively blocks the position for the amino-acid group of the native ligand TRP. Moreover, it tightly packs the indole-ring and provides a hydrogen bond (HB) interaction for the carboxyl-group of IAA in the 180° degree turned position. This positional stabilization of the IAA carboxyl group results in a stable salt-bridge to Arg84. The T44L mutation results in an extension of the hydrophobic pocket surrounding the indole-ring.

The bulky S88 side-chain results in an efficient switch of binding specificity from TRP towards IAA, however, it simultaneously facilitates IAN binding. Moreover, we observed that improvements in IAA binding positively correlate with those for binding of IAN. Structural data of intermediate variants either with bound IAA or bound IAN provide the explanation: both ligands share an almost identical position in the binding pocket without changing the surrounding residues. The only difference is that the IAA's carboxyl group interaction with the guanidino group is replaced by the electronegative nitrogen of the nitrile acting as interaction partner. The ITC-binding data confirm this similar binding mode. The ratio of the contributions of ΔS and ΔH are comparable between IAA and IAN in most variants.

The only discriminatory handle between IAA and IAN can be exerted by shifting the interaction between the guanidino-group of Arg84 and the substituents. Structural data on the final variant exemplify this subtle influence. The change T81M removes a HB partner of R84 which indirectly influences the salt-

bridge interaction to the carboxyl group (Kd change). The mutation A91H results in a slight rearrangement (XXX A) of the complete helical stretch resulting in a positional change of R84 fostering an interaction with the carboxyl- group (Kd change). Both positions exemplify that especially fine-tuning of binding specificities relies on residues well beyond the ones in contact with the ligand. The mutation M42F on the other hand results in a more effective packing of the hydrophobic pocket.

References

Benkova, E., M. Michniewicz, M. Sauer, T. Teichmann, D. Seifertova, G. Jurgens and J. Friml (2003). "Local, efflux-dependent auxin gradients as a common module for plant organ formation." Cell **115**(5): 591-602.

Brunoud, G., D. M. Wells, M. Oliva, A. Larrieu, V. Mirabet, A. H. Burrow, T. Beeckman, S. Kepinski, J. Traas, M. J. Bennett and T. Vernoux (2012). "A novel sensor to map auxin response and distribution at high spatio-temporal resolution." Nature **482**(7383): 103-106.

Cho, H., H. Ryu, S. Rho, K. Hill, S. Smith, D. Audenaert, J. Park, S. Han, T. Beeckman, M. J. Bennett, D. Hwang, I. De Smet and I. Hwang (2014). "A secreted peptide acts on BIN2-mediated phosphorylation of ARFs to potentiate auxin response during lateral root development." Nat Cell Biol **16**(1): 66-76.

Czechowski, T., M. Stitt, T. Altmann, M. K. Udvardi and W. R. Scheible (2005). "Genome-wide identification and testing of superior reference genes for transcript normalization in Arabidopsis." Plant Physiol **139**(1): 5-17.

Friml, J., A. Vieten, M. Sauer, D. Weijers, H. Schwarz, T. Hamann, R. Offringa and G. Jurgens (2003). "Efflux-dependent auxin gradients establish the apical-basal axis of Arabidopsis." Nature **426**(6963): 147-153.

Geldner, N., V. Dénervaud-Tendon, D. L. Hyman, U. Mayer, Y.-D. Stierhof and J. Chory (2009). "Rapid, combinatorial analysis of membrane compartments in intact plants with a multicolor marker set." The Plant Journal **59**(1): 169-178.

He, W., J. Brumos, H. Li, Y. Ji, M. Ke, X. Gong, Q. Zeng, W. Li, X. Zhang, F. An, X. Wen, P. Li, J. Chu, X. Sun, C. Yan, N. Yan, D. Y. Xie, N. Raikhel, Z. Yang, A. N. Stepanova, J. M. Alonso and H. Guo (2011). "A small-molecule screen identifies L-kynurenine as a competitive inhibitor of TAA1/TAR activity in ethylene-directed auxin biosynthesis and root growth in Arabidopsis." Plant Cell **23**(11): 3944-3960.

Kaper, T., L. L. Looger, H. Takanaga, M. Platten, L. Steinman and W. B. Frommer (2007). "Nanosensor detection of an immunoregulatory tryptophan influx/kynurenine efflux cycle." PLoS Biol **5**(10): e257.

Leverone, L. A., T. L. Stroup and J. L. Caruso (1991). "Western blot analysis of cereal grain prolamins using an antibody to carboxyl-linked indoleacetic Acid." Plant Physiol **96**(4): 1076-1078.

Liu, P. P., T. A. Montgomery, N. Fahlgren, K. D. Kasschau, H. Nonogaki and J. C. Carrington (2007). "Repression of AUXIN RESPONSE FACTOR10 by microRNA160 is critical for seed germination and post-germination stages." Plant J **52**(1): 133-146.

Mallory, A. C., D. P. Bartel and B. Bartel (2005). "MicroRNA-directed regulation of Arabidopsis AUXIN RESPONSE FACTOR17 is essential for proper development and modulates expression of early auxin response genes." Plant Cell **17**(5): 1360-1375.

Nakamura, A., K. Higuchi, H. Goda, M. T. Fujiwara, S. Sawa, T. Koshiba, Y. Shimada and S. Yoshida (2003). "Brassinolide induces IAA5, IAA19, and DR5, a synthetic auxin response element in Arabidopsis, implying a cross talk point of brassinosteroid and auxin signaling." Plant Physiol **133**(4): 1843-1853.

Navarro, L., P. Dunoyer, F. Jay, B. Arnold, N. Dharmasiri, M. Estelle, O. Voinnet and J. D. Jones (2006). "A plant miRNA contributes to antibacterial resistance by repressing auxin signaling." Science **312**(5772): 436-439.

Nishimura, T., K. Hayashi, H. Suzuki, A. Gyohda, C. Takaoka, Y. Sakaguchi, S. Matsumoto, H. Kasahara, T. Sakai, J. Kato, Y. Kamiya and T. Koshiba (2014). "Yucasin is a potent inhibitor of YUCCA, a key enzyme in auxin biosynthesis." Plant J **77**(3): 352-366.

Novak, O., E. Henykova, I. Sairanen, M. Kowalczyk, T. Pospisil and K. Ljung (2012). "Tissue-specific profiling of the Arabidopsis thaliana auxin metabolome." Plant J **72**(3): 523-536.

Parry, G., L. I. Calderon-Villalobos, M. Prigge, B. Peret, S. Dharmasiri, H. Itoh, E. Lechner, W. M. Gray, M. Bennett and M. Estelle (2009). "Complex regulation of the TIR1/AFB family of auxin receptors." Proc Natl Acad Sci U S A **106**(52): 22540-22545.

Perrot-Rechenmann, C. (2010). "Cellular responses to auxin: division versus expansion." Cold Spring Harb Perspect Biol **2**(5): a001446.

Petersson, S. V., A. I. Johansson, M. Kowalczyk, A. Makoveychuk, J. Y. Wang, T. Moritz, M. Grebe, P. N. Benfey, G. Sandberg and K. Ljung (2009). "An auxin gradient and maximum in the Arabidopsis root apex shown by high-resolution cell-specific analysis of IAA distribution and synthesis." Plant Cell **21**(6): 1659-1668.

Rademacher, E. H., B. Moller, A. S. Lokerse, C. I. Llavata-Peris, W. van den Berg and D. Weijers (2011). "A cellular expression map of the Arabidopsis AUXIN RESPONSE FACTOR gene family." Plant J **68**(4): 597-606.

Sabatini, S., D. Beis, H. Wolkenfelt, J. Murfett, T. Guilfoyle, J. Malamy, P. Benfey, O. Leyser, N. Bechtold, P. Weisbeek and B. Scheres (1999). "An auxin-dependent distal organizer of pattern and polarity in the Arabidopsis root." Cell **99**(5): 463-472.

Shen, J., Y. Zeng, X. Zhuang, L. Sun, X. Yao, P. Pimpl and L. Jiang (2013). "Organelle pH in the Arabidopsis endomembrane system." Mol Plant **6**(5): 1419-1437.

Simon, S. and J. Petrasek (2011). "Why plants need more than one type of auxin." Plant Sci **180**(3): 454-460.

Teale, W. D., I. A. Paponov and K. Palme (2006). "Auxin in action: signalling, transport and the control of plant growth and development." Nat Rev Mol Cell Biol **7**(11): 847-859.

Terrile, M. C., R. Paris, L. I. Calderon-Villalobos, M. J. Iglesias, L. Lamattina, M. Estelle and C. A. Casalongue (2012). "Nitric oxide influences auxin signaling through S-nitrosylation of the Arabidopsis TRANSPORT INHIBITOR RESPONSE 1 auxin receptor." Plant J **70**(3): 492-500.

Ulmasov, T., J. Murfett, G. Hagen and T. J. Guilfoyle (1997). "Aux/IAA proteins repress expression of reporter genes containing natural and highly active synthetic auxin response elements." Plant Cell **9**(11): 1963-1971.

Vert, G., C. L. Walcher, J. Chory and J. L. Nemhauser (2008). "Integration of auxin and brassinosteroid pathways by Auxin Response Factor 2." Proc Natl Acad Sci U S A **105**(28): 9829-9834.

Wang, J. W., L. J. Wang, Y. B. Mao, W. J. Cai, H. W. Xue and X. Y. Chen (2005). "Control of root cap formation by MicroRNA-targeted auxin response factors in Arabidopsis." Plant Cell **17**(8): 2204-2216.

Zhou, J., F. Yu, X. Wang, Y. Yang, C. Yu, H. Liu, Y. Cheng, C. Yan and J. Chen (2014). "Specific expression of DR5 promoter in rice roots using a tCUP derived promoter-reporter system." PLoS One **9**(1): e87008.

Figure 1

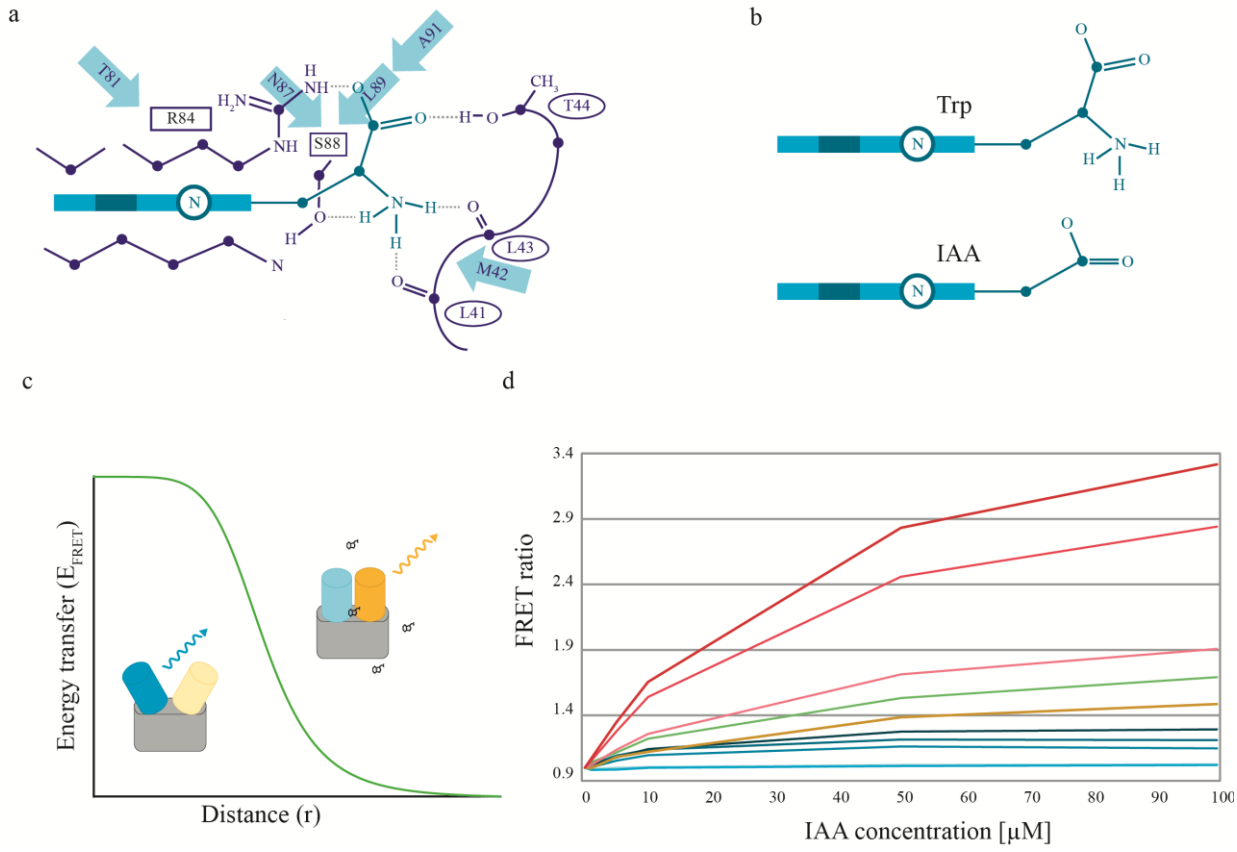

Figure 1: Mutations increasing auxin binding.

a) Structure of the binding pocket of TrpR. Trp is in the middle, the indole ring is perpendicular to the plane of the paper. Residues directly binding Trp are highlighted in purple. Backbone residues mutated in this study are shown as arrows. Modified from (Marmorstein *et al.* 1987).

b) Schemes of Trp and IAA.

c) In the absence of the ligand, the two fluorophores are distant or their chromophore dipoles are perpendicular to each other: the donor (blue) is exited and directly emits photons. Then the ligand (black) is bound, the orientation or distance changes and energy is directly transferred from the donor to the acceptor, which then emits more photons while the photon emission of the donor is quenched. The energy transferred (E_{FRET}) from the donor to the acceptor depends on the sixth power of the distance. See also (d).

d) FRET ratio change plotted against IAA concentration and contributions of the individual steps to the final sensor.

Figure 2

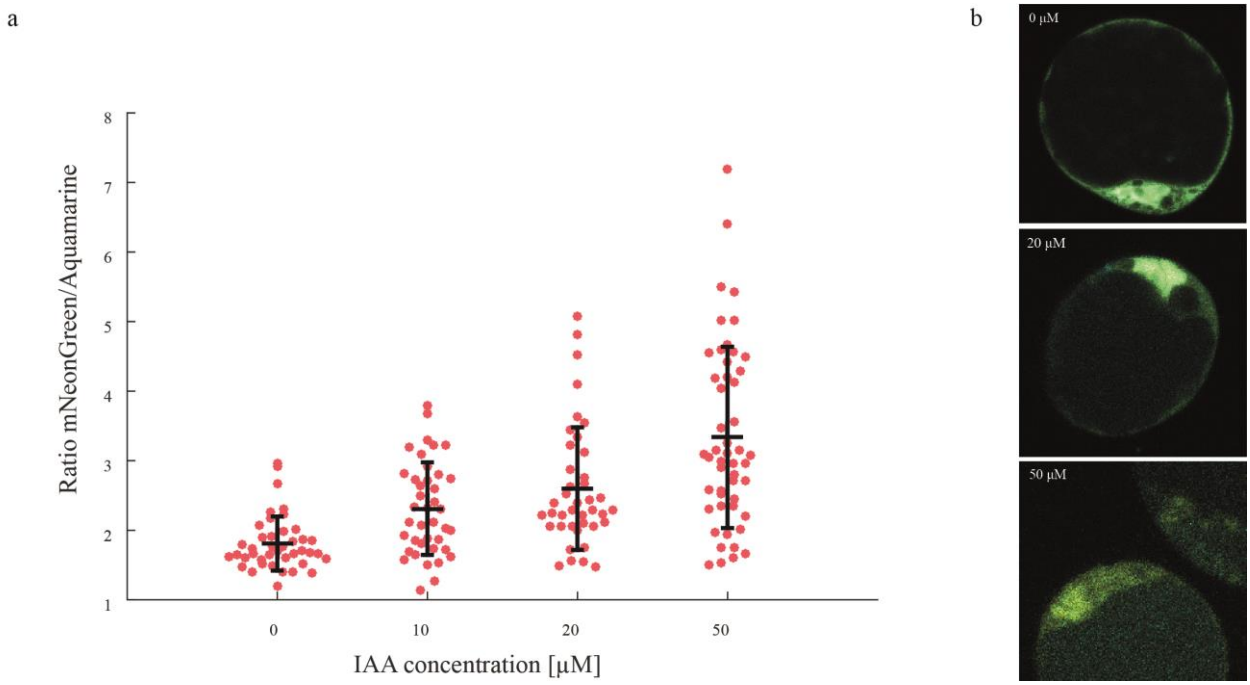

Figure 2: Auxin sensor response in protoplasts.

a) Bee plot of the FRET ratio in protoplasts treated with different IAA concentrations. Each dot indicates readout of a single protoplast. The cross shows the standard deviation and the mean.

b) Protoplasts expressing nuclear localized auxin sensor. The mNeonGreen signal (yellow) becomes increasingly dominant with increased IAA concentrations.

Figure 3

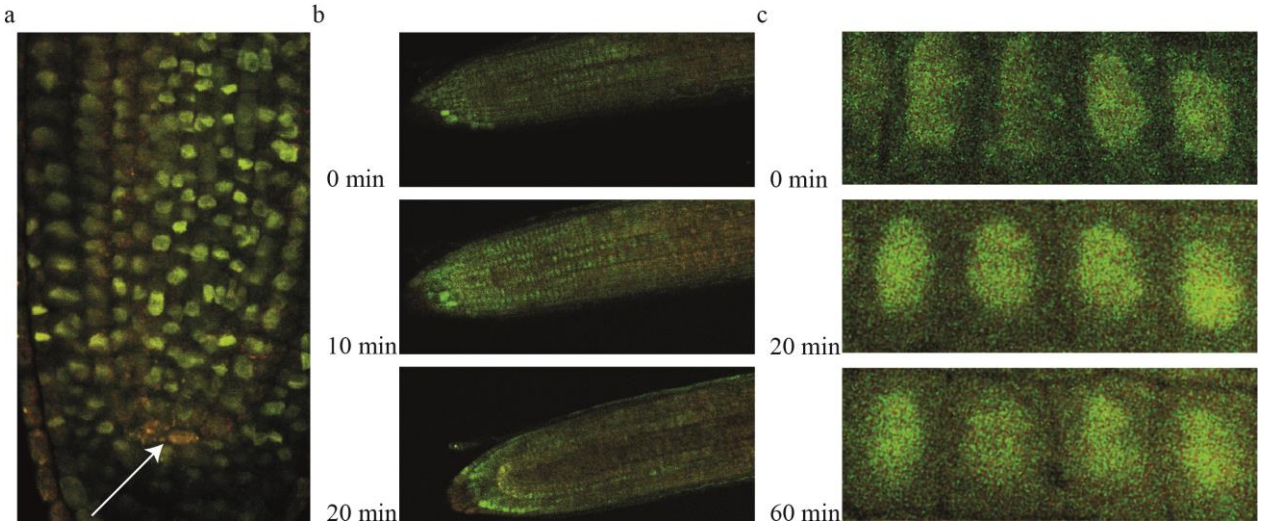

Figure 3. *pEF-1α::NLS:AuxSen* in the root. Overlay of donor (green) and acceptor (red) channels.

(a) Root tip, the arrow points to the auxin maximum in the meristem.

(b) FRET signal over time upon IAA treatment.

(c) Time course of auxin concentration upon gravistimulus. Only the bottom cells are shown.

Figure 4

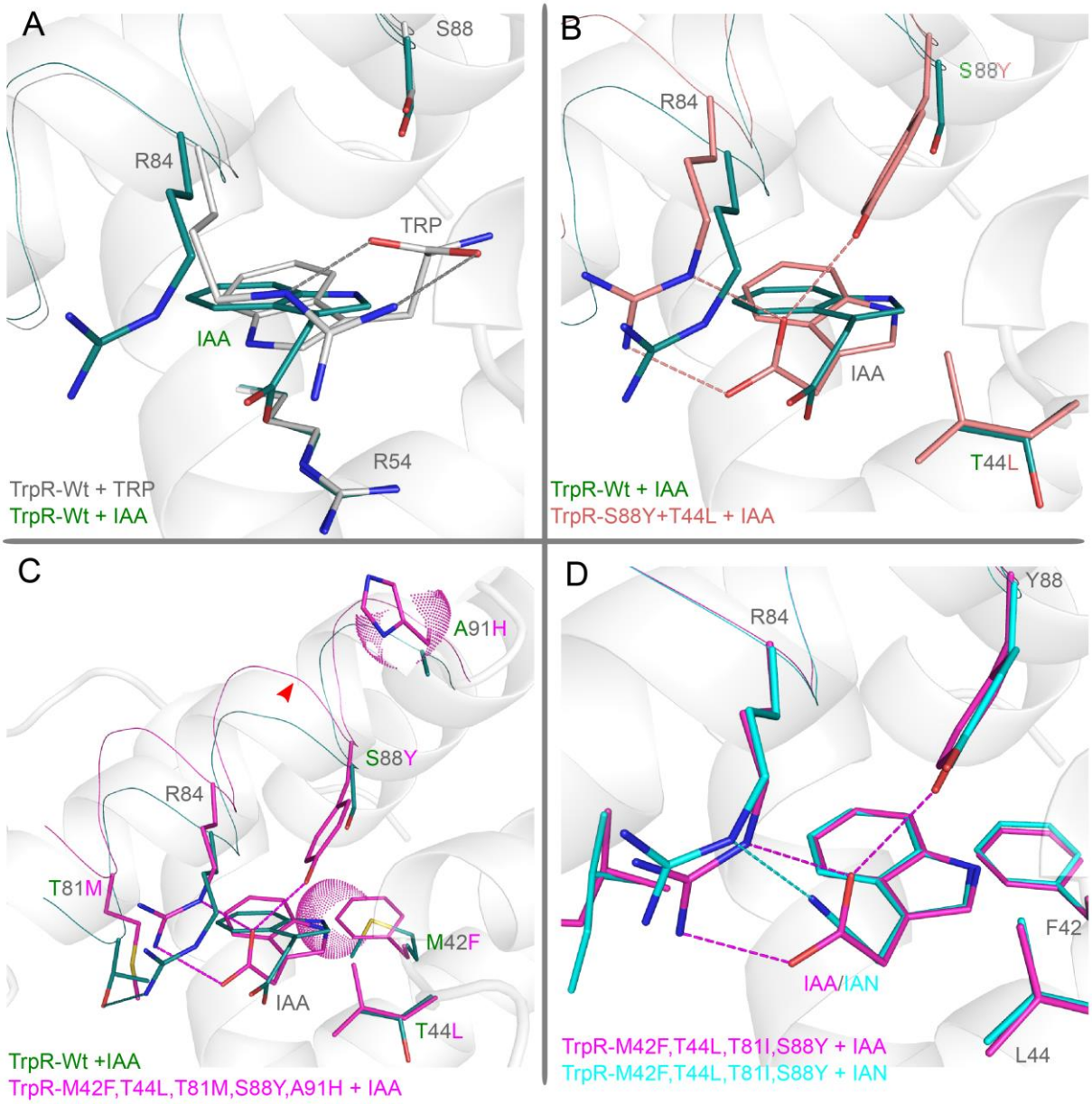

Figure 4. Structural understanding.

a) Structure of TrpR-Wt bound to the native ligand TRP (gray) and bound to the design-target IAA (green). IAA shows a ligand position turned by 180° compared to TRP.

b) Comparison between TrpR-Wt and an initial beneficial variant TrpR-S88Y+T44L (salmon) both bound to IAA. The bulky side-chain of Y88 results in a more stabilized position of the IAA promoting a stable salt bridge to R84. The T44L mutation results in disfavoring alternative positions for the carboxyl group.

c) Binding pocket of our final variant AuxSen (magenta). Next to the mutations S88Y and T44L already indicated in b the mutation T81M result in disfavoring R84 - IAN interaction as compared to IAA. A91H further promotes a rearrangement of the complete helical stretch (red arrow) which readjusts R84 in favor of a IAA interaction. The mutation M42F results in an extension of the hydrophobic pocket, additionally stabilizing the indole-ring.

d) Comparison between IAA (magenta) and IAN (cyan) binding in an intermediate variant (TrpR-M42F+T44L+T81I+S88Y). The binding mode and position in the pocket is almost identical for both ligands with no rearrangements in surrounding residues. The only difference stems from a different interaction propensity with the R84 moiety. Consequently position altering this interaction are prone to foster distinction between the two molecules.